2-22-2023 1:30 PM

# Oligo [poly(ethylene glycol) fumarate] gels with photo-sensitive pendent groups

Andrew Chung, *The University of Western Ontario*

Supervisor: Gillies, Elizabeth R., *The University of Western Ontario*

A thesis submitted in partial fulfillment of the requirements for the Master of Science degree in Chemistry

# Abstract

Stimuli-responsive hydrogels are 3D polymeric structures that offer attractive qualities within the biomedical field due to their excellent biocompatibility and tunability to be employed in drug release, wound healing, and implants. Aliphatic polyesters are biodegradable polymers that naturally degrade by the process of simple ester hydrolysis. Oligo[poly(ethylene glycol) fumarate] (OPF) is a linear polyester containing repeating units of poly(ethylene glycol) and unsaturated fumarate. OPF naturally degrades through hydrolytic cleavage into poly(ethylene glycol) (PEG) and fumaric acid which is a naturally occurring compound found in the Kreb's cycle. However, in some cases, it would be beneficial to activate or accelerate this degradation in a more controlled manner. This thesis explores the degradative behaviour of OPF functionalized with photoactivatable pendent groups that undergo intramolecular cyclization to cleave the backbone, thereby degrading the polymer. Next, the functionalized OPF is converted into a hydrogel by covalently cross-linking and the gel is characterized by the gel content and equilibrium water content. Hydrogel degradation is examined by $^{1}$H NMR spectroscopy and mechanical testing with and without UV light irradiation. It is shown that activation of the pendent groups can accelerate gel degradation.

## Keywords

Self-immolative spacers, self-immolative degradation, oligo[poly(ethylene glycol) fumarate], OPF, hydrogel, photosensitive

# Summary for lay audience

Polymers are large molecules that are composed of repeating units. Currently, there is interest in degrading polymers in response to stimuli such as light, heat, or acid. These degradable polymers are referred to as stimuli-responsive polymers. This thesis aims to explore a new method to trigger the degradation of polymers by introducing units that are responsive to ultraviolet light along the polymer backbone. When these units are activated by light, their reactivity changes and they can slice the backbone at a nearby unit. Overall, this process leads to accelerated degradation of the polymer in the presence of light. The new functional polymer is incorporated into a water-absorbing network, called a hydrogel, and it is shown that degradation of this hydrogel can be accelerated by irradiation with ultraviolet light. Overall, this work provides a proof of concept for a new way to control hydrogel degradation, which could be extended to relevant stimuli in the body for potential applications in new therapies.

# Co-Authorship statements

The work presented in this thesis was written by the author and revised by Dr. Elizabeth Gillies.

Chapter 1 was written by the author and revised Dr. Elizabeth Gillies.

Chapter 2 was written by the author and revised Dr. Elizabeth Gillies.

Chapter 3 describes studies designed by the author and Dr. Elizabeth Gillies. Experiments were primarily conducted by the author. SEC analysis was performed by Aneta Borecki, Dr. Zhengyu Deng, Dr. Burak Tavşanlı, and Dr. Xiaoli Liang. Compression test were performed by Dr. Burak Tavşanlı. The manuscript was written by the author and revised by Dr. Elizabeth Gillies. SEM imaging was performed by Xueli Mei.

Chapter 4 was written by the author and revised by Dr. Elizabeth Gillies.

# Table of contents

# List of Figures

# List of Tables

# List of Schemes

# List of Appendices

# Acknowledgements

I want to thank Dr.Gillies for the opportunity of being a part of the group and allowing me to take part in the graduate research experience. In addition, I must acknowledge her tireless effort and encouragement to see my success. It's been a wonderful opportunity and an uphill battle; I have learned a lot and I have gained a firmer understanding on the rigor and drive that is required to pursue scientific research.

Next, I want to thank my committee members for taking the time out of their busy schedule to read through my work to provide constructive criticism.

Special thanks to Aneta Borecki for the numerous amounts of SEC samples I had asked her to run. Furthermore, I would like to extend my gratitude to the post-docs Dr. Burak Tavşanlı, Dr. Xiaoli Liang, and Dr. Zhengyu Deng who also helped me run several SEC samples.

I must also give credit to past and present lab members for their incredible support through these years: Jay Jaehak Yu, Chuanfeng Li, Monica Vasquez, Jue Gong, Xueli Mei, Jared Pardy, Sherry Shen, Maya Fernando, Karanpreet Gill, and Quinton Sirianni. Beyond the group, I want to extend further gratitude to friends outside the research group, Paul Winiarz, and Mohammad Attaelmanan.

Thank you to my first mentor Dr. Farshid Shakrokhi who provided guidance and supported me through my first couple of rough months into research. Then, I would like to thank Dr. Zhengyu Deng again as my second mentor for providing his guidance, knowledge, and patience through the remainder of my research. You two were amazing mentors.

Finally, I want to thank my family members for their continual and unconditional support through these last 2 years.

# List of Abbreviations

| | |
|---|---|
| **ADMET** | acyclic diene metathesis |
| **ALG** | alginate |
| **°C** | degrees Celsius |
| **CAT** | catalase |
| **CMC** | carboxymethyl chitosan |
| **CS** | chitosan |
| **δ** | chemical shift |
| ***Đ*** | dispersity |
| **DNA** | Deoxyribonucleic acid |
| **DUM** | di(10-undecenyl) maleate |
| **ESI-MS** | electron spray ionization – mass spectrometry |
| **EWC** | equilibrium water content |
| **FT-IR** | Fourier Transformation infrared spectroscopy |
| **g** | grams |
| **GOx** | glucose oxidase |
| **h** | hours |
| **M** | molarity |

| | |
|---|---|
| **mg** | milligram |
| **MHz** | megahertz |
| $m_i$ | initial mass |
| **mL** | mililitres |
| **mm** | millimetre |
| $M_n$ | number average molecular weight |
| **mol** | mole |
| **mmol** | millimole |
| $M_w$ | weight average molecular weight |
| **MW** | molecular weight |
| **NB** | nitrobenzyl alcohol |
| **NMR** | nuclear magnetic resonance |
| **PAP** | phenylazophenol |
| **PBAT** | Polybutylene adipate terephthalate |
| **PBS** | phosphate buffer saline |
| **PEG** | poly(ethylene glycol) |
| **PEG-DA** | poly(ethylene glycol) diacrylate |

| | |
|---|---|
| **PEA** | poly(ester amide) |
| **pH** | log[H+] |
| **PPF** | poly(propylene glycol) fumarate |
| **ppm** | parts per million |
| **PGA** | poly(glycolic acid) |
| **PLA** | poly(lactic acid) |
| **PLGA** | poly(lactic-co-glycolic acid) |
| **PMMA** | poly(methyl methacrylate) |
| **PNSC** | N-Succinyl chitosan |
| **OPF** | oligo[poly(ethylene glycol) fumarate] |
| **SEC** | size exclusion chromatography |
| **SIP** | self-immolative polymer |
| **TEMED** | *N,N,N',N'* - tetramethylethylenediamine |
| **TFA** | trifluoroacetic acid |
| **THF** | tetrahydrofuran |
| **UV** | ultraviolet light |
| **(w/w) %** | weight by weight percent |

# Chapter 1

# 1 Introduction

## 1.1 Biodegradable polymers

The process of biodegradation can be defined as the change in chemical composition, mechanical, and structural properties with the formation of metabolic products through processes associated with living organisms.[1] This process occurs in two steps: i) the polymer is broken down and fragmented into lower molecular weight species; ii) subsequent degradation by the microorganism using extracellular enzymes and abiotic agents via processes such as oxidation, photodegradation, hydrolysis to depolymerize long polymer chains to oligomers.[1] Through a biomineralization process, oligomers are bio assimilated by micro-organisms and mineralized. In the final stage of biodegradation, aerobic or anaerobic degradation can occur. The presence of oxygen promotes aerobic degradation, generating $CO_2$ and $H_2O$. In the absence of oxygen, anaerobic degradation occurs followed by the generation of products such as methane, water, and carbon dioxide (**Figure 1.1**).[1]

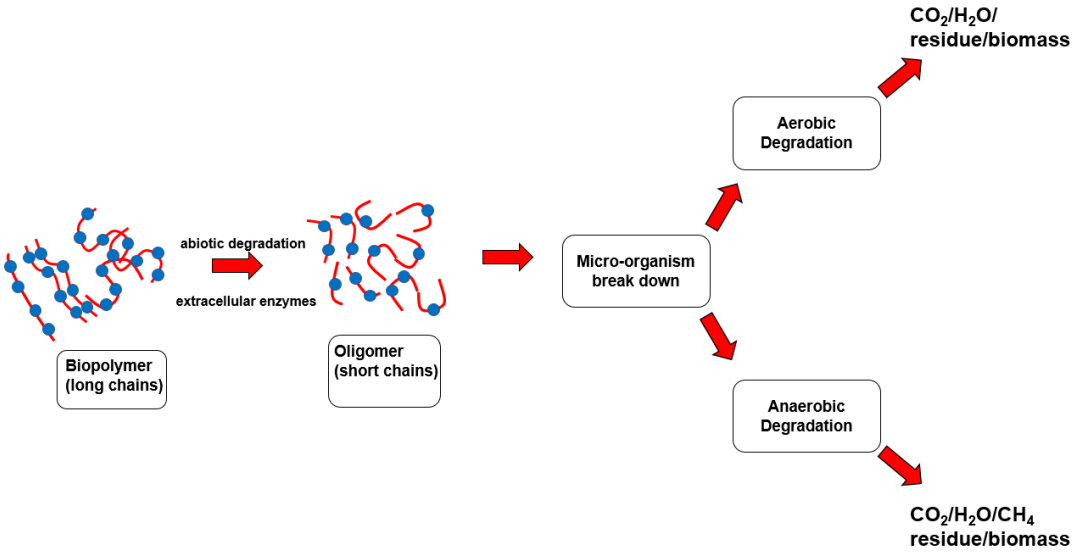


**Figure 1.1.** General overview of the degradative processes of biopolymers.

Natural biodegradable polymers are a class of macromolecules that are found in nature and contain biodegradable functional groups.[2] Commonly known natural biodegradable polymers include polysaccharides and polypeptides.[3-5] Biodegradable polymers have been demonstrated to have meaningful industrial applications within agricultural and biomedical fields.[6]

Synthetic biodegradable polymers are defined as a class of artificially manufactured macromolecules consisting of biodegradable groups.[1] However, like their natural counterparts, they are susceptible to degradation through the breakdown by living organisms. Some common classes of synthetic biodegradable polymers comprise of polyesters, polycarbonates, and polyurethanes.[7] These classes of polymers yield modifiable properties making them excellent candidates for several biomedical applications. Synthetic biodegradable polymers have been employed in drug delivery, tissue engineering, and other biomedical devices.[8]

Various factors such as the morphology, structure, molecular weight, and chemical treatment can affect the rate of a polymer's biodegradation.[1] For example, biodegradable polymers contain hydrolysable linkages that can be degraded by the microorganisms and hydrolytic enzymes.[1] Polymers containing a combination of hydrophobic and hydrophilic groups are more susceptible to degradation.[1] In terms of polymer morphology, amorphous regions of the polymer are easily accessible to be attacked by enzymes compared to the crystalline regions due to larger distances between chains in the amorphous region.[1] Enzymatic degradation of the polymer can be affected by the melting temperature ($T_m$) of the polymer. In general, vulnerability to biodegradation is inversely proportional to the melting point for polymers.[1] Biodegradation capability can also be altered with treatments such as ultraviolet (UV) light, that generate radical ions, leading to backbone cleavage. Oxidation may also occur affecting the polymer's ability to biodegrade.[1] Furthermore, biodegradability of a polymer may be hampered as the molecular weight of the polymer increases.

## 1.2 Biodegradable polyesters

### 1.2.1 Introduction to biodegradable polyesters

Biodegradable polyesters are a class of polymers that contain ester linkages in their backbone.[1, 8] There are several attractive qualities of polyesters and these include controlled biodegradability, excellent biocompatibility and convenient synthesis.[8, 9] Furthermore, polyesters have tunable physical and mechanical properties extending their range of applications within the biomedical field.[8, 10] Specifically, biodegradable polyesters are employed in drug delivery, tissue engineering, and medical devices.[8] Naturally, polyesters degrade through the mechanism of hydrolysis and this process can be catalyzed in the presence of base, acid, or enzymes.[8] When degradation is complete, the products are designed to be processed in the natural environment or in some cases resorbed by the body through a metabolic pathway.[7, 11] In the environment, the degraded polyester is consumed by the micro-organisms such as fungi and bacteria, and converted to water, carbon dioxide, and methane. Biodegradable polyesters can be broadly categorized into two major groups: aliphatic polyesters, or aromatic co-polyesters.[12] Examples of aliphatic polyesters include poly(lactic acid) (PLA), poly(caprolactone) (PCL), and poly(glycolic acid) (PGA) (**Figure 1.2**).[12, 13] While aliphatic polyesters are easily hydrolysable, aromatic polyesters are insensitive to most biodegradable processes by hydrolysis, enzymatic, or microbial attack.[2] Generally, aromatic polyesters are co-polymerized with an aliphatic monomer to improve their biodegradation capabilities.[2] For example, a random co-polymer such as poly(butylene adipate-co-terephthalate) (PBAT), involves the polycondensation between 1,4-butanediol and mixture of adipic acid and terephthalic acid (**Figure 1.3**).[2] When PBAT is co-polymerized with an aliphatic poly(ester), it was found to have excellent mechanical and thermal properties with concentrations of terephthalic acid at 35 mol%.[2] However, biodegradability can be diminished as the concentration of terephthalic acid is increased to 55 mol%.[2]

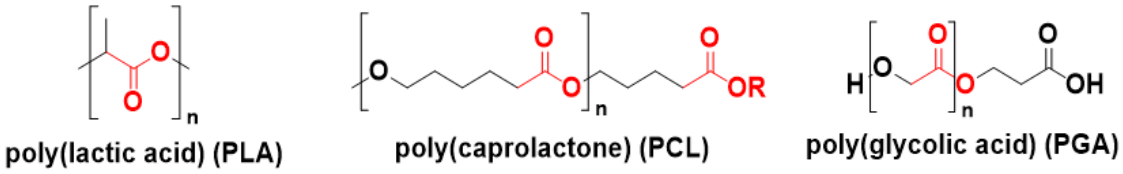


**Figure 1.2.** Common biodegradable synthetic polyesters.

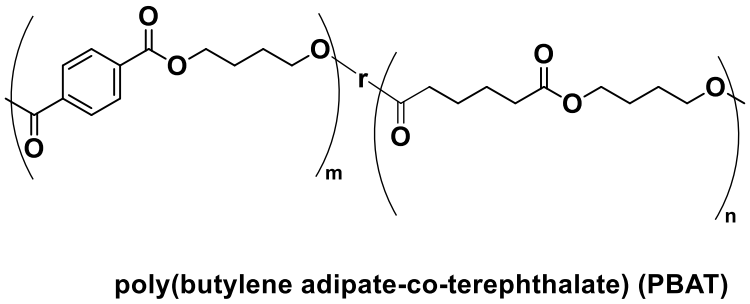


**Figure 1.3.** Biodegradable aromatic random co-polyester PBAT.

## 1.2.2 Aliphatic polyesters

Aliphatic polyesters are often sensitive to hydrolysis and typically have excellent mechanical, biocompatibility, and biodegradability within a physiological environment.[14-16] The mechanism of hydrolysis may either involve a bulk erosion or surface erosion process and the extent of degradation depends on the hydrophilicity and crystallinity of the polyester.[14, 15]

Straight chain polyesters offer the advantage of controlled and tunable degradation rates.[14] Due to the capability to modify the degradation behaviour of aliphatic polyesters, they are of growing interest as biomaterials for applications within living organisms.[14, 17] However, many polyesters are naturally hydrophobic and lack reactive side groups which affects the polymer's functionality within the body.[14] Therefore, it is important to investigate alternatives to improve a polyester's hydrophilicity whether it be through chemical or physical modifications.[14]

Aliphatic polyesters can be synthesized through three major routes: i) poly-condensation; ii) ring opening polymerization; iii) enzymatic polymerization.[18, 19 20] Polycondensation typically involves a diol and diacid, but a major drawback of this reaction is low degrees of polymerization leading to low molecular weight polymers.[15] Ring opening polymerizations can occur through either an anionic, cationic, or enzymatic process.[19] They involve the use of cyclic diesters such as a lactide and glycolide and result in high molecular weight polymer chains. There are usually minimal side reactions involved in these reaction such as racemization.[15] Finally, enzymatic polymerization is a technique carried out in mild conditions and aims to avoid the use of toxic reagents while recycling the catalyst.[15] Enzymes provide a direct polymerization such that no protected monomers are needed and they also afford regioselectivity and stereoselectivity.[15]

## 1.2.3. Applications of biodegradable polyesters

Degradable aliphatic polyesters such as PCL, PLA, PGA, and poly(lactic-co-glycolic acid) (PLGA) are commonly employed in several bioengineering applications.[15] For example, PGA has been used as resorbable sutures. These were first developed in 1962 by American Cyanamid Co. and became commercially available under the name if Dexon®. PLGA emerged 5 years later to form new resorbable sutures with the name Vircyl™.[21] However, these polyesters are known to be very hydrophobic which affects their cell adhesion and this factor plays a significant role in polymeric scaffolds.[15] Furthermore, these polyesters are known to undergo slow hydrolysis.[21] Aliphatic polyesters have also been investigated for drug delivery. For example, systems based on poly(lactic acid) were utilized for long-term delivery of anti-malarial drugs, contraceptives, and ocular therapies.[21] Overall, biodegradable polyesters are a promising class of polymers with a wide scope of applications and offer excellent tunability.

## 1.3 Stimuli-responsive polymers

Stimuli-responsive polymers refer to a class of macromolecules that change their chemical or physical properties in response to stimuli (e.g., pH, temperature, mechanical force, chemical, and electric or magnetic fields).[22-24] Furthermore, it is possible to synthesize a multi-responsive polymer through the incorporation of certain stimuli-responsive functional groups into the polymer.[22] For example, a backbone could be composed of a photo-responsive monomer such as azobenzene that exhibits temperature and light sensitivity. [22] Due to their ability to manifest as imitations of naturally occurring materials, these biomaterials are often selected to be exploited in sensors, biosensors, controlled drug delivery, and other applications.[22]

### 1.3.1 pH sensitive polymers

pH responsive polymers undergo changes in properties or degrade in response to a change in the pH of the environment.[25] They can contain degradable linkages such as acetals or ionizable functional groups that depending on the protonation state exhibit different conformations or solubilities.[25]

For example, pH responsive polymers are used in the synthesis of insulin delivery systems to manage glucose levels.[25] Anderson and co-workers in 2013 developed an injectable nano-network composed of alginate (ALG) or chitosan (CS) charged dextran nanoparticles that could encapsulate insulin (**Figure 1.4a**). They reported dextran nanoparticles containing insulin and other enzymes such as glucose oxidase (GOx) and catalase (CAT) coated with either chitosan or alginate (**Figure 1.4b**).[26] These nanoparticles carried either negative or positive charges on the surface of the coating and through charged interactions, the coated polymers formed a nanoscale network (**Figure 1.4c**). GOx catalyzes the conversion of glucose to gluconic acid which triggers the release of insulin into the surrounding area as a response to the change in pH. Mouse studies showed that hyperglycemic mice could maintain a normal blood sugar level (i.e., normoglycemia) after

subcutaneous injection of the nanoparticles. This work demonstrated a promising method for the controlled insulin release within mice and provides a new potential strategy for the treatment of diabetic patients.

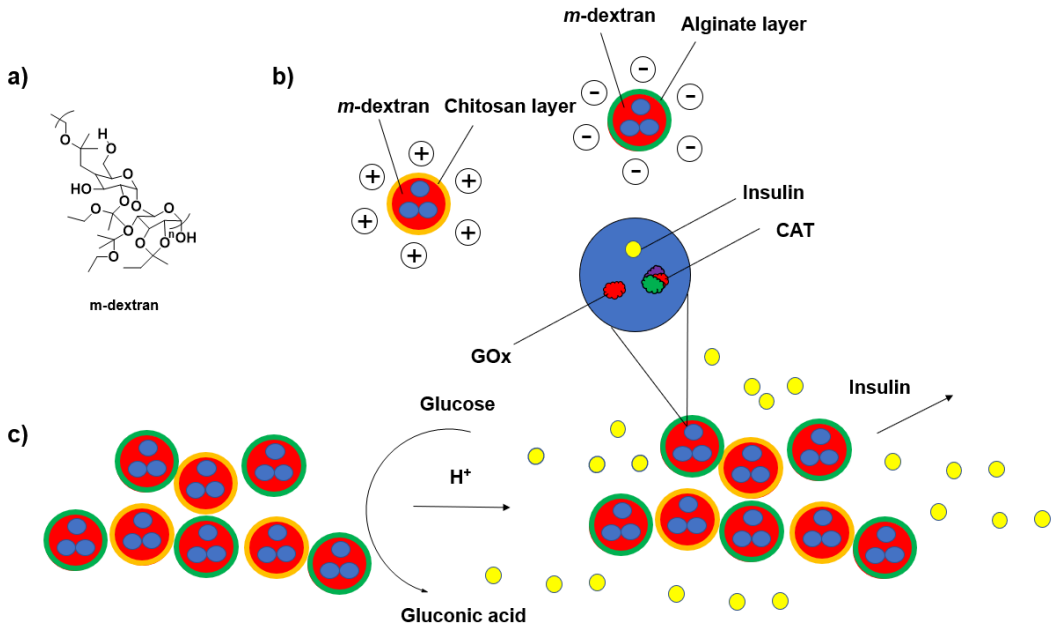


**Figure 1.4. a)** Polymer m-dextran **b)** m-dextran coated with chitosan and alginate layer and encapsulating insulin and other enzymes GOx and CAT **c)** nanoparticle network held together by opposite charges with triggered release during the generation of gluconic acid, as reported by Anderson and coworkers.[26] Reproduced with permission from reference 19. Copyright 2013, American Chemical Society.

## 1.3.2 Photo-sensitive polymers

Photo-sensitive polymers refer to macromolecules that undergo physiochemical changes in response to electromagnetic radiation from light sources such as UV, visible, and near infra-red (IR).[27, 28] These polymers can be triggered to undergo a reversible or irreversible degradation on demand, making them suitable

candidates for drug delivery and other applications such as biomimetic sensors and actuators.[28]

Recently, Orozco and co-workers developed a photosensitive nanocarrier built from *N*-succinyl chitosan that contained the ability to photo-isomerize to the trans configuration in the presence of UV irradiation and reversed to the cis configuration when exposed to visible light (**Figure 1.5**).[29] The cis to trans isomerization or vice versa, induced pore size changes in response to a change in polarity. The trans configuration resulted in a hydrophobic polymer while the cis configuration yielded a hydrophilic polymer.[29] These changes in configuration ruptures or destabilized the micellar structure allowing the cargo to be released.[29] Dofetilide was utilized as a cargo model and encapsulated within this polymeric framework. When the micellar structure was irradiated with UV light, rapid and controlled release of the drug cargo was observed.[29] This was the first nanocarrier reported to be functionalized with a cardiac targeting peptide with photo-triggerable anti-rhythmic drug delivery into cardiomytocytes with minimal cell cytotoxicity.

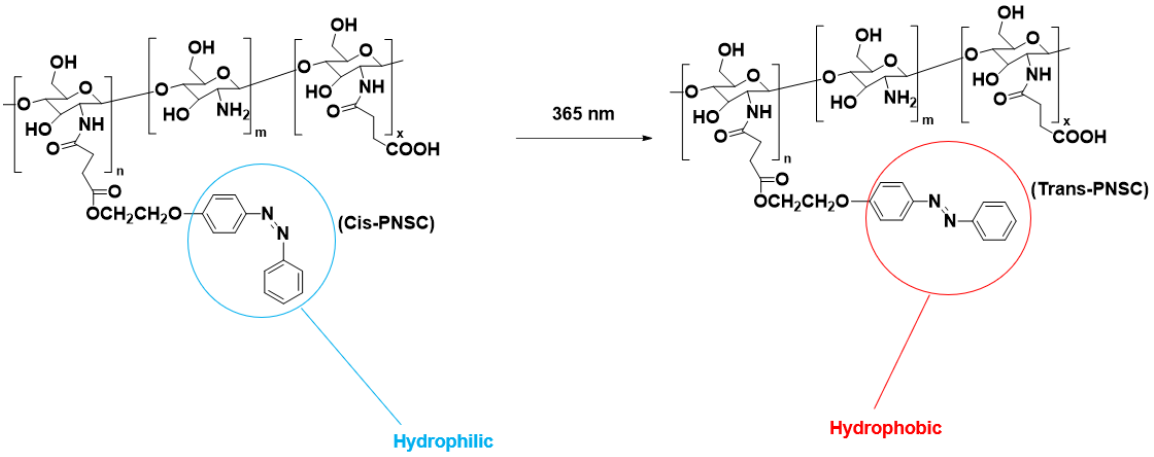


**Figure 1.5.** N-succinyl chitosan(PNSC) functionalized with photolabile 4-phenylazophenol (PAP) molecules that undergo photo-isomerization when irradiated with UV light as reported by Orozco and coworkers[29]. Reproduced with permission from reference 22. Copyright 2020, Wiley-VCH GmbH.

## 1.3.3 Self-immolative spacers

The first reported self-immolative spacers is often referenced to Katzellenbogen and coworkers in 1981.[30] Systems employing self-immolative spacers typically consist of: i) protecting group (trigger group), ii) self-immolative spacer, and iii) target compound (**Figure 1.6**).[31] When the system is subjected to a stimulus (e.g. light, change in pH or redox potential) the system initiates the "self-immolation" process. [31] This self-immolation refers to a cascade of processes such as 1,4- , 1,6-, or , 1,8- eliminations, often with subsequent decarboxylation reactions.[32 33] In other scenarios, self-immolation can occur through an intramolecular cyclization process.[31] This mechanism involves the release of the target compound which begins with the removal of the protecting group through an external stimuli and liberation of the nucleophilic group, followed by cyclization to cleave the chemical linkages and release the target compound.[34-36] In general, these processes are driven by an increase in entropy and/or irreversible formation of thermodynamically more stable compounds.[35]

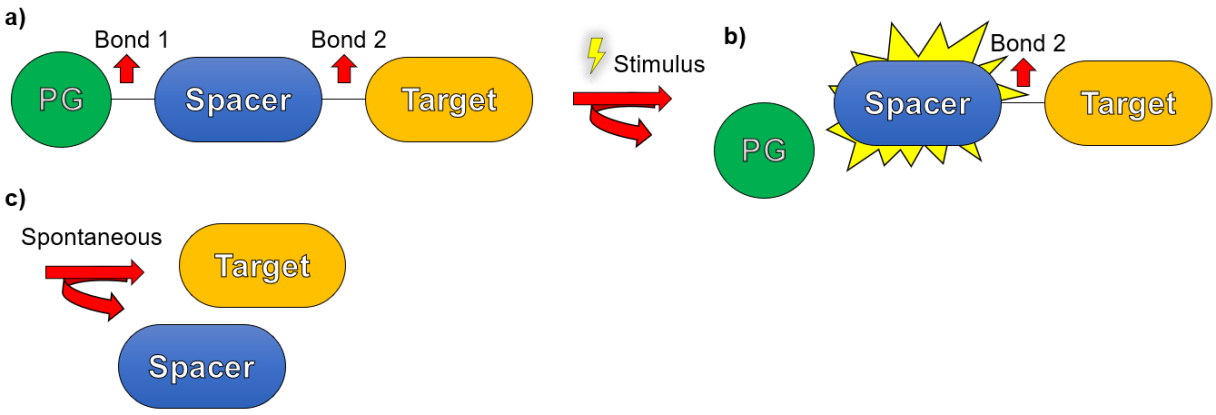


**Figure 1.6.** General design of a self-immolative spacer system consisting of PG = protecting group, spacer = moiety that undergoes chemical cleavage event, target = desired compound to be release. **a)** Self-immolative spacer system pre-cleavage event **b)** introduction of stimuli and subsequent cleavage of protecting group **c)** release of the target compound.

## 1.3.4. Cyclization spacers

Self-immolative spacers that degrade through cyclization commonly form 5- or 6-membered rings.[31] When the protecting group (PG) moiety is activated through the introduction of a specified stimulus, a nucleophilic group such as a hydroxyl, thiol, or amino group attacks a nearby carbonyl group, resulting in the formation of a 5- or 6-membered ring and the loss of the leaving group (LG) (**Figure 1.7**).[37, 38] Previously, the Gillies group has reported a poly(ester amide) (PEA) containing protected 2,4-diaminobutyric acid or homocysteine (HCY) units (**Figure 1.8**).[39] Upon cleavage of the pendent protecting groups, the amines or thiols respectively cyclized through reaction with the backbone esters, resulting in backbone scission. However, these PEA were not water-soluble, and their degradation was quite slow.

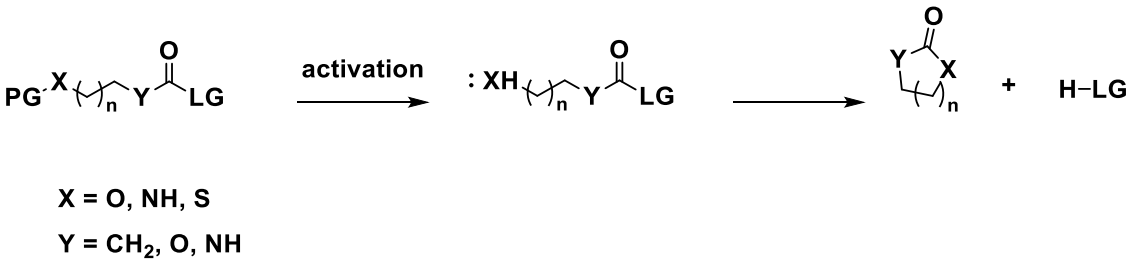


**Figure 1.7.** General scheme for an intramolecular cyclization degradation.

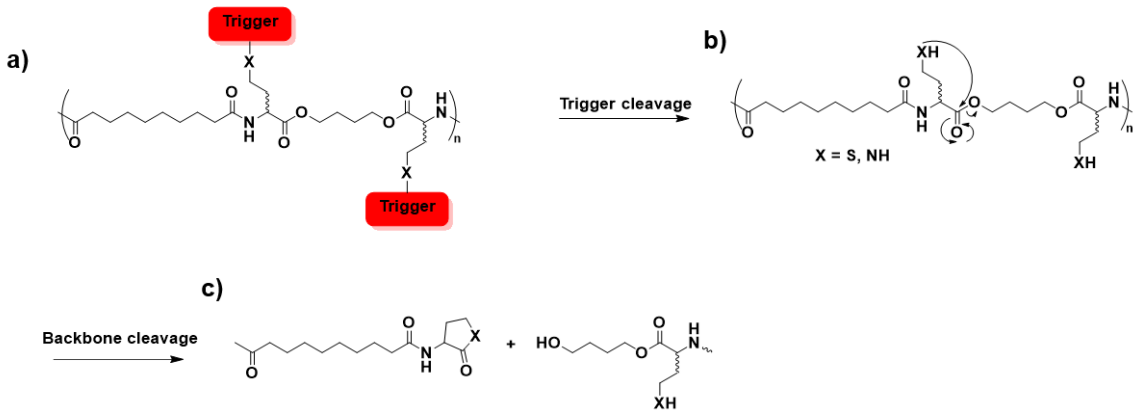


**Figure 1.8.** Self-immolative PEA through a cyclization mechanism reported by Gillies and coworkers (2013). **a)** PEA incorporated with trigger moieties **b)** cleavage of the trigger group and cyclization **c)** degradation products post cyclization.

Recently, Gennari and co-workers worked on cyclization spacers based on proline-derived compounds that could rapidly cyclize.[40] This degradation model leverages the cleavage of carbamate bonds where the nucleophilic amine attacks the adjacent carbamate, resulting in the formation of cyclic urea and a liberated hydroxyl compound (**Figure 1.9**). The author sought to improve upon slow cyclization spacers that are capable of on demand drug release, but suffer from low drug release rates, limiting their therapeutic efficacy.[40] Using this proline derived self-immolative spacer resulted in enhanced release of drugs such as camptothecin (CTX) and paclitaxel (PTX) having hydroxyl groups and consequently enhanced anti-cancer activity in vitro studies against IGROV-1 cancer cells.[40]

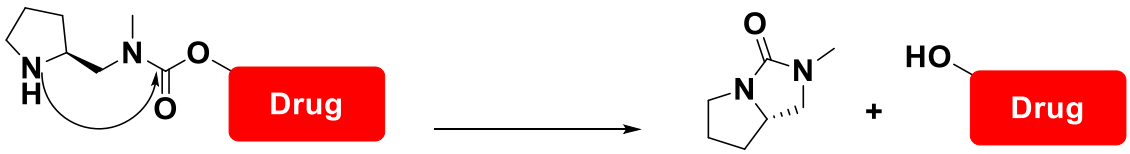


**Figure 1.9.** Proline derived cyclization spacer undergoing an intramolecular cyclization to release the drug loaded payload bearing a hydroxyl group.

# 1.4 Introduction to hydrogels

## 1.4.1 Background

Hydrogels were first described by Wichterle and Lim in 1984.[41] They were described as hydrophilic three-dimensional cross-linked polymeric networks derived from either a natural polymer (e.g. collagen, gelatine, and polysaccharides) or synthetic polymer (e.g. poly(acrylic acid), poly(acrylamide), and poly(2-hydroxyethyl methacrylate) (**Figure 1.10**).[42-44] Their structures enable them to swell through the process of absorbing water while remaining insoluble.[42, 45] Their water absorption capacity depends on the polymer properties and density of the network's cross-linked structure.[42] When the gel achieves a swollen state, the mass fraction of water is higher than the mass fraction of polymer and in most biomedical applications, the mass of water typically constitutes more than 50% of the gel.[42, 46] More importantly, researchers are recognizing that hydrogels can be synthesized to mimic the properties of natural tissues and can serve as a model to be tailored to several biomedical applications.[42]

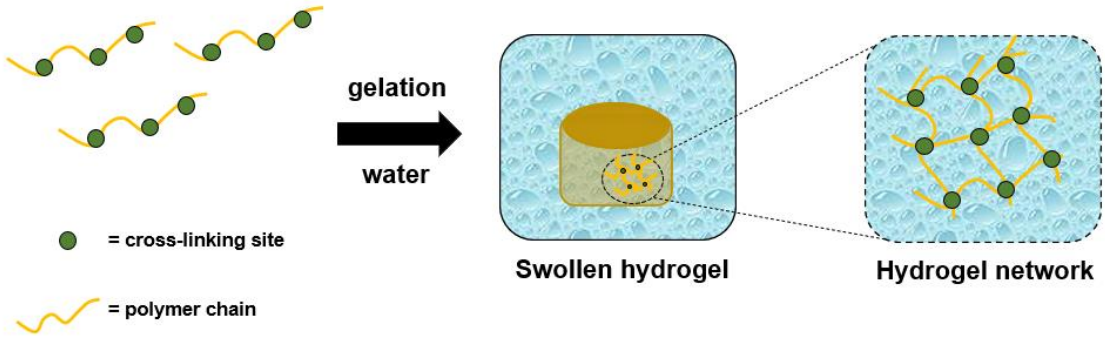


**Figure 1.10.** General schematic depicting a cross-linked polymer network hydrogel swollen in water.

### 1.4.2 Hydrogel cross-linking

Hydrogels can be developed based on several cross-linking protocols that accomplish a desired network and will dictate the gel's overall stability and resistance against disintegration.[43] In general, these cross-linking junctions can be a result of chemical bonds, physical bonds, or a combination of these.[42] Chemically cross-linked junctions involve the formation of irreversible covalent bonds while physically cross-linked junctions involves interactions that are transient in nature.[42, 47] Examples of chemical cross-linking reactions include radical reactions, addition reactions, click reactions, or enzymatic cross-linking.[48, 49] Examples of physical cross-links include hydrogen bonds, hydrophobic interactions, and ionic bonds.

Radical polymerization occurs through the production of a chemical initiator in response to irradiation with light or heating. The initiator reacts with a monomer or an appropriate cross-linker to facilitate the cross-linking process (**Figure 1.11**).[50, 51] Photoinitation may occur either through a type I reaction, which involves homolytic photodissociation of the photoinitiator molecule (**Figure 1.12**) or a type II reaction, where the excited initiator reacts with a co-initiator such as an electron donor or acceptor or hydrogen donor to produce radicals.[52] Type II initiation reactions are typically slower and less efficient than type I. Type II photoinitatiors often suffer from competitive processes that can occur during excitation of the photoinitiator such as reaction with the monomer, co-initiator or atmospheric oxygen.[52] The most widely used photoinitiator for hydrogel preparation is the type I water soluble photoinitator Irgacure 2959 (**Figure 1.13**). When the type I initiator is irradiated, it is cleaved into two radicals, benzoyl and alkyl group, and both initiate a radical polymerization of the hydrogel components.[52] The second method of radical polymerization involves the use of water soluble radical thermal redox initiators ammonium persulfate (APS) in the presence of the catalyst *N*,*N*,*N*,*N* – tetramethyldiamine (TEMED) (**Figure 1.14**). Typically for this method, the APS/TEMED and hydrogel components are heated to 37 °C to initiate the cross-linking process.[53]

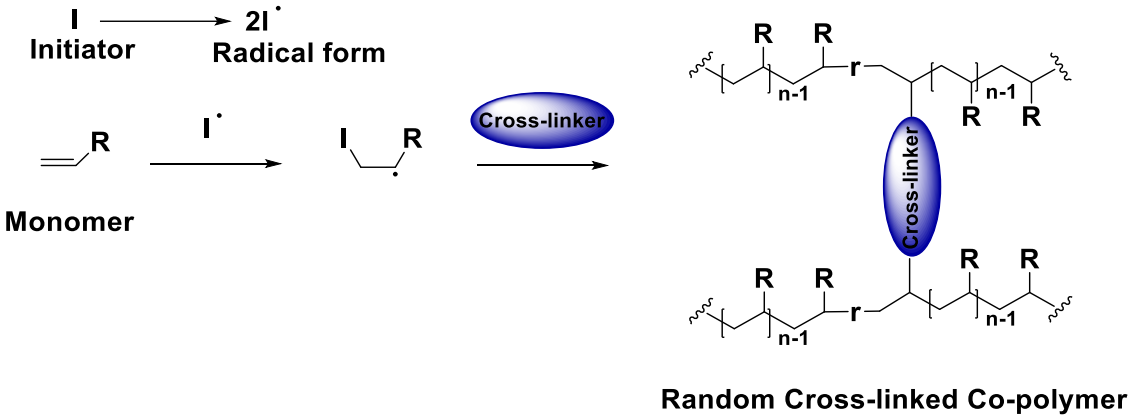


**Figure 1.11.** General scheme of a cross-linking method performed through free radical polymerization.[52]

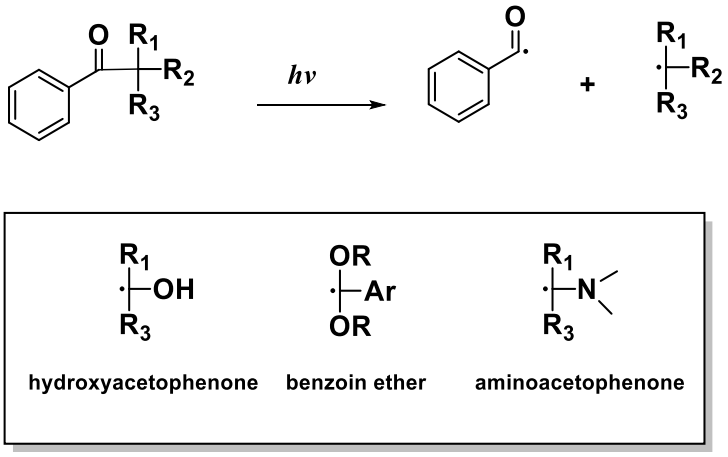


**Figure 1.12.** General overview of type I photoinitators.[52]

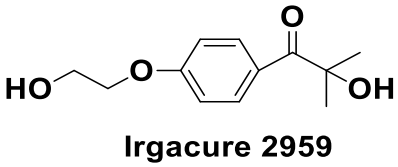


**Figure 1.13.** Chemical structure of the photoinitator Igracure 2959.[52]

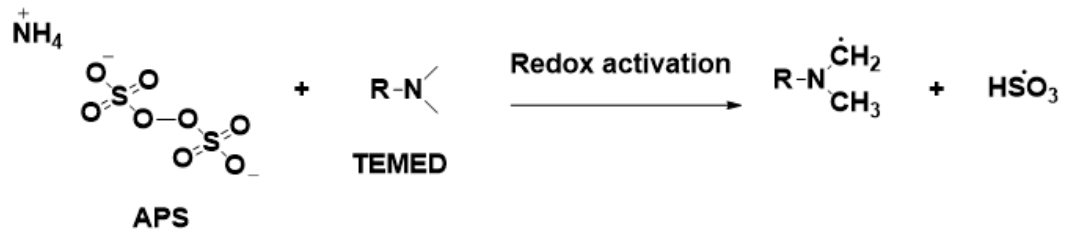


**Figure 1.14.** Redox activation of the water soluble radical initiators ammonium persulfate (APS) and *N,N,N,N* – tetramethyldiamine (TEMED).[52]

Hydrogels can be prepared using other cross-linking reactions such as Michael additions, involving the nucleophilic addition to an α,β-unsaturated carbonyl compound (**Figure 1.15**).[54] Alternatively, the hydrogels can be prepared through click chemistry, which encompasses a wide array of reactions including copper-catalyzed azide-alkyne cycloaddition, Diels-Alder, thiol-ene, tetrazine-norborene chemistry, thiol-epoxy, and thiol-maleimide couplings.[54] Cross-linking reactions performed by click chemistry, offer rapid polymerization kinetics and minimal reactivity with cellular components (**Figure 1.16**).[54] However, gels produced in this manner usually suffer from toxicity problems which can originate from the chemical cross-linker.[43]


**Figure 1.15.** General schematic of cross-linking through a Michael addition.[43]


**Figure 1.16.** General schematic of cross-linking through a click reaction.[43]

Examples of physical cross-links include chain entanglements, ionic interactions, inter- or intra-molecular hydrogen bonds, or hydrophobic interactions (**Figure 1.17**).[41, 42] The formation of physically cross-linked hydrogels can be manipulated by temperature, pH, the presence of ions, and UV light.[51, 55] These interactions are a reversible processes such that when stress is applied or the physical conditions are altered, the properties of the gel change in return. Gels composed in this manner are often weaker than their chemically constructed counterpart.

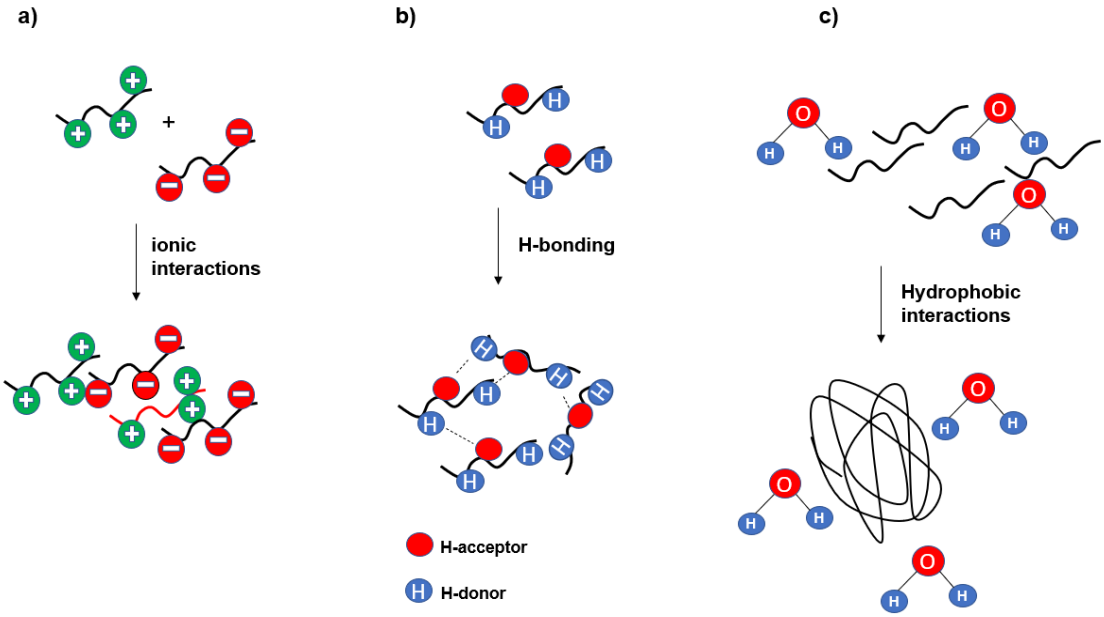


**Figure 1.17.** Schematic illustration of physical cross-linking in polymers **a)** ionic interactions **b)** hydrogen bonding **c)** hydrophobic interactions.

### 1.4.3 Oligo [poly(ethylene glycol) fumarate] gels

Oligo [poly(ethylene glycol) fumarate] (OPF) is a linear polyester, and is synthesized from a condensation polymerization between poly (ethylene glycol) (PEG) and fumaryl chloride.[56] OPF is synthesized in a molar ratio of 1:0.9 PEG to fumaryl chloride to produce oligomers end capped with PEG end groups. The number of PEG units incorporated within the oligomer is dependent on steric considerations.[56] Larger nominal molecular weight PEG groups result in obstruction of the fumarate unit addition with PEG. Thus, resulting in less PEG groups integrated into the oligomer backbone and a substantial amount of unreacted PEG.[56]

OPF oligomers can undergo a cross-linking reaction involving the unsaturated bonds of the fumarate unit found on the backbone.[57] Cross-linking is often facilitated with a cross-linking agent such as acrylic acid esters (PEG-diacrylate) or amides (*N*,*N*'-methylene bisacrylamide) due to the less reactivity of the double bonds.[57] Hydrogel fabrication of OPF are often considered to proceed towards completion due to the fixed length of PEG units between cross-linking sites.[57] Gel formulations that include large PEG chains with larger nominal weight tend to increase the swelling ratio of OPF hydrogels.[58] OPF naturally degrades through the mechanism of ester hydrolysis producing fumaric acid and PEG – fumaric acid is a naturally occurring biological compound found within the Kreb's cycle that makes it an excellent candidate to be exploited within the biomedical field due to minimal cytotoxicity (**Figure 1.18**).[57] OPF has been utilized in support tissue formation in bone, cartilage, osteochondral, tendon, cardiovascular, ocular, and neural tissue engineering.

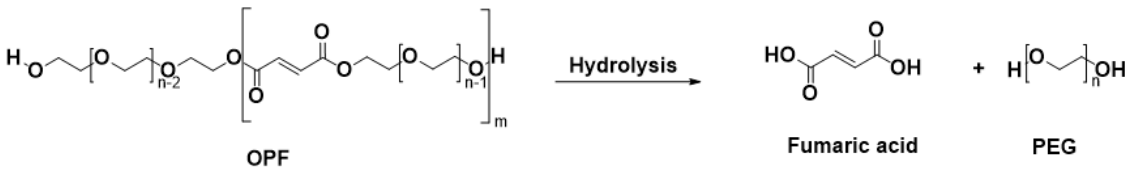


**Figure 1.18.** Hydrolytic degradation of OPF into its constituents fumaric acid and PEG.[56]

In 2005, Mikos and coworkers reported a hydrogel fabrication encapsulating plasmid DNA under physiological conditions using radical thermal initiators ammonium persulfate (APS) and *N*,*N*,*N'*,*N'* – Tetramethylethyldiamine (TEMED) (**Figure 1.19**).[59] Two hydrogel fabrications from different nominal molecular weight (OPF 3k and OPF 10k) were encapsulated with iodinated plasmid DNA ($^{125}$I-labeled DNA) and studied to measure the release of DNA plasmid into solution.[59] Release of the $^{125}$I-label DNA was quantified through a fluorescent method with Pico-Green dsDNA quantitation reagent and/or Oligreen ssDNA Quanitation Reagent termed Picogreen and Oligreen over the course of 40-60 days.[59] It was found that the OPF 3k formulation loaded with $^{125}$I-labeled DNA degraded completely by day 49 and releasing 97.8% +/- 0.3 of initial loaded DNA. In contrast, OPF 10k degraded completely by day 69 releasing 92.1 ± 4.3% of initial loaded DNA by picogreen analysis.[59] Overall, it was concluded that plasmid DNA release could be manipulated by modifying the oligomer properties by differing the nominal molecular weight used in the fabrication of the hydrogel.[59] Therefore, drawing attention to OPF as an attractive tool for controlled gene delivery.

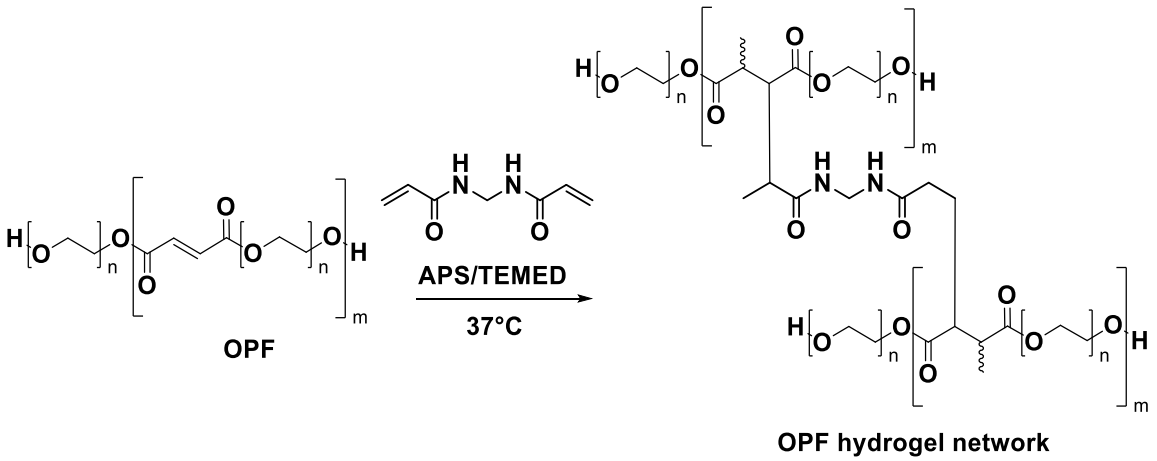


**Figure 1.19.** Hydrogelation of OPF with thermal initiator APS/TEMED as report by Mikos and co-workers (2005).[59]

## 1.4.4 Properties of hydrogels

The degree and type of cross-linking can affect properties of the hydrogel such as the mechanical strength, water content, and swelling.[43] Swelling ratio is the physical process of a material increasing in volume and mass by absorption of liquid.[44] Swelling ratio of the hydrogel can be modified through the use of: i) hydrophilic functional groups; ii) swelling media; iii) cross-linked bonding strength.[41] When the swollen hydrogel reaches thermodynamic equilibrium with the solvent medium, two swelling properties of the hydrogel can be calculated using equation (1) and equation (2). [44] Equation (1) represents the mass swelling ratio and equation (2) describes the equilibrium water content (EWC). The mass swelling ratio can be calculated by the difference between the swollen mass ($m_s$) and the initial mass ($m_i$) divided by the initial mass ($m_i$).[44] Next, the EWC can be calculated from the difference of the swollen mass ($m_s$) at equilibrium and the dry mass ($m_d$) post lyophilization of the swollen gel then the total is divided by the swollen mass ($m_s$).

$$Mass\ swelling\ ratio = \frac{m_s - m_i}{m_i}\ x100\% \qquad (1)$$

$$EWC = \frac{m_s - m_d}{m_s}\ x\ 100\% \qquad (2)$$

The gel content is defined as the percentage of polymeric material and cross-linker incorporated into the hydrogel during gelation.[60] The theoretical mass ($m_t$) describes the calculated ideal amount of polymer chains incorporated into the gel matrix if the reaction proceeds toward completion.[61] The gel content parameter relates to the mechanical strength of the gel and high gel content corresponds to a higher degree of cross-linking reactions that occurred during gelation.[44]

$$Gel\ content = \frac{m_d}{m_t}\ x\ 100\% \qquad (3)$$

Hydrogels can be characterized by their Young's moduli, a measure of the gel's stiffness. A compression test involves straining a hydrogel at a fixed rate along a single axis.[62] Gels can be mechanically characterized by measuring the relation between the stress and strain curve. When stress is applied, the gel begins to deform in proportion to the increasing stress.[63] When the stress is removed, the gel restores to its original shape due to its elasticity.[63] The values recorded from the stress and strain (equation 4 and equation 5, respectively) of the gel generate a stress-strain curve where the Young's modulus is derived from the slope of the stress-strain curve (**Figure 1.20**).[62] Equation 4 describes the stress applied to an object which is calculated from the compression force applied over the cross-sectional area of the object.[63] Equation 5 denotes the strain on the object which is related to the deformation of an object. This is described as the change in height of the object ($H$) from the initial height ($H_o$). [63]

$$Stress\ (\sigma) = \frac{compression\ force}{cross\text{-}sectional\ area} \quad (4)$$

$$Strain\ (\varepsilon) = \frac{H - H_o}{H_o} \quad (5)$$

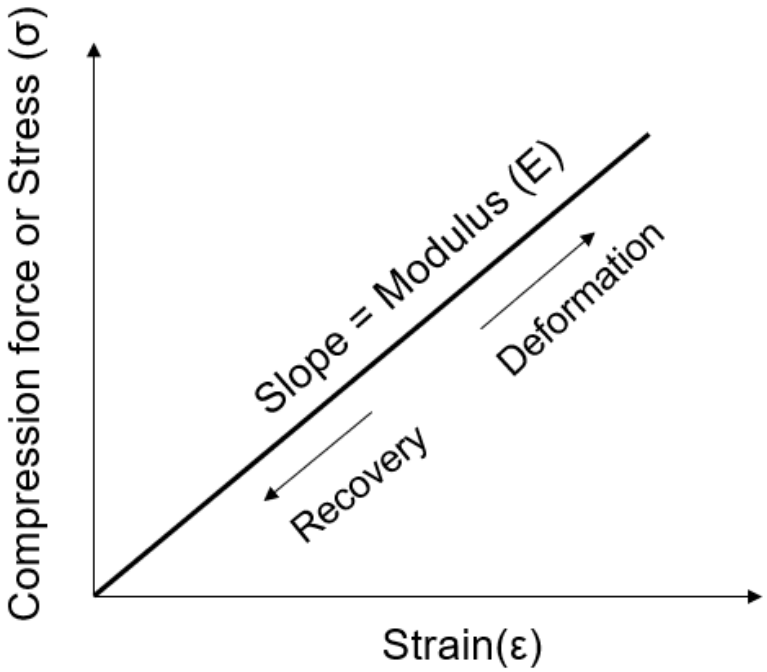


**Figure 1.20**. Stress-strain curve with the slope corresponding to the elastic modulus.[63]

These mechanical properties can be manipulated by modifying the cross-linking density within the gel matrix.[64] However, increasing the cross-linking density typically results in gels with low swelling capacity.[64] Overall, there are several methods that can be used to tune the behaviour of hydrogels through their mechanical and swelling properties.

### 1.4.5 Biomedical applications of stimuli-responsive hydrogels

Hydrogels are well suited for biomedical applications due to their permeability, water content, structure, and viscoelasticity resembling that of natural tissues.[61, 65] Stimuli-responsive hydrogels can undergo structural or mechanical changes in response to environmental stressors (i.e. light, temperature, pH, chemical and biological triggers).[65] Stimuli-responsive polymers have been developed to undergo sol-gel transitions that are affected by factors including temperature, pH, and ionic strength.[61] Stimuli-responsive hydrogels can be tailored to provide various properties such as controllable gelation, degradation, or stiffness change.[65]

Xu and coworkers recently developed a light-sensitive hydrogel that behaved as a liquid bandage adhesive, utilizing photochemically reactive ortho-nitrobenzene species and Schiff-base reactions.[66] These biomaterials adhere to organ or skin tissue and could achieve wound closure. The authors sought to create material that did not utilize toxic initiators or cross-linking agents. Therefore, a naturally occurring polysaccharide – chitosan - was selected, which has been approved by the Food and Drug Administration (FDA) owing to its hemostatic and antibacterial potential.[66] Using carboxymethyl chitosan (CMC) as a backbone to construct the macromolecule, the *o*-nitrobenzyl alcohol (NB) analogue was modified to synthesize NB-CMC. When the NB-CMC is exposed to UV-light, the *o*-nitrobenzene group was transformed into an *o*-nitrosobenzaldehyde that could react with free amino groups on tissue surfaces (**Figure 1.21**). The NB-CMC hydrogel was found to rapidly integrate into tissue and yield strong adhesive properties as a consequence of covalent bonds in the hydrogel-tissue interface.[66]

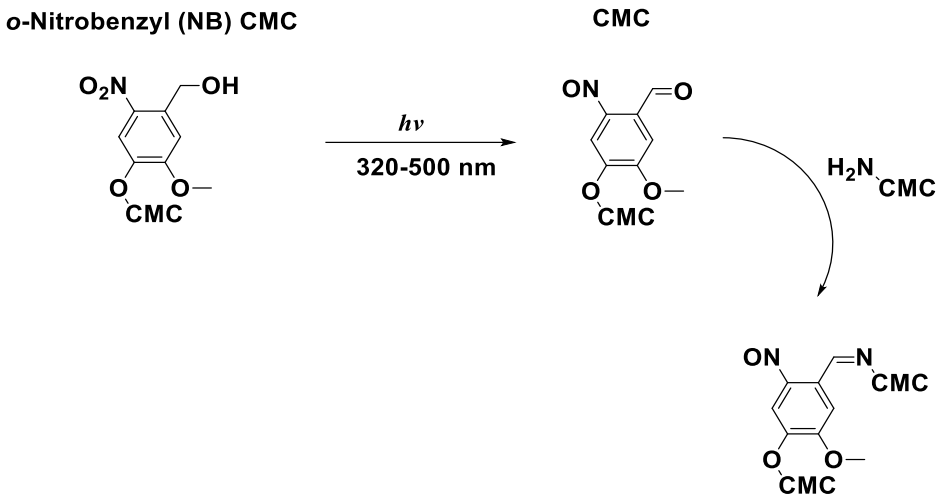


**Figure 1.21.** *o*-Nitrobenzene modified carboxylmethyl chitosan (CMC) irradiated with UV light to form o-Nitrosobenzaldehyde followed by cross-linking of free amino groups on the backbone of CMC reported by Xu and co-workers (2020).[66]

In another example, Yang and co-workers developed a pH-sensitive amphiphilic hydrogel for localized drug delivery.[67] The backbone of the macromolecule consisted of poly(ethylene glycol)-*block*-poly(propylene glycol)-*block*-poly(ethylene glycol) (PEO-PPO-PEO) terminated with benzaldehyde on both ends (**Figure 1.22**).[67] The hydrogel was prepared by an inime forming cross-linking reaction between glycol chitosan and the block copolymer triggered by the increase from a slightly acidic to neutral pH.[67] The gel was then drug loaded with doxorubicin (DOX) and paclitaxel (PTX). The authors found that the drug release could be tuned by adjustment of the pH. It was demonstrated that decreasing the pH from physiological pH to adopt a slightly acidic environment could accelerate dual drug release, making this a viable drug delivery system effective against cancerous tissue.

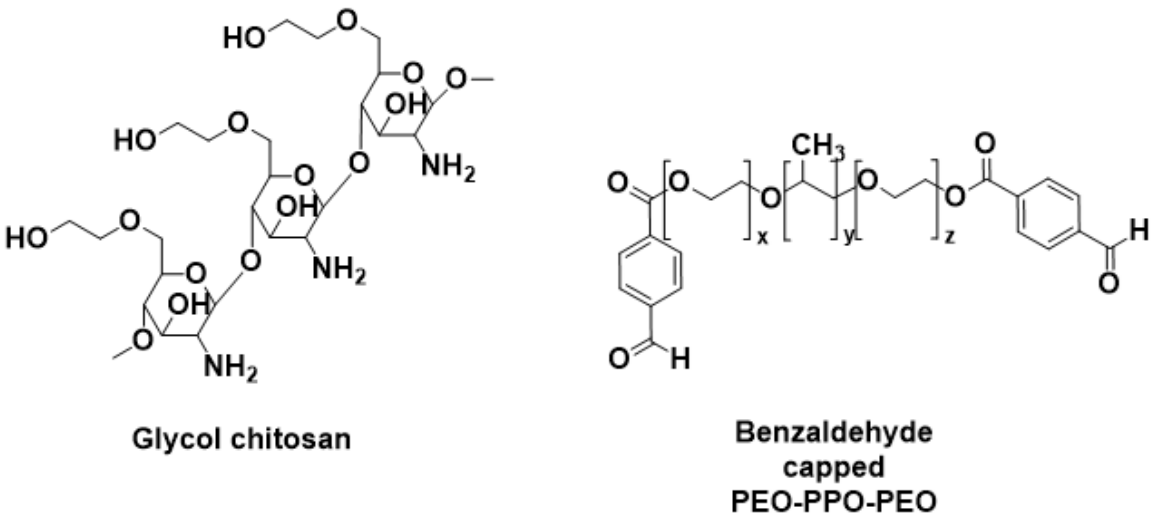


**Figure 1.22.** Preparation of cross-link glycol chitosan and benzaldehyde terminated block co-polymer as report Yang and co-workers (2011).[67]

## 1.5 Thesis objectives

The overall goal of this thesis is to develop new mechanisms to control and trigger the degradation of polyester hydrogels. The initial objective is to synthesize a photo-sensitive OPF derivative by functionalizing the double bonds of the fumarate units with pendent amino groups installed with a photo-cleavable protecting group (**Figure 1.23**). Upon photochemical cleavage of these groups, should be followed by the liberation of the free amine, and consequently undergoes an intramolecular cyclization to cleave the adjacent backbone ester group by the formation of a lactam ring. Degradation of these polymers will be studied by NMR spectroscopy and size exclusion chromatography (SEC). Next, the functionalized OPF will be integrated into a hydrogel network (**Figure 1.24**). The hydrogel will be characterized and its degradation in response to UV light will be examined. This work will demonstrate a proof of concept for the accelerated degradation of OPF-like hydrogels in response to stimuli, that could later be applied to more biologically relevant stimuli such as enzymes.

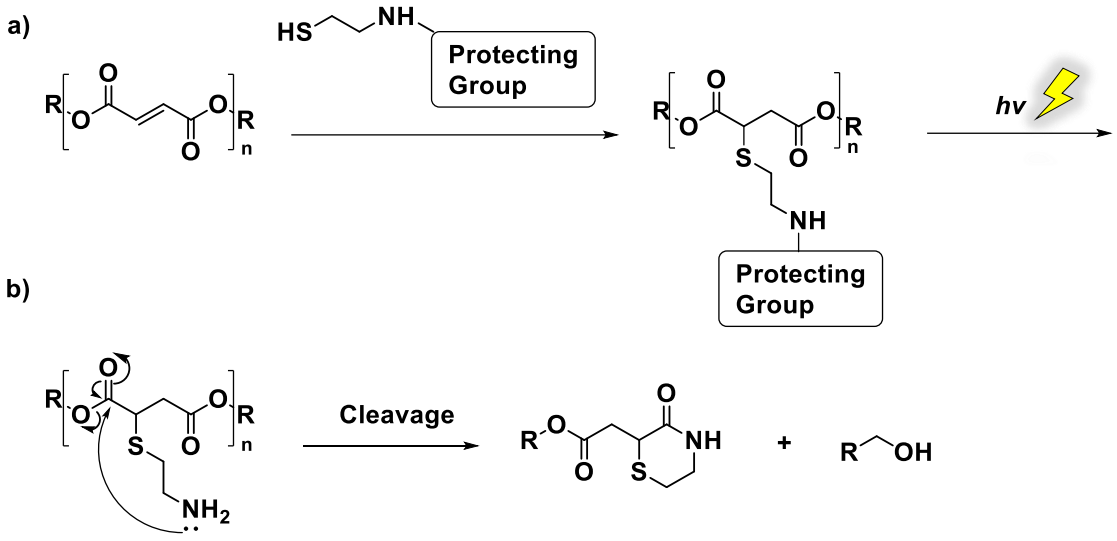


**Figure 1.23.** General schematic of a triggerable pendent functionalized poly(esters). **a)** Functionalization of a poly(ester) with a protected pendent group followed by UV-irradiation. **b)** Poly(ester) with a liberated free amine and undergoes cyclization to generate a lactam ring and an alcohol.

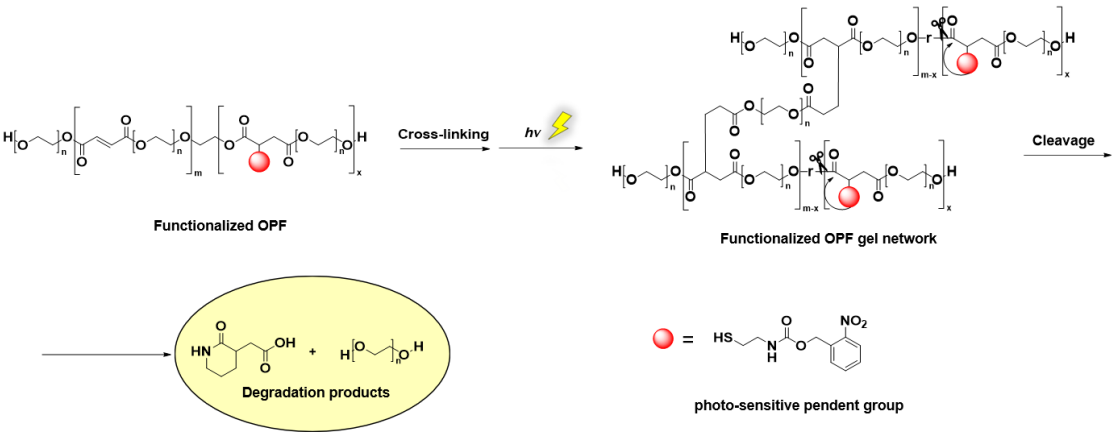


**Figure 1.24.** Schematic illustration of a stimuli responsive OPF hydrogel network.

# Chapter 2

# 2 Oligo [poly (ethylene glycol) fumarate] hydrogels with photo-sensitive pendent groups

## 2.1 Experimental

### 2.1.1 General Experimental Details

***General Materials*.** OPF,[56] 2-(tritylthio)ethanamine (**1**),[68] and 2-nitrobenzyl(4-nitrophenyl)carbonate (**2**),[69] were synthesized as previously reported. Toluene, acetonitrile (MeCN), dichloromethane ($CH_2Cl_2$), and pyridine were purchased from Caledon Laboratory Chemicals (Georgetown, ON, Canada). Hydrochloric acid (HCl), triethylamine ($NEt_3$), poly(ethylene glycol) ($M_n$ = 1500 g/mol) (PEG-1500), trifluoroacetic acid (TFA), trityl chloride, potassium persulfate (KPS), *N*,*N*,*N*',*N*'-tetramethylethylenediamine (TEMED), potassium carbonate, and poly(ethylene glycol) diacrylate (PEG-DA) ($M_n$ = 575 g/mol) were purchased from Sigma Aldrich. Cysteamine hydrochloride was purchased from Fluka Analytical. Fumaryl chloride was purchased from Acros Organics. Sodium hydroxide was purchased from Fisher Scientific. 4-Nitrophenyl chloroformate was purchased from TCI. Hydroquinone was purchased from Anachemia Chemicals Ltd. Diethyl fumarate was purchased from Alfa Aesar. All solvents and reagents were used as received unless otherwise indicated. Toluene was distilled over sodium/benzophenone under a nitrogen atmosphere before use. $NEt_3$ and $CH_2Cl_2$ were distilled over calcium hydride ($CaH_2$) under a nitrogen atmosphere before use.

***General procedures***. NMR spectra was recorded at 25 °C on a Bruker Avance HDIII 400 MHz equipped with a Bruker HX smartprobe, Bruker Neo 600 MHz

equipped with a Bruker HX iprobe, or Varian INOVA 600 MHz spectrometer equipped with a Varian AutoXDB direct-detection NMR probe. The $^{1}H$ NMR and $^{13}C$ NMR chemical shifts (δ) are reported in parts per million (ppm) relative to tetramethylsilane and calibrated against the residual solvent signals of deuterated chloroform ($CHCl_3$, 7.26 ppm) or water (HOD, 4.80 ppm). Coupling constants (J) are expressed in Hertz (Hz). Fourier-transform infrared spectroscopy (FTIR) was performed using a PerkinElmer Spectrum Two FTIR spectrometer with an attenuated total reflectance (ATR) attachment and a single reflection diamond. The size exclusion chromatography (SEC) instrument was equipped with a Viscotek gel permeation chromatography (GPC) Max VE2001 solvent module. Samples were analyzed using the Viscotek VE3580 RI detector operating at 30°C. The separation technique employed two Agilent Polypore (300 x 7.5 mm) columns connected in series and to a Polypore guard column (50 x 7.5 mm). Samples were dissolved in chromatography grade tetrahydrofuran (THF) at approximately 5 mg/mL concentration and filtered through 0.22 µm syringe filters. Samples were injected using a 50 µL loop (56 µL volume). The THF eluent was filtered and eluted at 1 mL/min for a total of 30 minutes. The number average molecular weight ($M_n$), weight average ($M_w$), and polydispersity ($Đ$) were determined relative to PEG standards with molecular weight ranges of 400 – 106,500 g/mol. High-resolution mass spectrometry (HRMS) was conducted on a Synapt high definition mass spectrometer using electrospray (ESI) ionization in either the positive or negative ion mode. Samples were irradiated with either a UV box equipped with a diode array (wavelength: 365-370 nm, intensity: 10 $mW/m^2$) or a mercury lamp with an energy and power density of UVA (12 $mW/cm^2$), UVB (10 $mW/cm^2$), UVC (2.7 $mW/cm^2$), and UVV (9.6 $mW/cm^2$).

## 2.1.2 Synthetic procedures

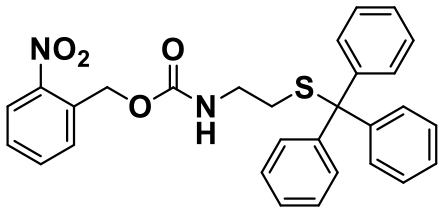

***Synthesis of Compound 3***. Nitrobenzyl(4-nitrophenyl) carbonate (**2**) (4.10 g, 12.8 mmol, 1.0 eq) was dissolved in 150 mL of MeCN and then 2-(tritylthio)ethanamine (**1**) (5.35 g, 16.7 mmol, 1.3 eq) and $NEt_3$ (7.2 mL) were added. The reaction was stirred at room temperature overnight. The reaction was then concentrated under reduced pressure and the products were redissolved in 150 mL of $CH_2Cl_2$. The mixture was transferred to a separatory funnel and the organic layer was washed with 0.5 M $K_2CO_3$ solution (2 x 100 mL). The organic layer was then washed with brine (2 x 50 mL) and the solvent was removed again under reduced pressure to obtain Compound **3** as an off-white solid. The crude product was crystallized from 1:4 ethyl acetate: hexanes and recrystallized then washed with cold diethyl ether to provide 5.33 g of a white solid. Yield = 83%. $^1$H NMR (400 MHz, $CDCl_3$): δ 8.09 (d, *J* = 9.0 Hz, 1H), 7.62-7.55 (m, 2 H), 7.49 – 7.37 (m, 7 H), 7.29 (t, *J* = 7.4 Hz, 6 H), 7.22 (t, *J* = 7.2 Hz, 3 H), 5.48 (s, 2 H), 4.90 (br, 1 H), 3.03 (dt, *J* = 6.3 Hz, 2 H), 2.44 (t, 6.3 Hz, 2 H). $^{13}$C NMR (101 MHz, $CDCl_3$): δ 144.6, 133.7, 129.5, 128.7, 128.5, 128.0, 126.8, 124.9, 124.9, 77.0, 63.2, 39.8, 32.2. FT-IR: 3059 $cm^{-1}$, 1695 $cm^{-1}$, 1575 $cm^{-1}$, 1520 $cm^{-1}$. MS positive ion mode (m/z): calc'd for $C_{29}H_{26}N_2NaO_4S$: 521.1511; found 521.1505 [$M+Na^+$]

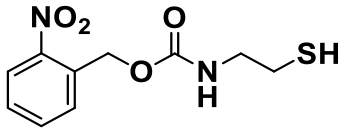

***Synthesis of Compound 4***. Compound **3** (5.32 g, 10.7 mmol, 1.0 eq) was dissolved in 20 mL of anhydrous $CH_2Cl_2$. Triethylsilane (8.52 mL, 53.4 mmol, 5.0 eq) was added to the solution followed by the addition of TFA (4.08 mL, 53.4 mmol, 5.0 eq). The reaction was stirred at room temperature under argon gas for 2 hours

while monitoring by thin layer chromatography for completion. The TFA and $CH_2Cl_2$ were removed in vacuo and the crude mixture was purified by silica column chromatography (1:4 ethyl acetate:hexanes) to obtain 2.02 g of Compound **4** as an off-white solid. Yield = 74%. $^1$H NMR (400 MHz, $CDCl_3$): δ 8.09 (d, *J* = 8.3 Hz, 1H), 7.67 – 7.58 (m, 2H), 7.48 (t, *J* = 7.6 Hz, 1H), 5.52 (s, 2H), 5.27 (br, 1H), 3.40 (dt *J* = 6.3 Hz, 2H), 2.69 (dt, *J* = 6.4 Hz, 2H), 1.38 (t, *J* = 8.5 Hz, 1). $^{13}$C NMR (101 MHz, $CDCl_3$): δ 155.8, 147.6, 133.8, 133.1, 128.7, 125.1, 63.5, 44.1, 25.0. FT-IR: 2933 $cm^{-1}$, 1691 $cm^{-1}$, 1575 $cm^{-1}$, 1515 $cm^{-1}$. MS positive ion mode (m/z): calc'd for $C_{10}H_{12}N_2NaO_4S$: 279.0415; found 279.0410 [$M+Na^+$]

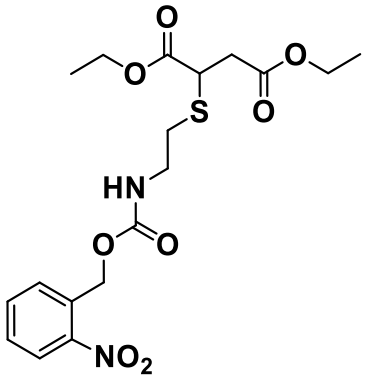


***Synthesis of Compound 5.*** Compound **4** (0.33 g, 1.3 mmol, 1.1 eq) and diethyl fumarate (0.20 g, 1.2 mmol, 1.0 eq) were dissolved in 10 mL of MeCN. To this mixture, triethylamine (0.36 mL, 2.32 mmol, 2.0 eq) was added and the reaction was stirred overnight at 23 °C. The mixture was concentrated under reduced pressure to obtain a crude yellow oil. The crude material was purified by silica chromatography (1:4 ethyl acetate:hexanes) to obtain 0.47 g of Compound 5 as a yellow oil. Yield = 96%. $^1$H NMR (400 MHz, $CDCl_3$): δ 8.09 (d, J = 9.1 Hz, 1H), 7.66 – 7.59 (m, 4H), 7.46 (t, J = 7.5 Hz, 2H), 5.51 (s, 2H), 5.29 (br, 1 H), 4.21-4.14 (m, 8H), 3.69 – 3.65 (m, 1H), 3.47 (q, J = 6.2 Hz, 4H), 2.99 – 2.76 (m, 3H), 2.68 (dd, J = 17.1, 6.8 Hz) 1.29 – 1.23 (m, 6H). $^{13}$C NMR: (101 MHz, $CDCl_3$): δ 171.6, 170.6, 155.7, 133.7, 133.2, 128.5, 124.9, 77.3, 63.3, 61.6, 61.1, 41.2, 40.0, 36.3, 32.1, 14.11. FT-IR: 2982 $cm^{-1}$, 1722 $cm^{-1}$, 1578 $cm^{-1}$, 1520 $cm^{-1}$. MS positive ion mode (m/z): calc'd for $C_{18}H_{24}N_2NaO_8S$: 451.1151; found 451.1170 [$M+Na^+$]

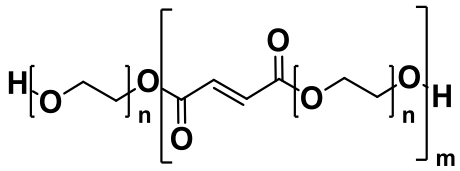

***Synthesis of OPF.*** PEG-1500 was dried through azeotropic distillation using dry toluene and a Dean Stark apparatus under inert atmosphere (adapted from the Lucas and coworkers).[57] Fumaryl chloride was purified by distillation under argon gas at 170 °C, stored under argon gas and placed in the freezer until use. The PEG-1500 (20 g) was dissolved in 130 mL anhydrous $CH_2Cl_2$ with stirring and purged under argon gas. Both distilled fumaryl chloride (1.3 mL, 12 mmol, 0.9 eq) and anhydrous $NEt_3$ (3.4 mL, 24 mmol, 2 eq) were dissolved in 12 mL of anhydrous $CH_2Cl_2$ and slowly added to the reaction using an addition funnel over 2 hours at 0 °C. After complete addition of the fumaryl chloride and $NEt_3$, the reaction was stirred for 30 min at 0 °C then left to stir at 23 °C for 24 h. About 1% (w/w) of hydroquinone inhibitor (0.2 g) was then added to the mixture and the solvent was removed by rotary evaporation to obtain a brown crude product. The product was redissolved in 280 mL of ethyl acetate by heating at 40 °C for 30 mins with high stirring. The salts were removed from the warm suspension by vacuum filtration and then the filtrate was cooled to 0 °C for 2 h to precipitate the product. The precipitate was collected by vacuum filtration and then the dissolution and precipitation process was repeated. Finally, the precipitate was stirred in 1.0 L of diethyl ether, filtered, washed with diethyl ether (3 x 100 mL) and dried to give 10.8 g of OPF as a white solid. The polymer was stored under argon in the freezer until further use. Yield = 54%. $^{1}$H NMR (CDCl3, 400 MHz): δ 6.9 (s, 1.34 H), 4.36-4.34 (m, 3 H) 3.82-3.45 (m, 136 H). $^{13}$C NMR (101 MHz, $CDCl_3$): δ 164.6, 133.4, 70.3, 68.7, 64.2. FT-IR: 2883 $cm^{-1}$, 1722 $cm^{-1}$, 1101 $cm^{-1}$. $M_n$ = 5949 g/mol, $Đ$ =2.20.

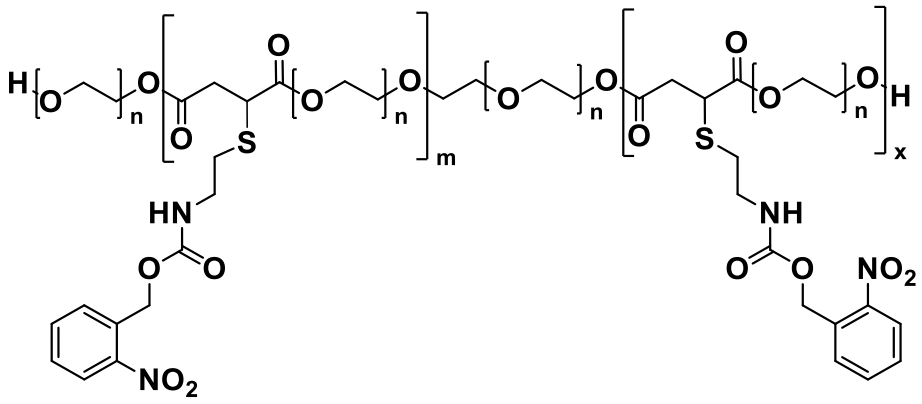

***Post-polymerization functionalization of OPF*** **(synthesis of *OPF-NB-100*).** **OPF** (400 mg, 0.253 mmol of alkene, 1.0 eq) was dissolved in 5 mL of MeCN. Compound **4** (194 mg, 0.758 mmol, 3.0 eq) was subsequently added to the reaction mixture followed by the addition of triethylamine (0.26 mL, 53 mmol, 10 eq). The reaction was stirred at room temperature overnight. The solvent was removed *in vacuo* resulting in a brown solid. 100 mL of diethyl ether was added to the crude mixture and the resulting suspension was stirred for 15 mins. The precipitate was collected by vacuum filtration and washed with diethyl ether (3 x 30 mL) and dried to yield 200 mg of the product. The purified product was stored under argon and in the freezer. Yield = 50 %. $^{1}$H NMR (400 MHz, $CDCl_3$) δ 8.06 (d, *J* = 8.2 Hz, 1H), 7.66-7.59 (m, 2H), 7.46 (t, *J* = 7.1 Hz, 1H), 5.89 (s, 1H), 5.50 (s, 2H), 4.41-4.18 (m, 4H), 3.81-3.40 (m, 136H), 3.02 -2.67 (m, 4H). $^{13}$C NMR: δ 171.8, 170.7, 155.9, 133.8, 128.9, 128.6, 125.0, 72.7, 70.6, 68.9, 64.3, 63.3, 61.8, 41.1, 40.2, 36.2, 32.2. FT-IR: 3411 $cm^{-1}$, 2884 $cm^{-1}$, 1960 $cm^{-1}$, 1729 $cm^{-1}$. $M_n$ = 6164 g/mol, $Đ$ = 1.95.

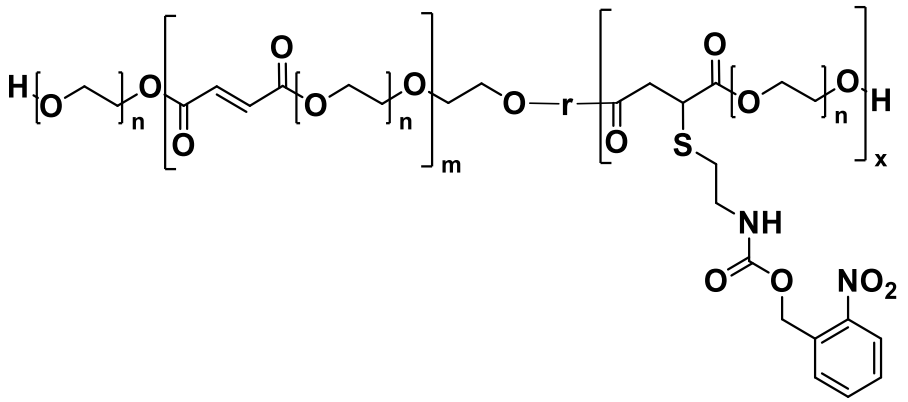

***Synthesis of OPF-NB-50.*** This polymer was synthesized by the same procedure used for the synthesis of OPF-NB-100 except that 19.62 mg (0.077 mmol of alkene, 1.0 eq) of compound **4** was used to provide 280 mg of product. Yield = 93%. $^{1}$H NMR (400 MHz, $CDCl_3$): δ 8.07 (d, *J* = 8.1 Hz, 0.24 H), 7.68 – 7.54 (m, 0.54 H), 7.46 (t, *J* = 7.9 Hz, 0.28 H), 6.88 (s, 0.76 H), 5.88 (s, 0.28 H), 5.50 (s, 0.67 H), 4.43 – 4.28 (m, 2.48 H), 4.24 - 4.18 (m, 1.39 H), 3.89 – 3.35 (m, 136H), 3.07 – 2.63 (m, 4H). $^{13}$C NMR: δ 164.62, 133.45, 128.61, 124.73, 72.40, 70.35, 68.68, 68.62, 64.24, 61.49, 39.90, 31.94, 1.68. $M_n$ = 5945 g/mol, ***Đ*** **=**1.74. FT-IR: 3440. cm $^{1}$, 2883. cm$^{-1}$, 1949.15 cm$^{-1}$ ,1525 cm$^{-1}$., 1465 cm$^{-1}$. $M_n$ = 6088 g/mol g/mol, ***Đ*** = 2.31.

## 2.1.3 Degradation studies

***Degradation of model compound studied by $^{1}$H NMR spectroscopy.***10 mg of the model compound was dissolved in a deuterated phosphate buffer (pH 7.4, 0.1M): deuterated MeCN (3:5) solution and a $^{1}$H NMR spectrum was obtained. The sample was irradiated with diode array for 30 mins and the peak at ~5.37 ppm was monitored by $^{1}$H NMR spectroscopy to ensure a complete cleavage of the photogroup. In parallel, a control sample was prepared but was not irradiated. Both the irradiated and non-irradiated samples were incubated at 37 °C for 9 days and $^{1}$H NMR spectra were obtained periodically.

***Analysis of polymer degradation by $^{1}$H NMR spectroscopy.*** 20 mg samples of each of OPF, OPF-NB-50, and OPF-NB-100 were dissolved in 0.8 mL of

phosphate buffered $D_2O$ (pH = 7.4, 0.1 M). For samples with remaining fumarate alkenes, 1% (w/w) of the inhibitor of hydroquinone was added to prevent any cross-linking (i.e. OPF and OPF-NB-50). Each sample was irradiated with a diode array for 30 mins, while control samples was incubated in a 37 °C oven without UV irradiation. The samples were then incubated at 37 °C for 7 days in the dark and $^1H$ NMR spectra were obtained at various time intervals.

***Analysis of polymer degradation by SEC.*** 40 mg samples of each of OPF, OPF-NB-50, and OPF-NB-100 were dissolved in 0.8 mL of 0.1 M phosphate buffer (pH = 7.4). For samples with remaining fumarate alkenes, 1% (w/w) of the inhibitor of hydroquinone was added to prevent any cross-linking (i.e., OPF and OPF-NB-50). Each sample was irradiated with a diode array for 30 mins, while control samples were prepared in the absence of UV irradiation. The samples were then incubated at 37 °C for 7 days and 100 µL aliquots were removed at various time points, lyophilized to remove the water, redissolved in THF, filtered, and analyzed by SEC.

## 2.1.4 Hydrogel studies

***Preparation of hydrogels (*OPF *I* *OPF-NB-50).*** Hydrogels were formulated with compositions of 30% (w/w) polymer. A 4:1 mass ratio of OPF or OPF-NB-50 (200 mg) and PEG-DA (44.64 µL) was dissolved in 290 µL of distilled water. TEMED (8.75 µL) was added to the mixture and the solution was stirred for 1 min. Subsequently, 0.2 M KPS (290 µL) in distilled water was added to the mixture. The resulting solution was stirred for approximately 10 seconds in an ice bath and then the contents of the mixture were transferred into a 1 mL syringe. The final concentrations of the KPS and TEMED were 0.1 M. The sample was incubated at 37 °C overnight.

***Determination of the gel content, equilibrium water content, and mass swelling ratio.*** Gel content and the equilibrium water content measurements were performed in triplicate. The initial mass ($m_i$) of the hydrogel after preparation was recorded and the theoretical mass ($m_t$) of the polymer involved in the cross-linking

was calculated as $m_i$ x 0.3 based on the 30% (w/w) in the formulation. The gel was then swelled in PBS buffer solution for 24 h and the swollen mass ($m_s$) was recorded. The gels were then immersed in distilled water for at least 24 h to remove salts and non-cross-linked materials. Finally, the swollen gel was frozen with liquid nitrogen and lyophilized to obtain a dried gel mass ($m_d$). The gel content, EWC, and mass swelling ratio were calculated using the equations (1-3).

$$Gel\ content = \frac{m_d}{m_t}\ x\ 100\% \quad (1)$$

$$EWC = \frac{m_s - m_d}{m_s}\ x\ 100\% \quad (2)$$

$$Mass\ swelling\ ratio = \frac{m_s - m_i}{m_i}\ x100\% \quad (3)$$

***Measurement of the compression moduli****.* Gels prepared from OPF and OPF-NB-50 were prepared in 1 mL syringes. Cylindrical gels were prepared with diameter x height dimensions of ~6 mm x 5 mm and equilibrated in PBS overnight (n = 3). Unconfined compression tests were conducted using a UniVert system (Cellscale, Waterloo, ON, Canada) equipped with a 10 N or 0.5 N load cell in a 37 °C PBS bath, OPF and OPF-NB-50 gels were tested using 10 N and 0.5 N load cell, respectively. To provide a complete contact between the gel and plates an initial compressive contact of 0.01 N was applied and compressed to 20% strain at a rate of 0.5% $s^{-1}$. Measurements were taken before and after UV irradiation for a total of 10 days. Gels (n = 3) were irradiated for 8 hours of UV irradiation followed by 16-hour incubations at 37 °C each day. Non-irradiated gels (n = 3) were incubated for 8 hours on the first day and followed by subsequent 24-hour incubation periods at 37 °C. Irradiated and non-irradiated gels were measured at the $5^{th}$ and $10^{th}$ day. Nominal stress was calculated by dividing the applied force by the cross-sectional area of the gels. The compression moduli were calculated from the slope of the linear region of the stress-strain curve between 5% and 15% strain.

***Hydrogel degradation analysis by $^{1}$H NMR spectroscopy*.** Dried gels (15 mg) of OPF-NB-50 and OPF-NB-100 were separately immersed in 800 µL of deuterated PBS and 1 µL of MeCN was added an internal standard. The immersed gels were irradiated with a mercury lamp for 8 h each day over 9 days and incubated overnight at 37 °C. A parallel set of samples were prepared in similar fashion without the irradiation of UV light. Gel degradation was monitored by $^{1}$H NMR spectroscopy.

# Chapter 3

# 3 Results and discussion

## 3.1 Synthesis of a photo-labile model compound

A model compound was synthesized to demonstrate that the predicted cyclization reaction could occur upon photochemical unmasking of a pendent amino group. 2-(Tritylthio)ethanamine (**1**)[68] and 2-nitrobenzyl(4-nitrophenyl)carbonate (**2**)[69] were combined in the presence of triethylamine in acetonitrile to provide compound **3** (**Scheme 3.1**). Cleavage of the trityl protecting group was conducted using TFA in the presence of triethylsilane in $CH_2Cl_2$ to give compound **4**. Next, **4** was treated with diethyl fumarate in MeCN in the presence of triethylamine to provide the model compound **5**.

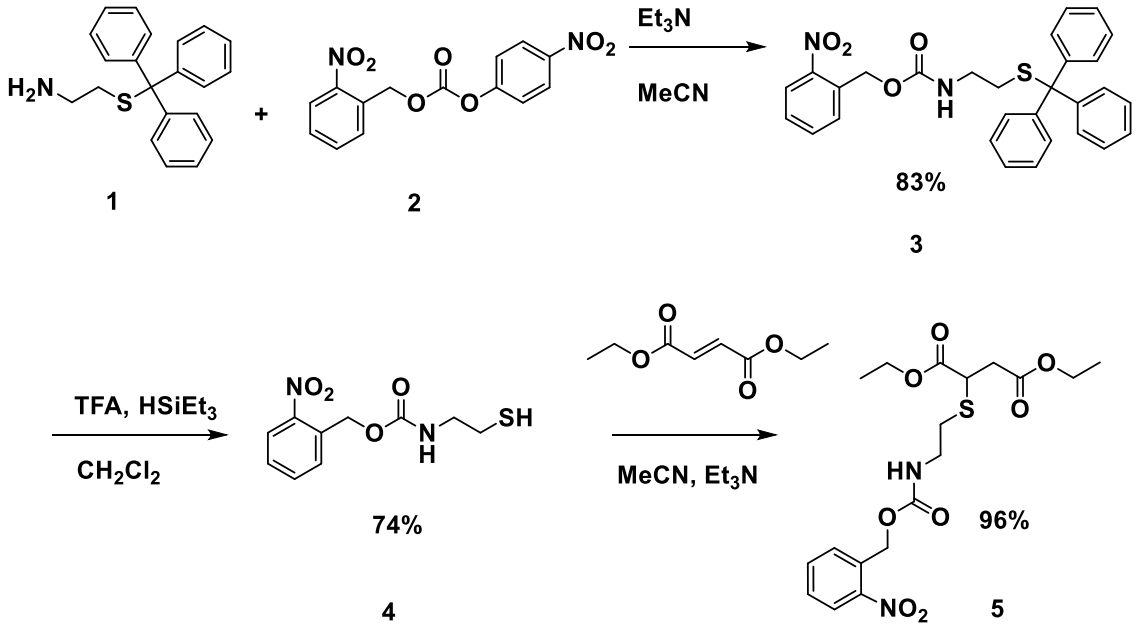


**Scheme 3.1.** Synthetic route towards a photosensitive model compound (**5**).

The new small molecules **3** - **5** were characterized by $^{1}H$ NMR spectroscopy, $^{13}C$ NMR spectroscopy, FT-IR spectroscopy, and electrospray ionization mass spectrometry (ESI-MS). In the $^{1}H$ NMR spectrum of **5**, peaks from 8.1 - 7.5 ppm correspond to the protons on the aromatic ring (**Figure 3.1**). Peaks from 5.52 - 5.46 ppm represent the methylene protons next to the carbamate linkage and the N-H proton. Peaks from 4.2 - 4.1 ppm indicate the methylene protons next to the ester oxygen. The peak at 3.67 ppm corresponds to the methine proton adjacent to the thioether. The peaks between 2.95 ppm to 2.68 ppm are a series of multiplets corresponding to the methylene protons adjacent to the ester and the methylene protons neighbouring the sulfur atom. Finally, the peaks corresponding to the methyl protons are at ~1.3 ppm.

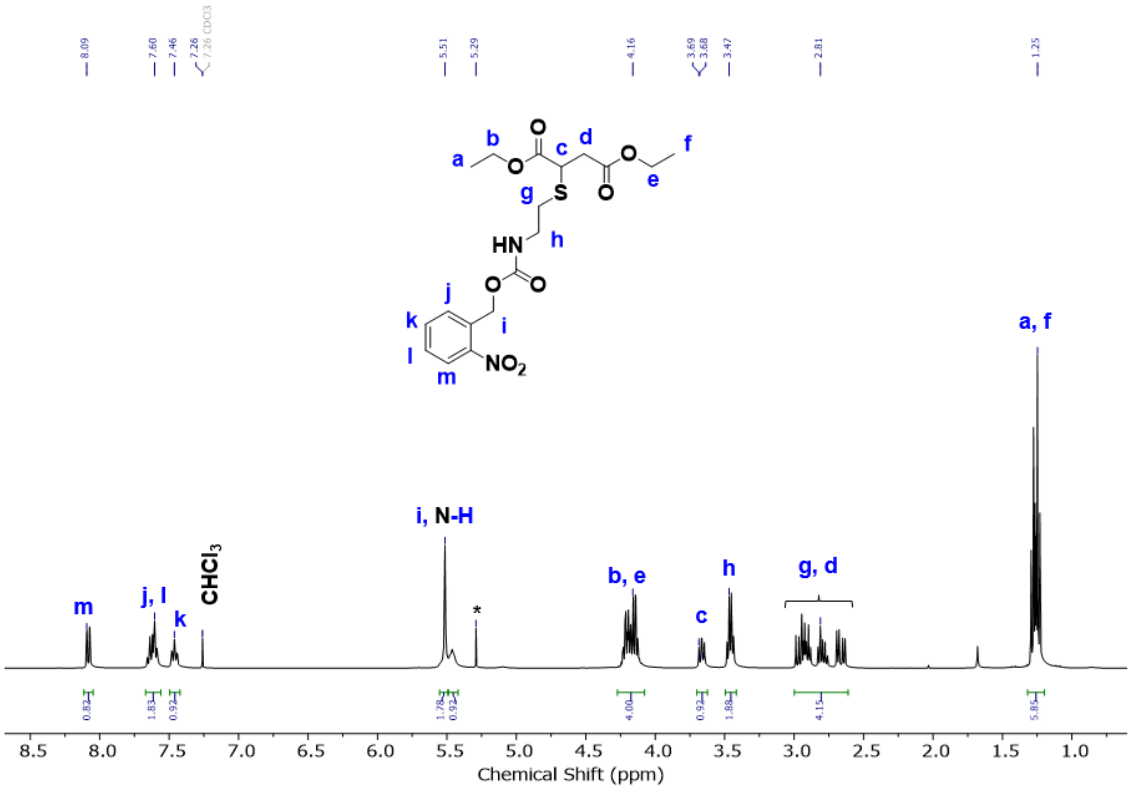


**Figure 3.1.** $^{1}H$ NMR ($CDCl_3$, 400 MHz) spectrum of compound (**5**).

## 3.2 Degradation of the model compound after photochemical cleavage

The cyclization of the model compound after photochemical cleavage of the pendent group was examined. Compound **5** was dissolved in a mixture of 3:5 deteurated phosphate buffer (pH = 7.4, 0.1 M):$CD_3CN$ to ensure a complete dissolution. Two samples were prepared, one sample was irradiated with UV light for 30 min. Another sample was prepared in the absence of UV light and both compounds were incubated at 37 °C and monitored over the course of several days. After 30 min of UV irradiation, the peaks corresponding to the aromatic protons had significantly decreased in intensity (**Figure 3.2**). The peak at ~5.36 ppm corresponding to the benzylic methylene protons of the pendent group had substantially decreased in intensity. The peak at 3.3 ppm corresponding to the methylene group adjacent to the carbamate shifted upfield to ~3.1 ppm. These changes suggest that within the span of 30 min, the *o*-nitrobenzyl group underwent a Norrish II mechanism in response to UV light. This would generate a nucleophilic primary amine to attack the adjacent ester, forming a 6-membered ring. After this initial period, further changes were observed over the next several days. For example, a new quartet appeared at 3.52 ppm corresponding to released ethanol. In addition, the peak at 3.1 ppm corresponding to the methylene group adjacent to the pendent amine gradually disappeared. Furthermore, additional changes occurred in the spectra from 3.2 - 2.6 ppm presumably corresponding to the cyclization reaction. In contrast, when model compound **5** was not irradiated with UV light, no changes in the spectra occurred over 8 days (**Figure 3.3**). These results demonstrate that the observed changes for the irradiated compound could not be attributed to simple ester hydrolysis. While the cyclization was rather slow in this solvent mixture containing >60% acetonitrile, it would be anticipated to be more rapid in a fully aqueous system.[38, 39]

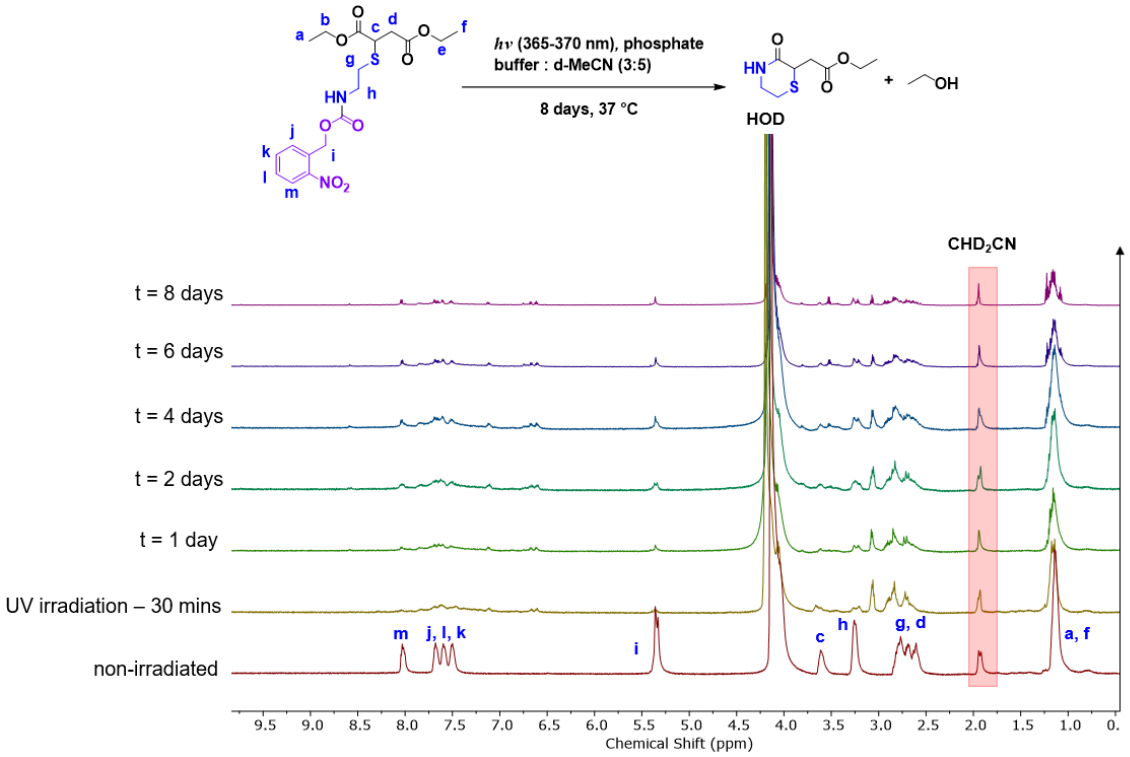


**Figure 3.2.** $^{1}$H NMR spectrum of compound **5** (3:5 deuterated phosphate buffer (pH = 7.4, 0.1 M):$CD_3CN$, 600 MHz) before and after UV irradiation (365–370 nm) and at various time points after incubation at 37 °C. Note that the intensity of the peaks decreases over time, likely due to some precipitation of the cyclized product, as the solution was observed to become turbid.

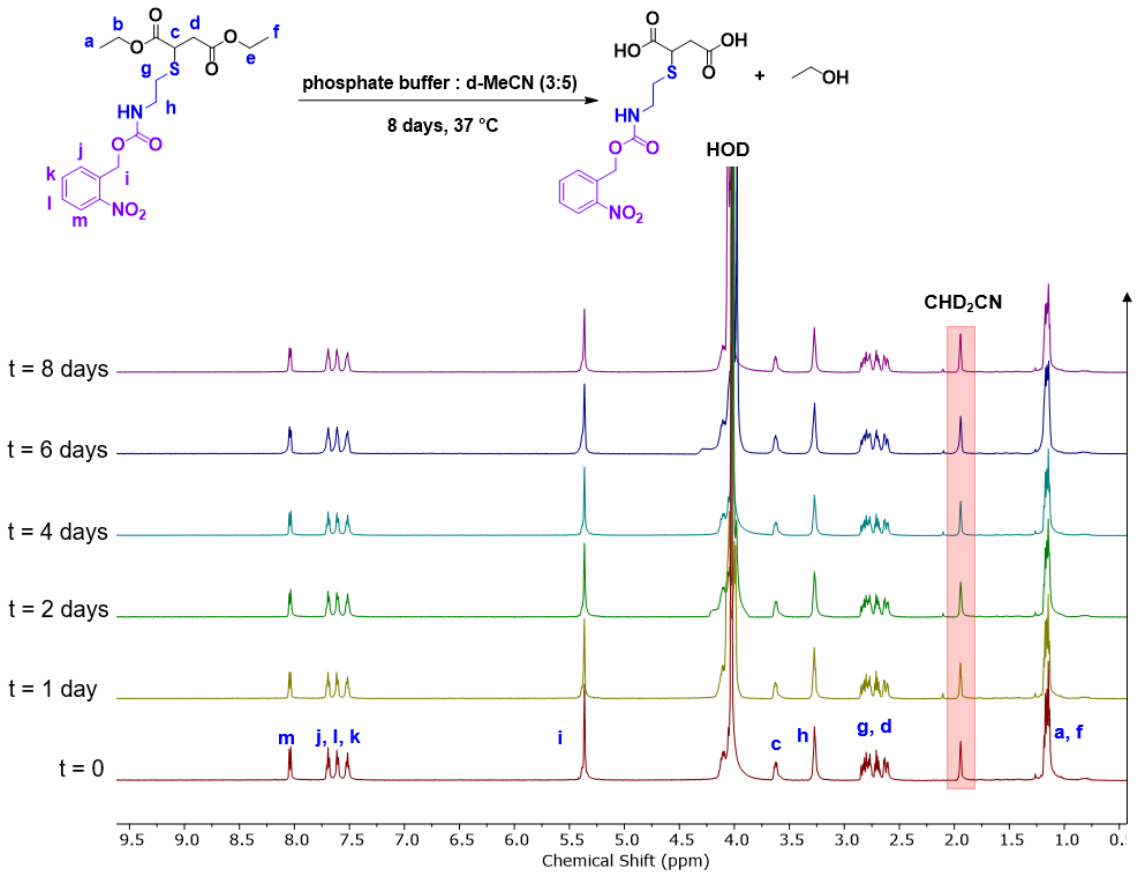


**Figure 3.3.** $^{1}$H NMR spectrum of compound **5** (3:5 deteurated phosphate buffer (pH = 7.4, 0.1 M):$CD_3CN$, 600 MHz) after incubation and at various time points at 37 °C.

## 3.3 Synthesis and functionalization of OPF

OPF was synthesized as previously reported,[56] except that the polymerization was run for 24 h instead of 48 h to minimize the chance of spontaneous cross-linking (**Scheme 3.2**). The polymer had an $M_n$ of 5950 g/mol and $Đ$ of 1.74 based on SEC in THF relative to PEG standards. $^{1}$H NMR spectroscopy in $CDCl_3$ showed an intense peak at 3.64 ppm associated with PEG (**Figure 3.4**). There are also peaks at 4.34 ppm that are due to the methylene protons adjacent to the fumarate unit.

Further downfield, a peak appears at 6.90 ppm that represents the remaining alkene protons of the fumarate.

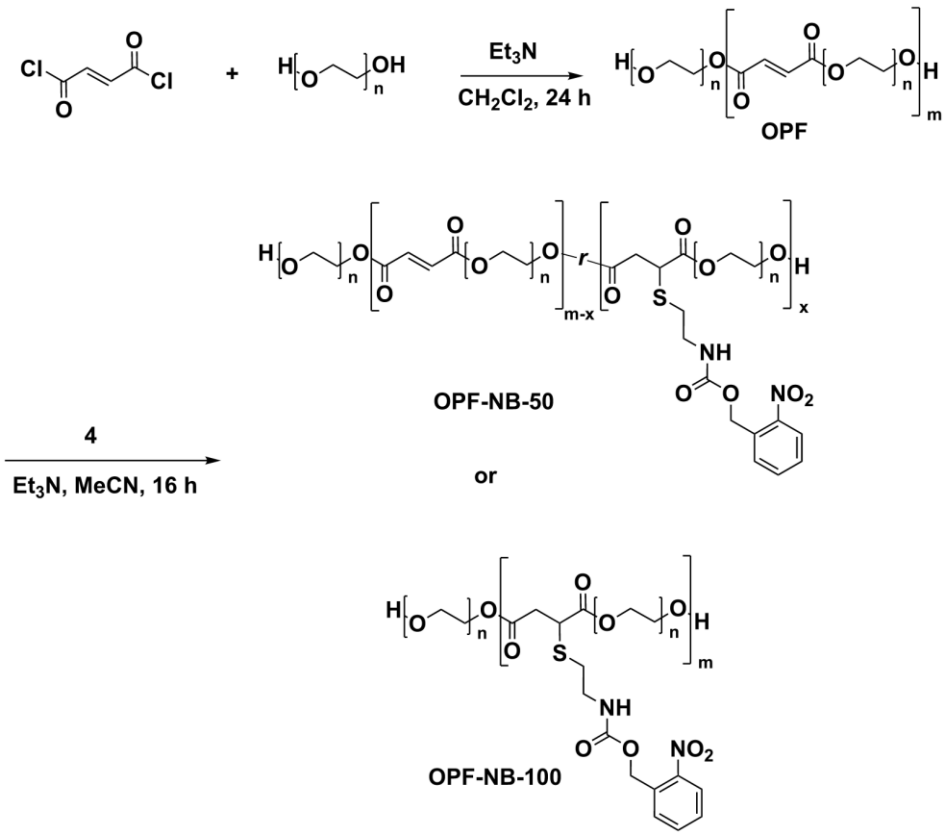


**Scheme 3.2.** Synthesis of OPF and its conversion to OPF-NB-50 or OPF-NB-100.

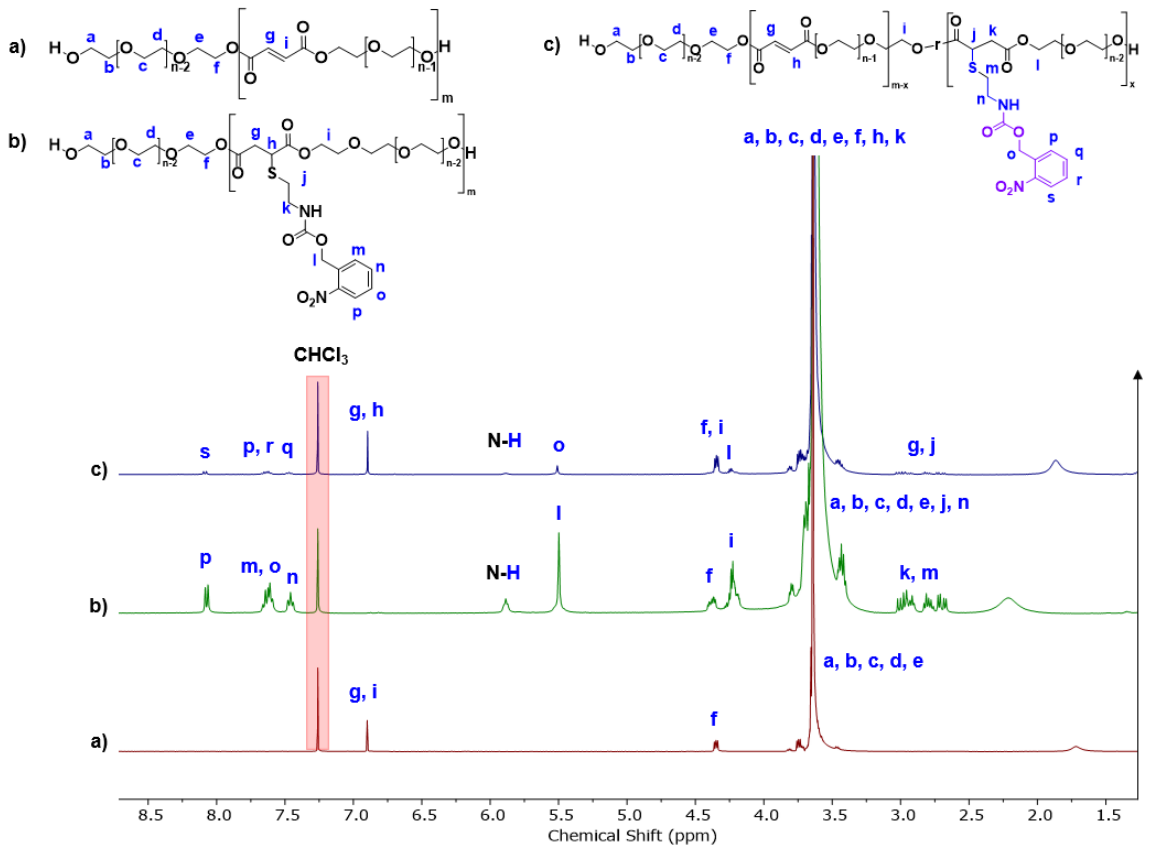


**Figure 3.4.** $^{1}$H NMR spectra ($CDCl_3$, 400 MHz) of **a)** OPF, **b)** OPF-NB-100, and **c)** OPF-NB-50.

To fully functionalize the OPF with the photochemically-responsive pendent group, the OPF was reacted with 3.0 equivalents of thiol **4** in MeCN to provide OPF-NB-100 (**Scheme 3.2**) based on disappearance of the peak corresponding to the alkene in the $^{1}$H NMR spectrum (**Figure A10**). The choice of solvent for the functionalization reaction was important as this would result in significantly differing $M_n$ values for the resulting polymers and varying functionalization kinetics. Polar protic solvents such as methanol resulted in smaller chains likely due to transesterification of the ester bonds. Other protic solvents such as isopropanol and ethanol failed to fully dissolve the polymer. Furthermore, co-solvent mixtures involving the use of THF to aid in the dissolution in ethanol and isoproponal resulted in slow reaction rates and incomplete functionalization.[70] On the other hand, the use of MeCN resulted in complete disappearance of the fumarate alkene

peaks over 16 h, indicating quantitative functionalization **(Figure A13)**. SEC indicated the $M_n$ of the fully functionalized polymer was found to be 6164 g/mol and similar *Đ* to the starting OPF. Next, the random co-polymer OPF-NB-50 was prepared by reaction with 0.5 equivalents of thiol **4** relative to the calculated moles of alkene, resulting in functionalization of ~45% of the alkene bonds based on the reduction in the peak integral corresponding to the alkene (Figure A10). SEC showed that the polymer chains had an Mn value of 5955 g/mol.

## 3.4 Degradation studies of OPF and functionalized OPF

OPF, OPF-NB-50, and OPF-NB-100 were studied to determine how rapidly degradation would occur at 37 °C in phosphate buffer at pH 7.4 in the presence of UV light (**Figure 3.5**) and in the absence of UV light. The inhibitor hydroquinone was added to the solutions of OPF and OPF-NB-50 to avoid undesired crosslinking reactions. For the non-functionalized OPF (**Figure 3.6**), no significant changes were observed when it was irradiated for 30 minutes with UV light. After one day of incubation at 37 °C, the alkene region between 7.0 and 6.5 ppm began to change, with a decrease in the intensity of the initial alkene peak and the emergence of new peaks, which likely correspond to alkenes next adjacent carboxylates, arising from simple hydrolysis of the polymer.

Specifically, two doublets appeared at 6.95 ppm and 6.53 ppm, with a coupling constant of $J$ = 14.9 Hz, consistent with a trans configuration. This desymmetrization of the alkene would arise if one side of the fumarate was hydrolyzed resulting in two different alkene protons to couple to each other. In addition, the peak corresponding to the methylene group of PEG, adjacent to the fumarate, began to decrease and a new peak arose at 4.25 ppm presumably corresponding to the same methylene but with an adjacent fumarate carboxylate. These changes continued over the next several days, with the methylene peak reaching 4.5% of its initial integration after 7 days. The same results were obtained

for OPF that was not treated with UV light but was incubated in the same manner over 7 days (**Figure 3.7**).

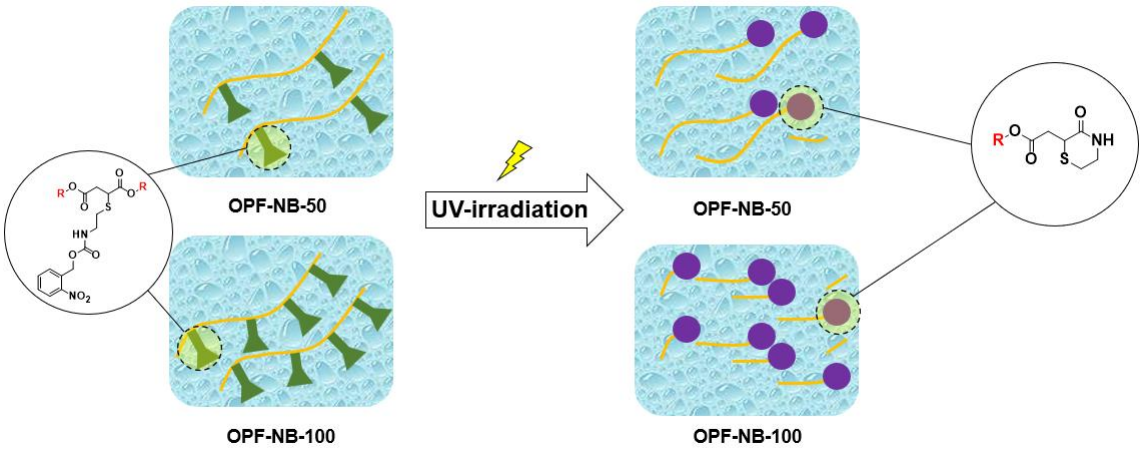


**Figure 3.5.** Schematic depicting the degradation of the functionalized OPF chains containing *o*-nitrobenzyl carbamate-functionalized amines, undergoing cyclization and consequently breaking down the backbone.

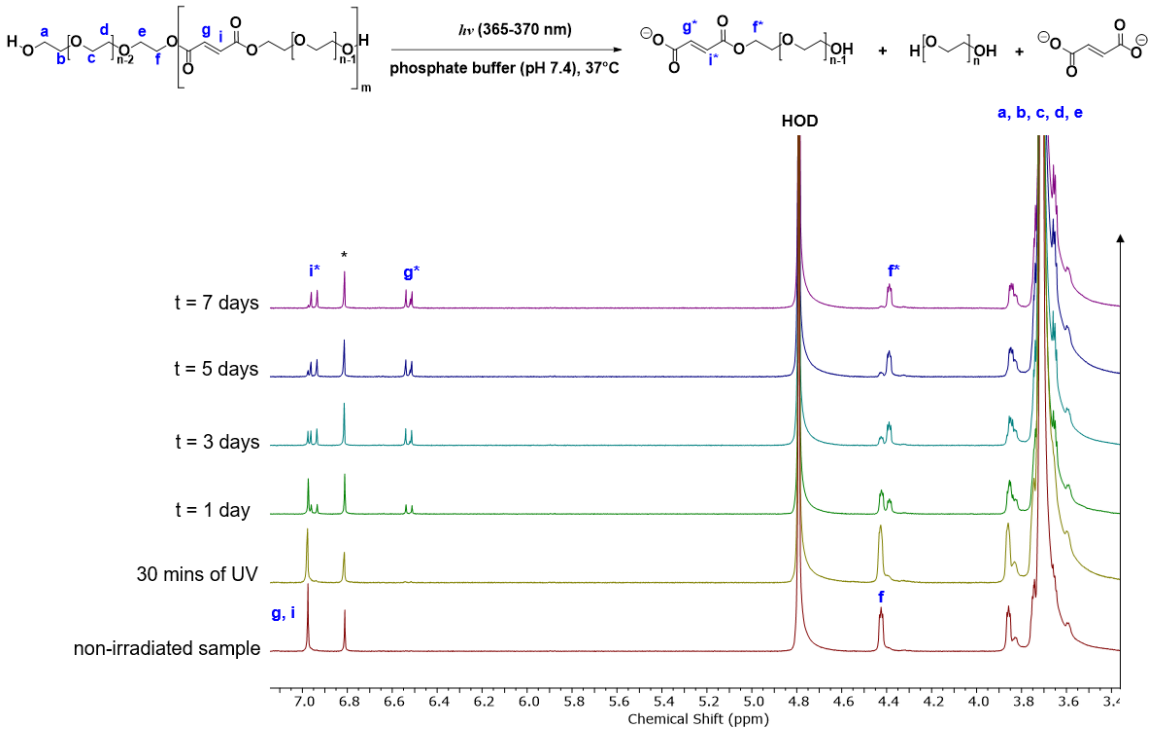


**Figure 3.6.** $^{1}$H NMR spectrum (deuterated phosphate buffer (pH 7.4, 0.1 M)), 600 MHz) of OPF, before and after UV irradiation (365-370 nm) and at various time points after incubation at 37 °C. (* = hydroquinone, t = incubation period at 37 °C).

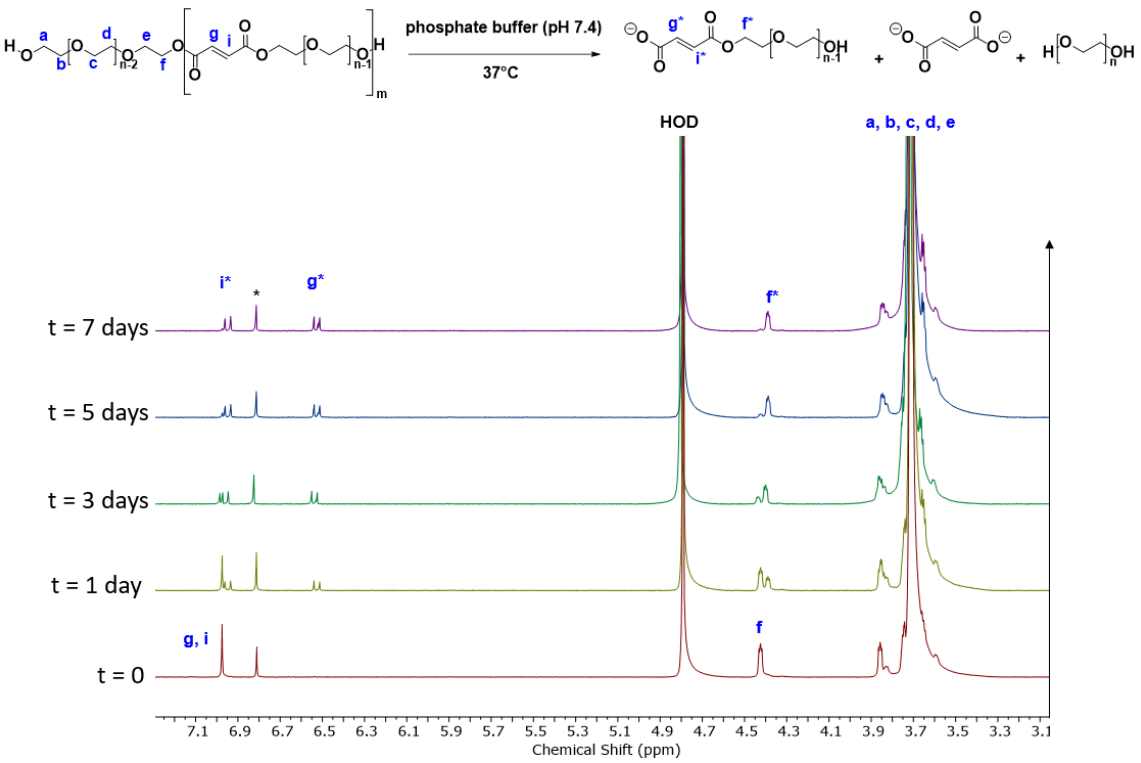


**Figure 3.7.** $^{1}$H NMR spectra (deuterated phosphate buffer (pH 7.4, 0.1 M), 600 MHz) of OPF without UV light irradiation and after incubation. (* = hydroquinone, t = incubation period at 37 °C).

Next, the degradation of OPF-NB-100 was investigated. Peaks from the polymer were relatively broad, due to the functionalized polymer's limited solubility in deuterated phosphate buffer (**Figure 3.8**). However, it was found that after irradiation with UV light for 30 min, peaks corresponding to the *o*-nitrobenzyl carbamate disappeared. Then, over the next several days there was a reduction in the intensity of the peaks from 4.4 – 4.2 ppm corresponding to the methylene groups adjacent to the ester groups, and changes in the region between 3.2 – 2.8 ppm, consistent with cyclization or hydrolysis related to ester cleavage as in the model compound and according to assignments by Lv and co-workers.[71] Unfortunately, the broadness of the relevant peaks and their low intensity made quantification of these changes in the NMR spectra impossible.

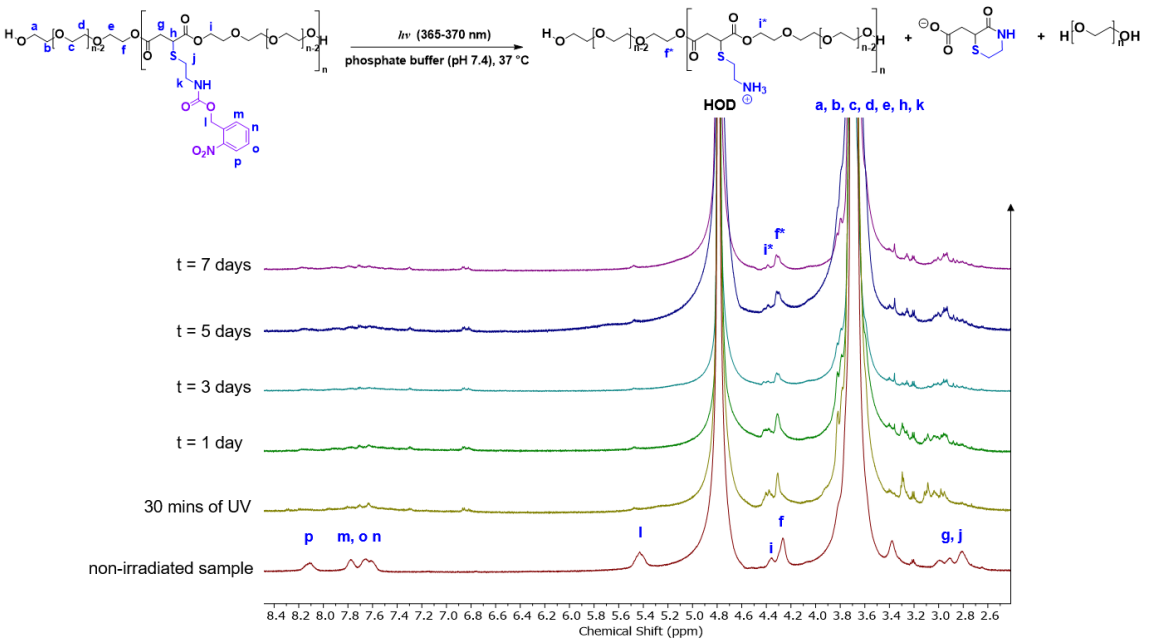


**Figure 3.8.** $^{1}$H NMR spectra of OPF-NB-100 (deuterated phosphate buffer (pH 7.4, 0.1 M), 600 MHz) before and after irradiation with UV light (365-370 nm) followed by incubation at 37 °C at various time points. (t = incubation period).

When OPF-NB-100 was not irradiated with UV light, no significant changes in the $^{1}$H NMR spectra were observed (**Figure 3.9**). These results indicated that the rate of background ester hydrolysis for the functionalized OPF was much slower than that of OPF. The slower ester hydrolysis rate for OPF-NB-100 can likely be attributed to increased hydrophobicity and steric hindrance associated with the esters in this polymer compared with OPF.

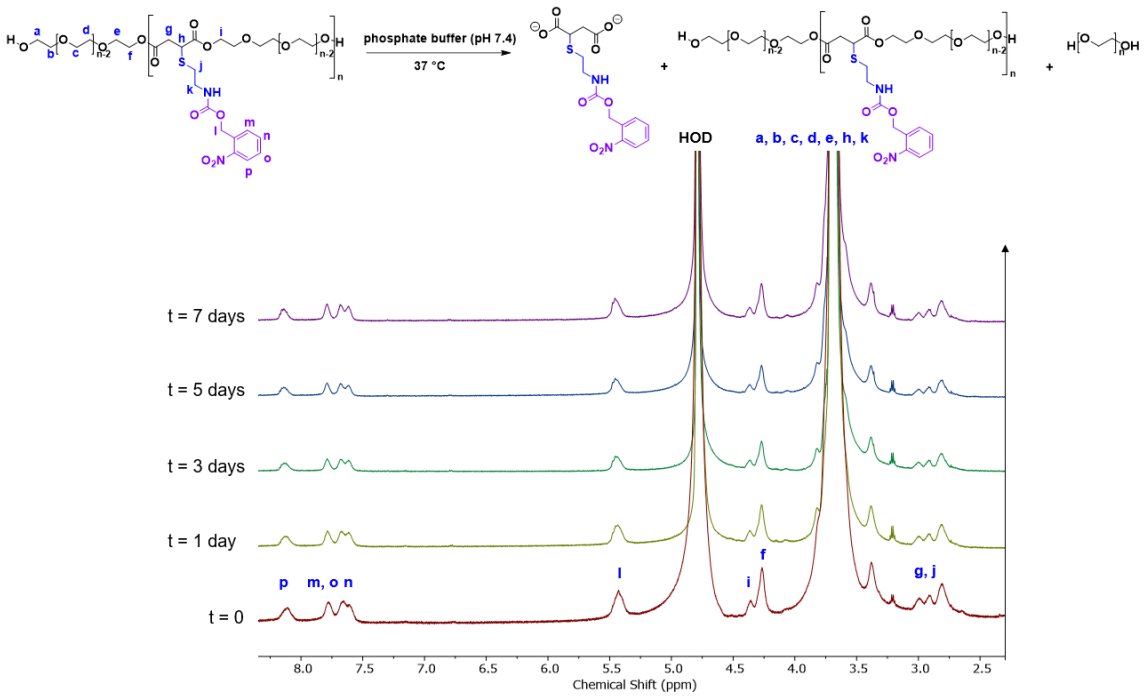


**Figure 3.9.** $^{1}$H NMR spectrum of OPF-NB-100 (deuterated phosphate buffer (pH 7.4, 0.1 M), 600 MHz) after incubation at 37 °C at various time points. (t = incubation period).

**Figure 3.10** shows the degradation of OPF-NB-50 monitored by $^{1}$H NMR spectroscopy. The peaks from 8.2 - 7.6 ppm and the peak at 5.5 ppm correspond to the *o*-nitrobenzyl group. Post UV irradiation, these signals disappeared, indicating complete cleavage of the protecting group, and unmasking of the free amine. After this, the changes were consistent with those observed for OPF and OPF-NB-100. For example, the peaks from 4.4 – 4.2 ppm corresponding to the methylene protons adjacent to the ester groups decreased in intensity. In addition, new alkene peaks emerged corresponding to cleavage of the esters of the remaining fumarate groups. Furthermore, changes in the peaks between 3.3 – 2.7 ppm were observed, consistent with probable cyclization.

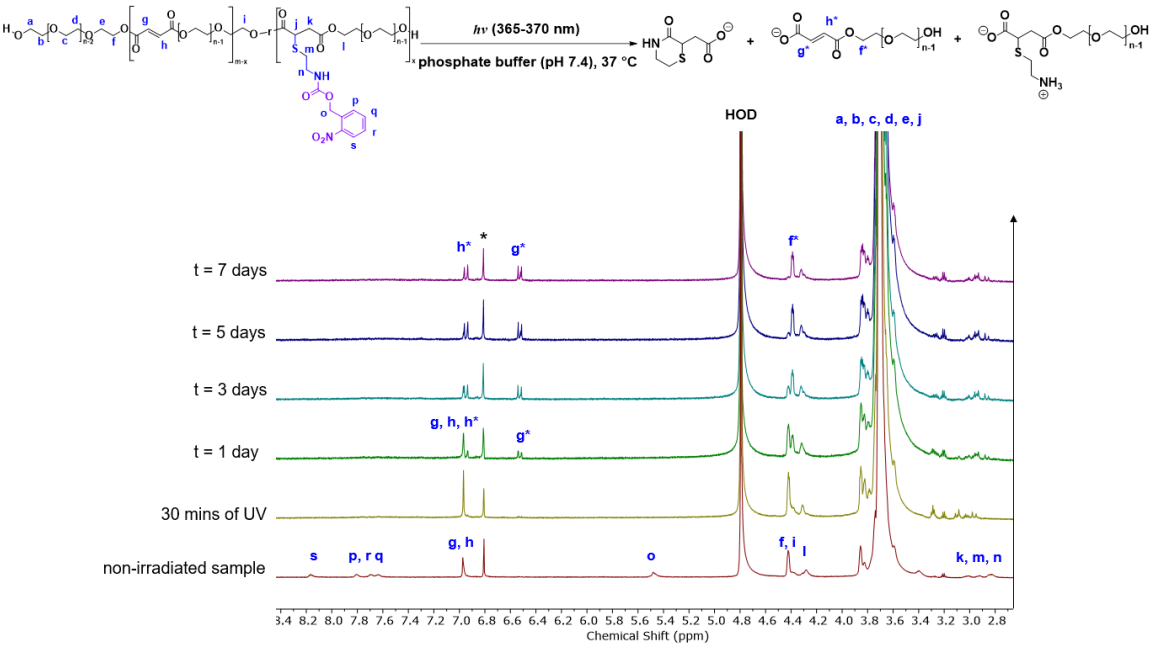


**Figure 3.10.** $^{1}$H NMR spectrum of OPF-NB-50 (deuterated phosphate buffer (pH 7.4, 0.1 M), 600 MHz) before and after UV irradiation (365-370 nm) followed by incubation at 37 °C at various time points. (* = hydroquinone, t = incubation period).

In the control experiment, where OPF-NB-50 was not irradiated with UV light, the peaks corresponding to the *o*-nitrobenzyl group remained intact (**Figure 3.11**) but hydrolytic cleavage adjacent to the fumarate occurred, as evidenced by the intensity of the alkene peak at 6.9 ppm decreasing, and new doublets emerging at 6.9 and 6.5 ppm as for unfunctionalized OPF. In addition, the peak 4.4 ppm corresponding to the methylene protons adjacent to the esters decreased somewhat in intensity. However, there were no significant changes in the spectrum from 3.3 - 2.7 ppm, suggesting that cyclization did not occur.

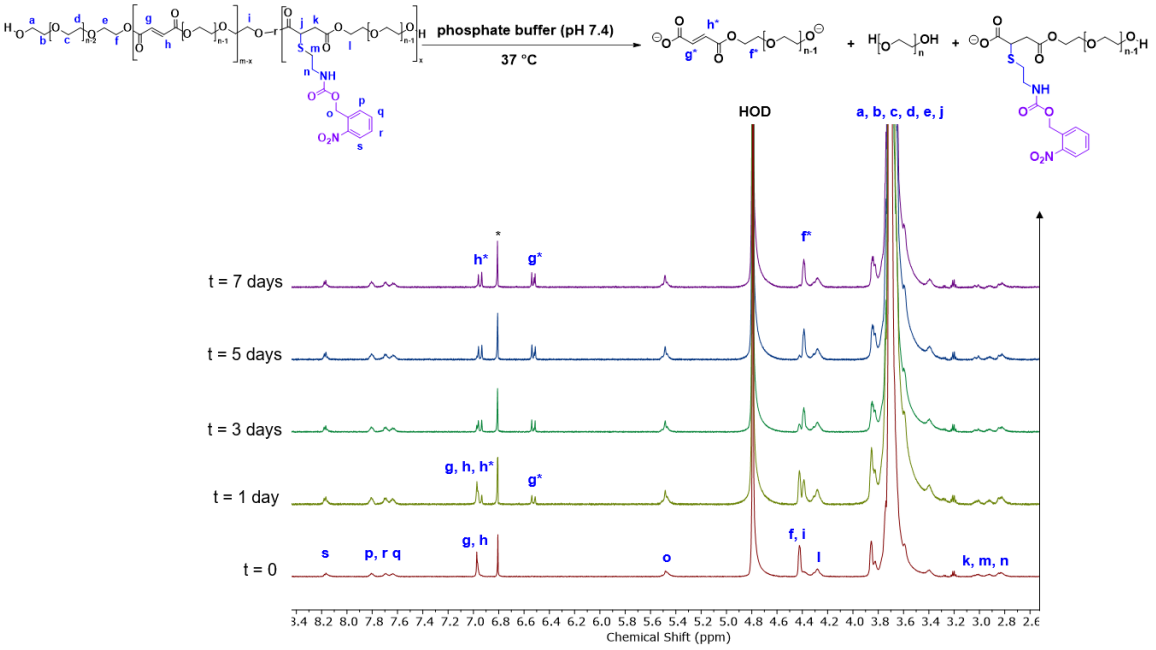


**Figure 3.11.** $^{1}$H NMR spectrum of OPF-NB-50 (deuterated phosphate buffer (pH 7.4, 0.1 M), 600 MHz) in the absence of UV-irradiation and after incubation at 37 °C. (* = hydroquinone, t = incubation period).

As degradation of the polymers was difficult to quantify by $^{1}$H NMR spectroscopy alone, the process was also studied by SEC. The samples were irradiated with UV light for 30 mins in a 50 mg/mL polymer solution. Then, SEC samples were obtained for irradiated and non-irradiated solutions of the polymers in phosphate buffer (pH = 7.4) incubated at 37 °C over 7 days. Quantitation of the SEC traces were integrated from the retention times from 14 mins to 20 mins and plotted as %initial $M_n$ and $M_w$ against time.

**Figure 3.12** shows the degradation of OPF. In the span of 7 days, there was a significant shift in the retention volume to larger volumes, confirming that the OPF underwent ester hydrolysis, as observed in the NMR spectroscopy study. Non-irradiated OPF exhibited the same behaviour (**Figure 3.13**). These results agree with those of the NMR spectroscopic study indicating that UV light did not have a significant effect on the polyester if there were no photo-responsive groups. The $M_n$ of the initial polymer distribution decreased from 100% to 21% of its initial value

after 1 day and down to 16% after 3 days (**Figure 3.14**). Furthermore, a peak emerged at 18.3 min corresponding to the release of PEG-1500. By 7 days, the polymer had almost completely broken down to PEG, with similar corresponding initial $M_n$ of 16%.

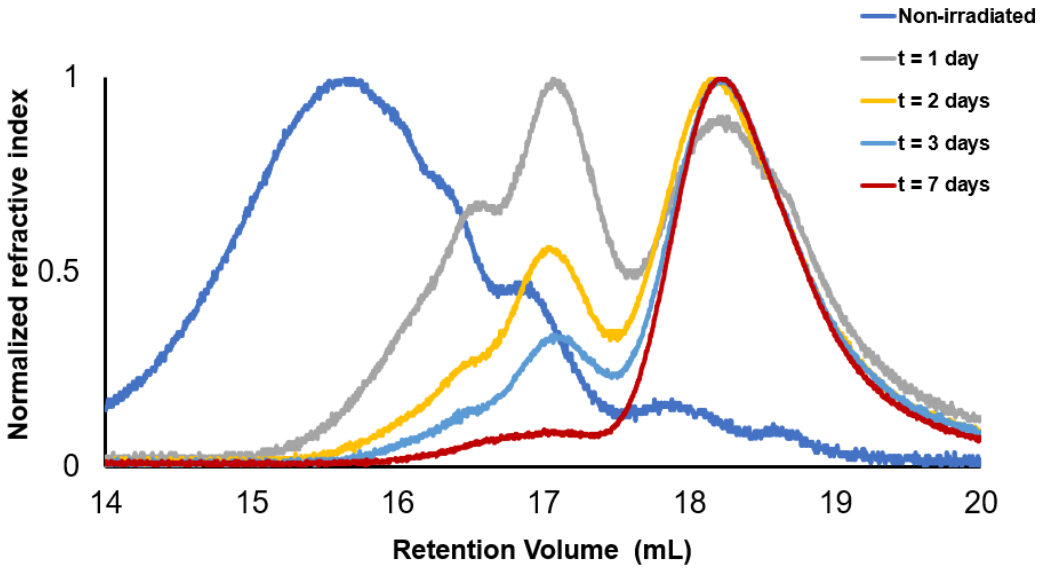


**Figure 3.12.** SEC traces of OPF (THF) before and after UV irradiation (365-370 nm) followed by incubation periods in phosphate buffer (pH = 7.4) at 37 °C at various time points over 7 days.

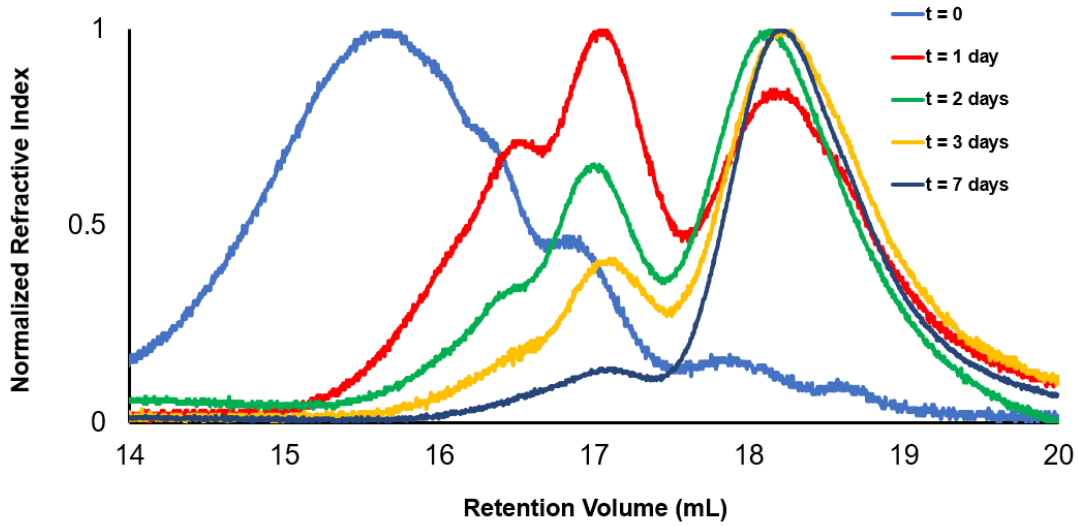


**Figure 3.13.** SEC traces of non-irradiated OPF (THF) after incubation in phosphate buffer (pH = 7.4) at 37 °C at various time points over 7 days.

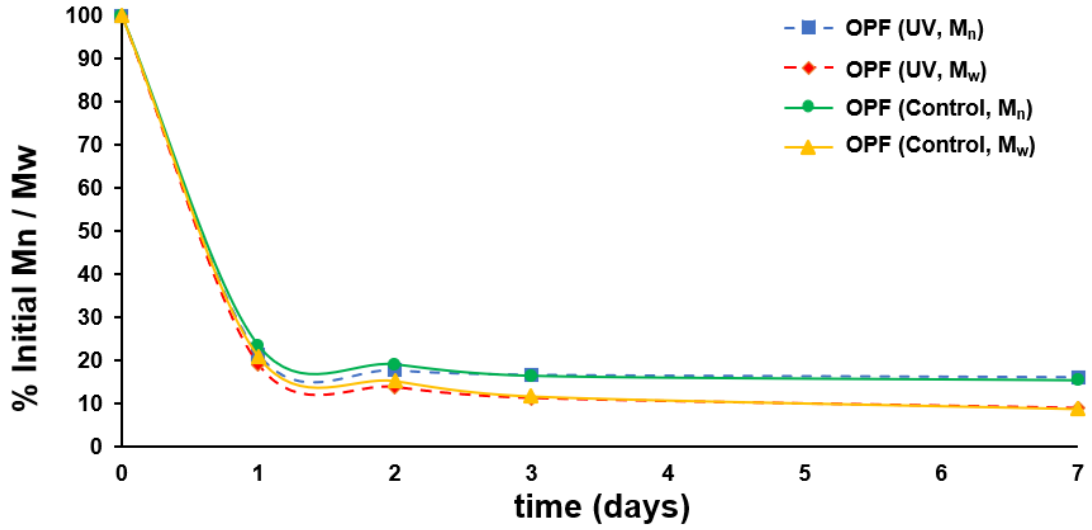


**Figure 3.14.** Molecular weight loss (%) of irradiated and non-irradiated OPF over 7 days of incubation at 37°C in phosphate buffer (pH 7.4).

**Figure 3.15** shows the degradation profile of OPF-NB-100 in phosphate buffer (pH 7.4) incubated at 37 °C over several days after irradiation with UV light. After 1 day of incubation, the retention volume shifted from 15.9 mL to 16.7 – 17.0 mL. This significant shift in retention volume is likely attributed to the liberation of the amine group and resulting cyclization and release of PEG-1500. The degradation continued over 7 days, resulting primarily in the peak due to PEG-1500. **Figure 3.16** depicts the degradation of non-irradiated OPF-NB-100. Minimal shifts in the retention volume were observed over 3 days, after which a small degree of further degradation was observed by 7 days. Whereas irradiated OPF-NB-100 underwent a 70% decrease in the initial Mn% and 65% decrease in the initial Mw% over 1 day, decreases of only about 9% were observed for the non-irradiated control (**Figure 3.17**). Near 7 days, the degradation rates of the irradiated and non-irradiated converged to some extent, as the polymers were converted to free PEG chains.

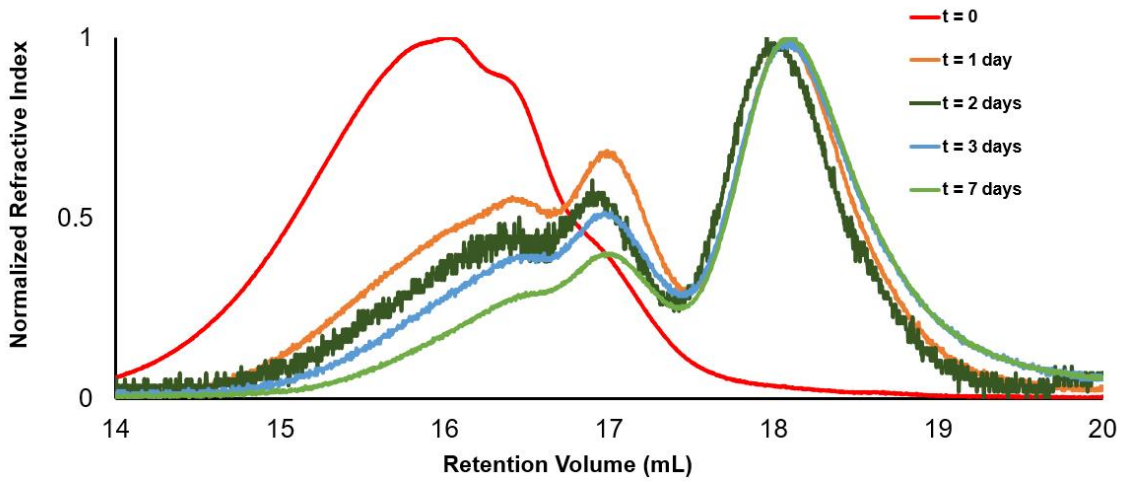


**Figure 3.15.** SEC traces of OPF-NB-100 (THF) before and after UV-irradiation (365-370 nm) followed by incubation periods in phosphate buffer (pH = 7.4) at 37 °C at various time points over 7 days.

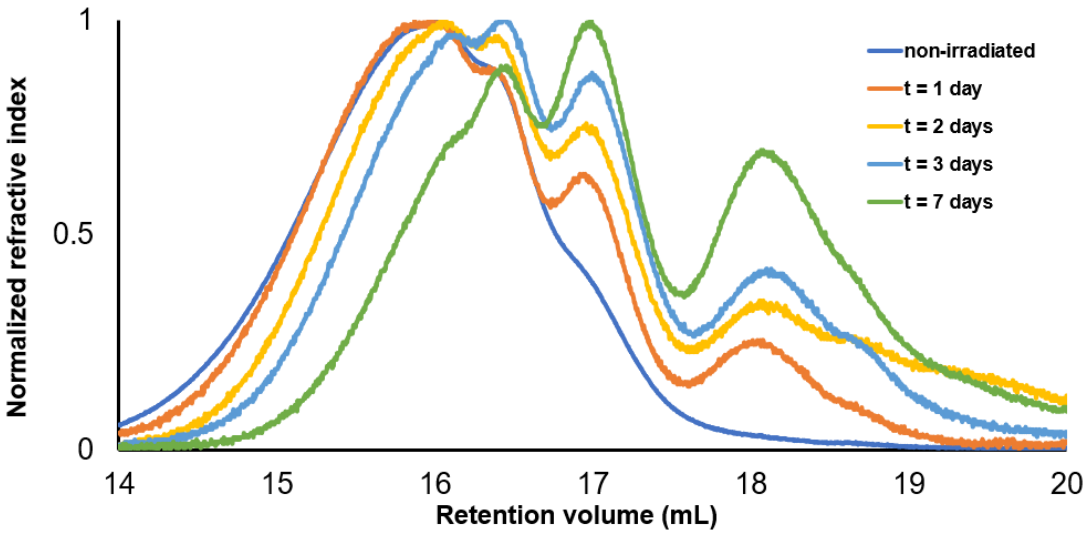


**Figure 3.16.** SEC traces of OPF-NB-100 (THF) after incubation in phosphate buffer (pH = 7.4) at 37 °C at various time points over 7 days.

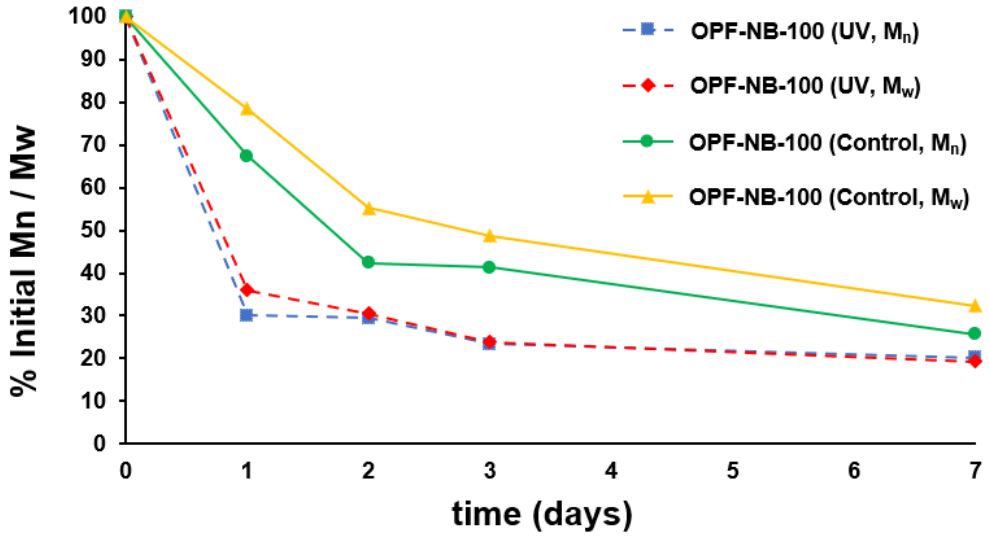


**Figure 3.17.** Molecular weight loss (%) of OPF-NB-100 over 7 days of incubation at 37°C in phosphate buffer (pH 7.4).

Finally, the degradation of OPF-NB-50 was also investigated by SEC. **Figure 3.18** and **Figure 3.19** shows the degradation of OPF-NB-50 after being subjected to 30

min of UV irradiation and in the absence of UV light respectively. The polymer underwent degradation largely to PEG over 7 days, with a decrease in Mn to 23 % of its original molar mass over 1 day and to 18 % after 7 days (**Figure 3.20**). $M_w$ was reduced to 22% of the initial value after 1 day and 12% after 7 days. As only about 50% of the fumarate double bonds were functionalized to enable cyclization, this degradation arose due to simultaneous intramolecular cyclization and hydrolysis of the esters adjacent to the remaining fumarates. For the control, non-irradiated OPF-NB-50, the Mn decreased to 31% of its initial value after 1 day, and 23% of the initial value after 7 days (**Figure 3.19**). $M_w$ was reduced to 33% of the initial value after 1 day and 17% after 7 days. The differences between the irradiated and non-irradiated polymers can be attributed to cyclization-mediated cleavage of the irradiated polymer. However, as both polymers had residual fumarate bonds, some hydrolysis could occur regardless of irradiation.

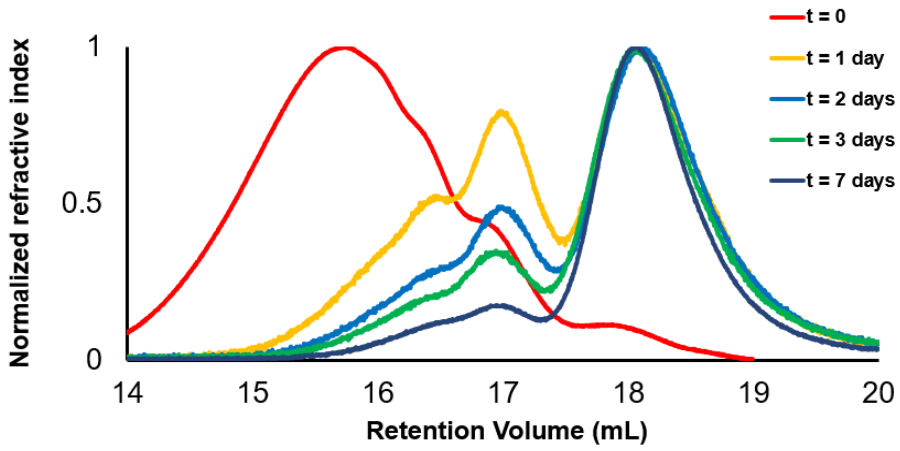


**Figure 3.18.** SEC traces of OPF-NB-50 (THF) before and after UV-irradiation (365-370 nm) followed by incubation periods in phosphate buffer (pH = 7.4) at 37 °C at various time points over 7 days.

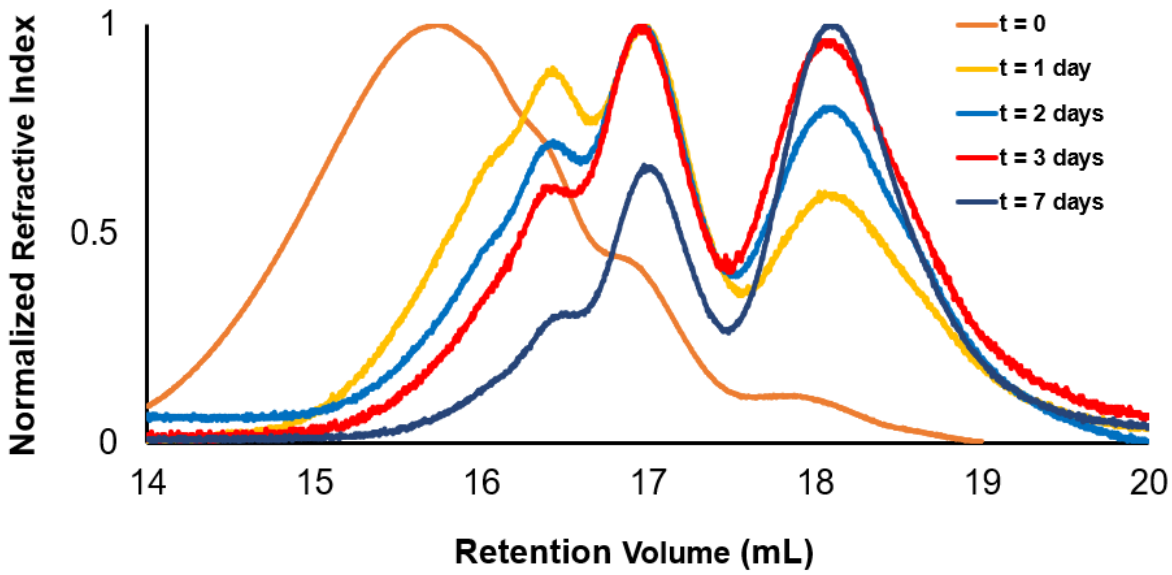


**Figure 3.19.** SEC traces of OPF-NB-50 (THF) after incubation in phosphate buffer (pH = 7.4) at 37 °C at various time points over 7 days.

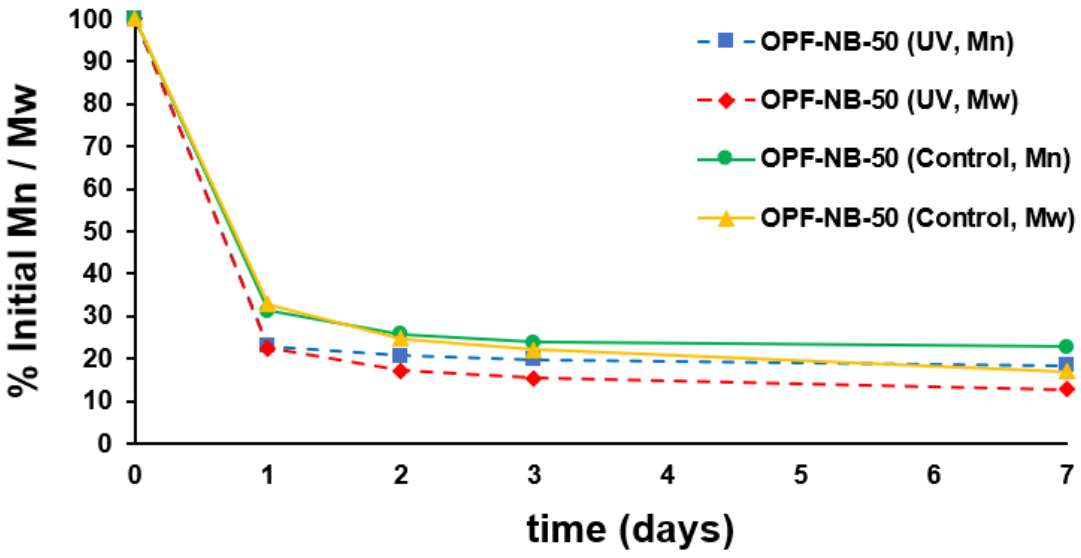


**Figure 3.20.** Molecular weight loss (%) of OPF-NB-50 over 7 days of incubation at 37 °C in phosphate buffer (pH 7.4)

# 3.5 Synthesis, characterization, and degradation of hydrogels

Hydrogels were prepared by using a 4:1 weight ratio of (OPF/OPF-NB-50) to PEG-DA followed by the addition of water-soluble radical initiator with final concentrations of 0.1 M KPS in the presence of 0.1 M TEMED catalyst (**Scheme 3.3** and **Scheme 3.4**). This procedure was adapted from the Mikos group, while reducing the amount of cross-linker content from 2:1 OPF:PEG-DA due to the reduced content double bonds in OPF-NB-50.[72] Furthermore, the cross-linker content was decreased to reduce the number of cross-linking reactions between PEG-DA and itself, which would lead to non-stimuli-responsive components in the network. 30% (w/w) polymer was used in the formulation because formulations of OPF-NB-50 at lower polymer content such as 15% or 25% w/w resulted in viscous liquids or very fragile gels respectively.

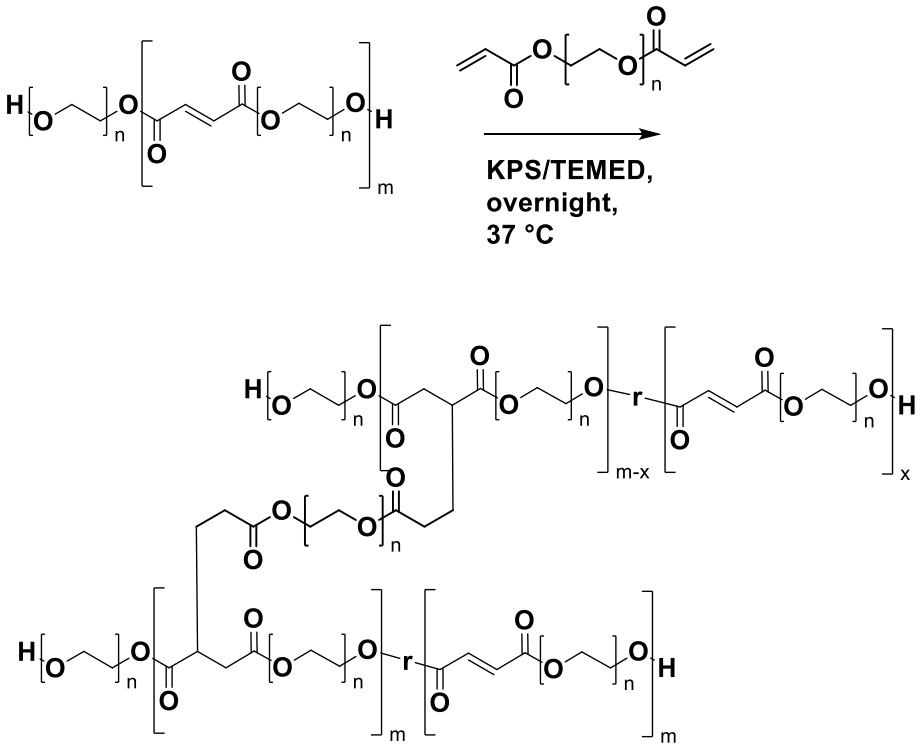


**Scheme 3.3.** Radically initiated cross-linking of OPF.

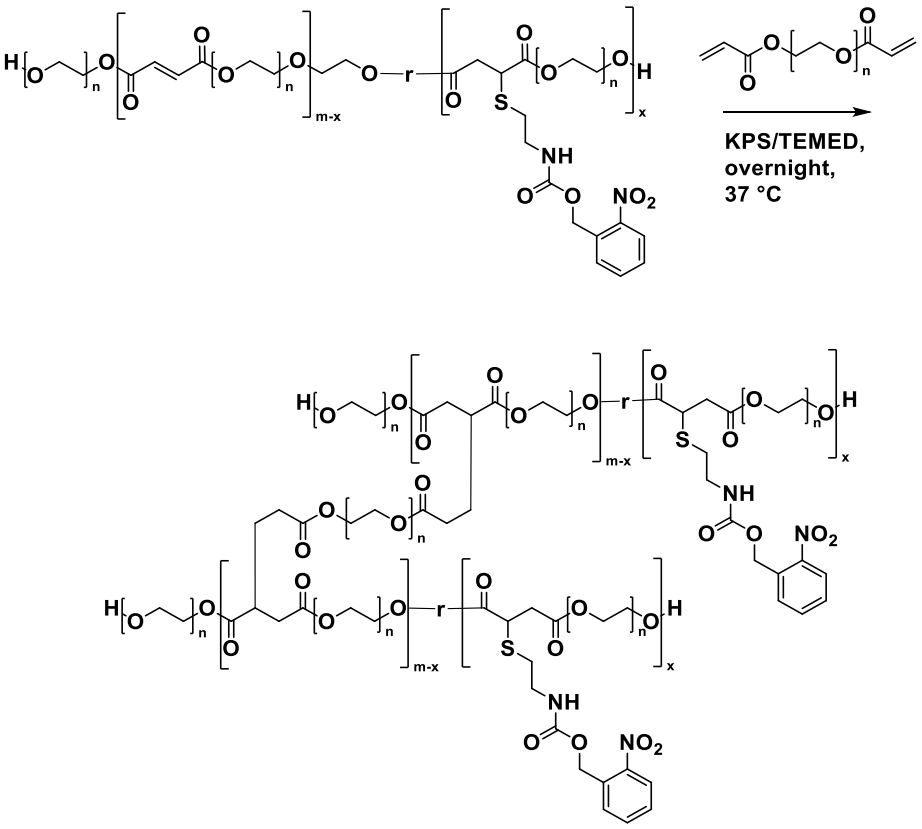


**Scheme 3.4.** Radically initiated cross-linking of OPF-NB-50.

The gel content, equilibrium water content, and mass swelling ratios of the OPF and OPF-NB-50 hydrogels were measured (**Table 3.1**). The mass swelling ratio after equilibrating both gels of OPF and OPF-NB-50 in PBS showed similar results, despite it being anticipated that the OPF-NB-50 gel would have a larger mass swelling ratio due to the lower degree of cross-linking density within the polymer and consequently larger pores. However, the gel content of the OPF-NB-50 network was lower, at 47% compared to 77% for the OPF hydrogel. Both gels were equilibrated in distilled water to measure the equilibrium water content (EWC). The OPF-NB-50 gel contained ~96% water, whereas OPF gel contained 93% water. The EWC for the OPF-NB-50 would be higher because the gel content is lower than OPF.

Scanning electron microscopy (SEM) images taken at a 20 μm scale revealed that the surface of the OPF-NB-50 gels contained a porous structure (**Figure A19**). In contrast, SEM imaging of the 30 wt% OPF at a 20 μm scale did not show any visible pores on the surface of the gel which suggest higher cross-linking density.

**Table 3.1. Gel characterization of OPF and OPF-NB-50 gels**

| 30 wt% | Gel content | Mass swelling ratios | EWC |
|---|---|---|---|
| **OPF** | **77 ± 1** | **64 ± 1** | **93.0 ± 0.4** |
| **OPF-NB-50** | **47 ± 1** | **63 ± 1** | **95.7 ± 0.2** |

The degradation of the OPF and OPF-NB-50 hydrogels were then studied by $^{1}$H NMR spectroscopy after immersing the hydrogels in pH 7.4 deuterated PBS. OPF and OPF-NB-50 hydrogels were irradiated with a diode array for periods of 8 h each day and subsequently incubated at 37 °C overnight. This process was repeated for 8 days. It should be noted that longer irradiation times were used for these hydrogels compared to the polymer solutions as it was more difficult for the UV light to penetrate the gels. Control hydrogels were not irradiated but were incubated at 37 °C and 1 μL of acetonitrile was used as a reference peak.

Before UV irradiation, no peaks were observed for OPF-NB-50, as the polymer motion was constrained in the network (**Figure 3.21**). When OPF-NB-50 hydrogel was irradiated with UV light, a sharp peak at 3.7 ppm emerged over several days. This peak is likely associated with the release of free PEG molecules into solution.

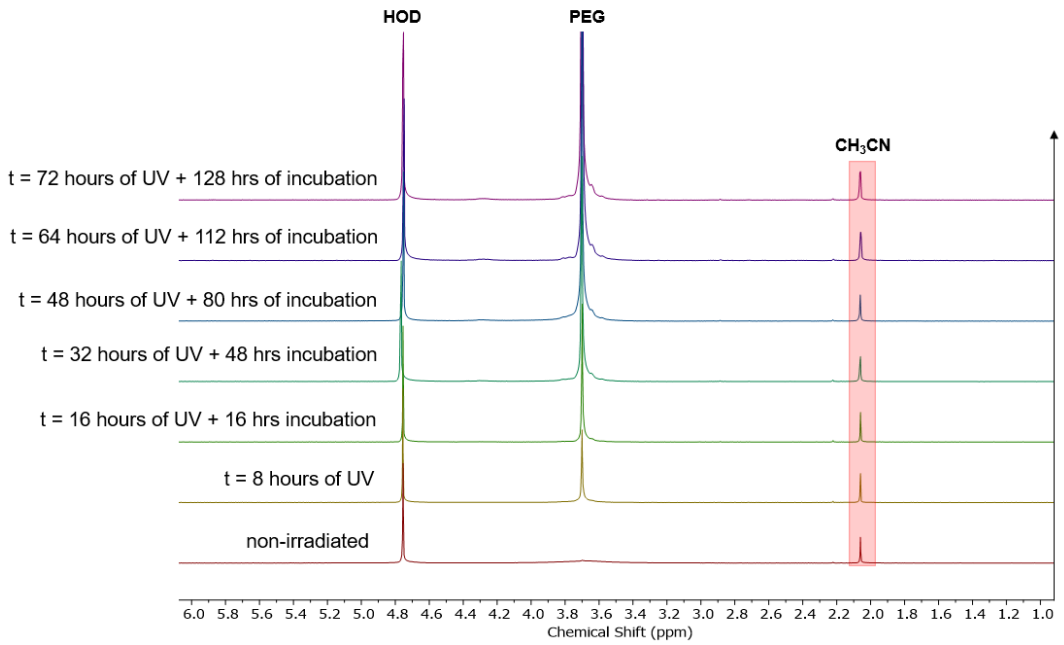


**Figure 3.21.** $^{1}H$ NMR spectra ($D_2O$, 600 MHz) of OPF-NB-50 hydrogel in PBS before and after UV irradiation (365-370 nm) followed by various irradiation and incubation periods (t = hours of UV treatment + incubation periods at 37 °C at pH = 7.4).

For the non-irradiated OPF-NB-50 sample, the PEG peak at 3.70 ppm was much broader and could be detected even in the initial sample, likely corresponding to PEG chains incorporated into the network, but retaining some mobility (**Figure 3.22**). Over time, the peak height increased compared to the $CH_3CN$ peak, suggesting that the chains became more mobile, presumably due to some degree of ester hydrolysis. However, the peak remained broader than that observed for the irradiated OPF-NB-50 hydrogels.

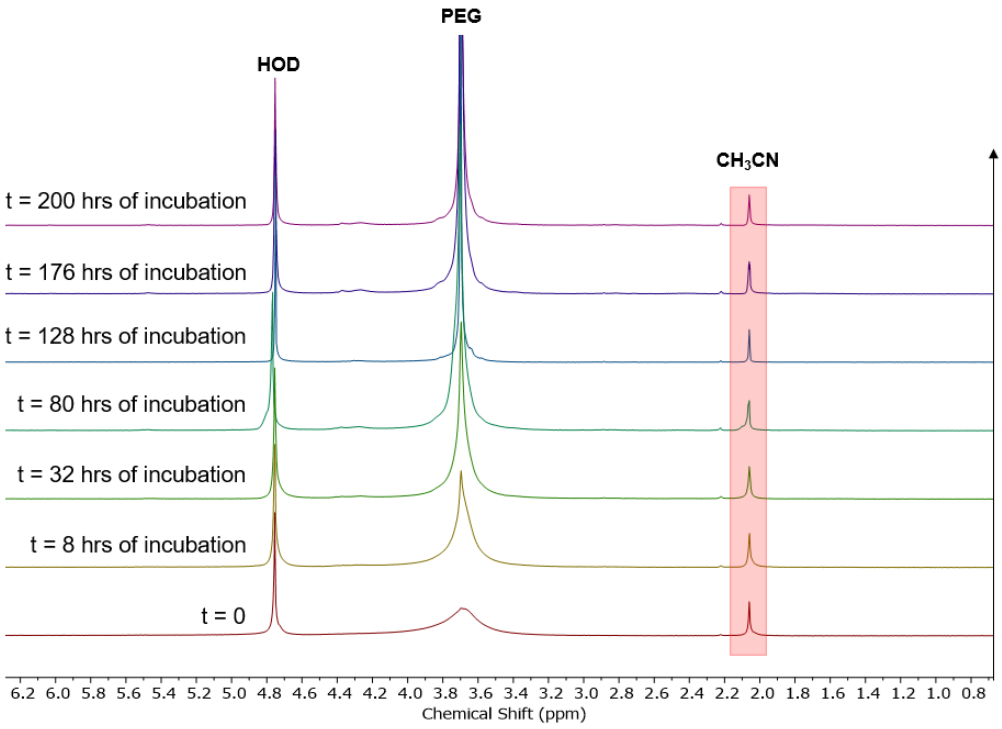


**Figure 3.22**. $^{1}$H NMR spectra ($D_2O$, 600 MHz) of the non-irradiated OPF-NB-50 hydrogel in PBS after various incubation periods (t = incubation periods at 37 °C at pH = 7.4).

OPF hydrogels were also subjected to similar treatments to observe their degradation behaviour. Both irradiated and non-irradiated OPF hydrogels degraded to some extent over 8 days, but the ratio of the PEG peak height to that of $CH_3CN$ remained much lower than that of the OPF-NB-50 hydrogels (**Figure 3.23-3.24**). This degree of degradation presumably arose from background hydrolysis of the esters in the network. Interestingly, whereas the background degradation of OPF itself was much faster than non-irradiated OPF-NB-50, the OPF hydrogel appeared to degrade more slowly than the OPF-NB-50 hydrogels. This change can likely be attributed to the consumption of the fumarate alkenes during the cross-linking as these moieties seemed to accelerate background hydrolysis in the free polymers.

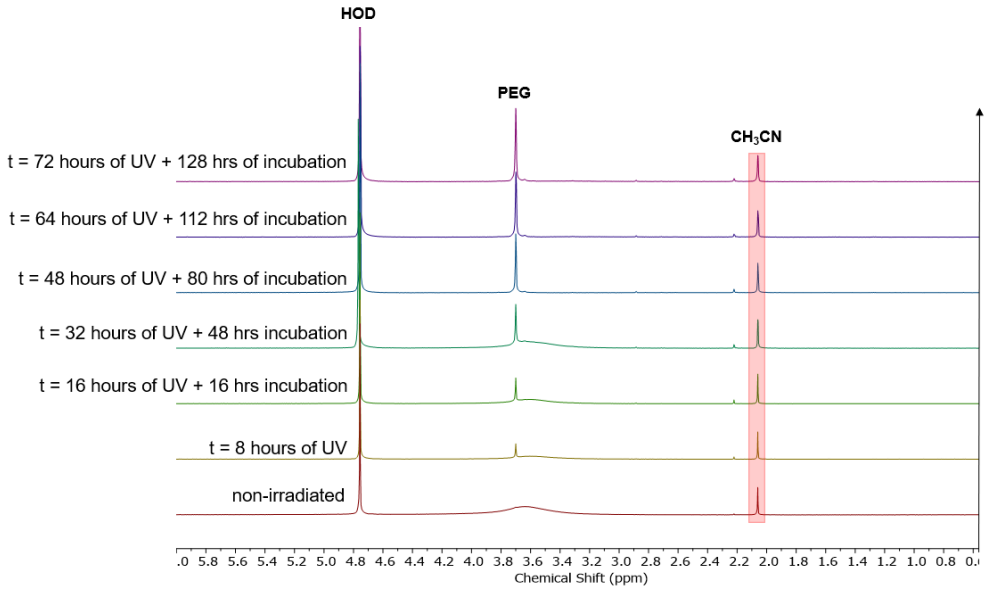


**Figure 3.23.** $^{1}H$ NMR spectra ($D_2O$, 600 MHz) of 30 wt% OPF hydrogel in PBS before UV irradiation and after various UV irradiation (365-370 nm) and incubation periods (t = hours of UV treatment + incubation periods at 37 °C at pH = 7.4).

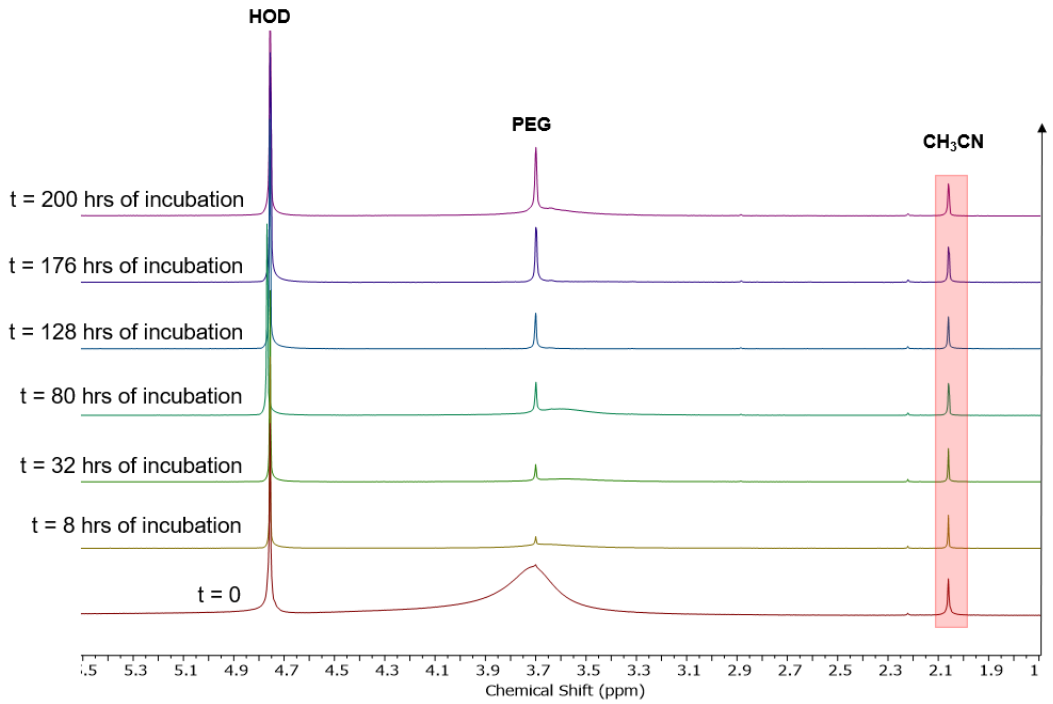


**Figure 3.24.** NMR spectra ($D_2O$, 600 MHz) of the 30 wt% OPF hydrogel in PBS after various incubation periods (t = incubation periods at 37 °C at pH = 7.4).

## 3.6 Compressive moduli of the degrading hydrogels

Initially, the OPF-NB-50 hydrogel appeared as a soft light orange gel while the OPF gel was a stiffer dark orange gel. After equilibrating the two gels in PBS for one day, the OPF-NB-50 gel became white and opaque while the OPF gel became yellow and transparent. Each of the OPF-NB-50 and OPF gels were prepared in triplicate. One set of triplicates served as the irradiated set followed by periods of incubation while the other would be incubated without UV-irradiation. Similar to the previous gel degradation experiment, it was hypothesized that the functionalized gels would require long periods of irradiation to ensure the complete cleavage of *o*-nitrobenzyl protecting group. Thus, the cylindrical gels were immersed in a PBS solution and irradiated for 8 h each day with a mercury lamp for 10 days.

The compressive moduli were measured initially, and then after 5 days of treatment (**3**). The initial modulus of the OPF-NB-50 gel was 9.58 ± 3.97 kPa

(**Figure 3.25**). The relatively high standard deviations can be attributed to variability in the gel-to-gel preparation. After 5 days of UV irradiation, the modulus of the irradiated OPF-NB-50 hydrogel was too low to accurately measure. This is likely to be attributed to chemical bond cleavage events resulting in the breakdown of the gel network. In contrast, the non-irradiated gels showed an insignificant reduction in stiffness which remained at 8.8 ± 4.0 kPa after 5 days of incubation and 8.2 ± 3.7 kPa after 10 days. These results suggest that the presence of UV light leads to a predominantly photochemically induced cleavage process rather than ester hydrolysis.

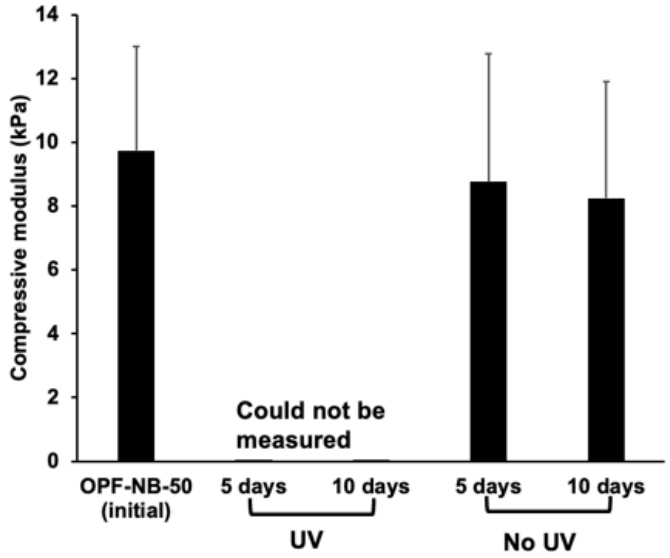


**Figure 3.25.** Compressive moduli of non-irradiated and irradiated OPF-NB-50 hydrogels in PBS. Irradiated samples (UV) were irradiated for 8 h followed by incubation at 37 °C for 16 h each day for total of 10 days. Compression tests were performed prior to treatment and after 5 and 10 days. The control samples were incubated at 37 °C for the same amount of time. Error bars correspond to the standard deviation on triplicate samples.

Finally, the OPF gels were also tested to evaluate the effects of UV light on chemically similar but non-UV-responsive materials. Initially, the OPF hydrogel

had a compressive modulus of 164 ± 18 kPa (**Figure 3.26**). This modulus is much higher than that of the OPF-NB-50 hydrogel, a result that can likely be attributed to a higher density of cross-links when all of the double bonds remained unfunctionalized. After 5 days of UV light treatment and incubation, the compressive modulus decreased to 153 ± 23 kPa then after 10 days, it fell to 148 ± 24 kPa. Control OPF hydrogels behaved similarly with the modulus dropping to 153 ± 14 kPa after 5 days, and 143 ± 8 KPa after 10 days. While there was a trend towards lower moduli with continued irradiation, this could be explained by minor hydrolytic cleavage of some bonds in the network. The change was not statistically significant and confirmed that the reduction in modulus for OPG-NB-50 hydrogels upon UV treatment was not due to non-specific photochemical breakdown of the network.

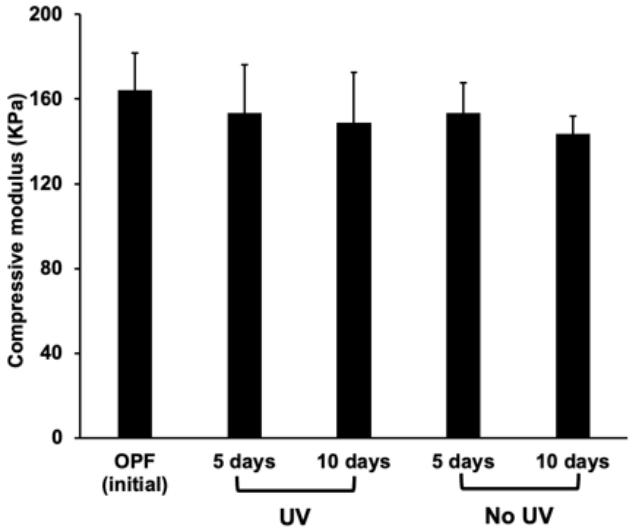


**Figure 3.26.** Compressive moduli of non-irradiated and irradiated OPF hydrogels in PBS. Irradiated samples (UV) were irradiated for 8 h followed and incubation at 37 °C for 16 h each day for total of 10 days. Compression tests were performed prior to treatment and after 5 and 10 days. The control samples were incubated at 37 °C for the same amount of time. Error bars correspond to the standard deviation on triplicate samples.

# Chapter 4

# 4 Conclusions and Future work

In conclusion, this work presents preliminary results of the functionalization and degradation of oligo [poly(ethylene glycol) fumarate] with novel photo-sensitive moieties. These gels can be incorporated into gel networks to trigger on demand degradation of OPF gels (**Figure 4.1**).

Chapter 3 illustrated the synthesis of a novel photo group derived from a *o*-nitrobenzyl alcohol and incorporation of these pendent groups into gel matrices. This novel pendent group was used to functionalized a previously synthesized oligomer OPF.[56] Different levels of functionalized OPF (0%, 50%, 100%) was compared to study the effects of the cyclization spacers in the presence of UV light and monitored by $^{1}$H NMR spectroscopy and SEC. The SEC results show that the non-functionalized OPF rapidly degraded in 0.1 M of phosphate buffer (pH 7.4) at 37 °C due to its susceptibility to simple ester hydrolysis. In comparison, functionalized OPF exhibited to yield enhanced triggered degradation when irradiated with UV-light compared to the absence of UV light proportional to the level of functionalization. Therefore, it would be possible to tune the rate of degradation of the oligomer based on the number of functionalization and alkene bonds consumed.

When the photo-sensitive pendent group gels were prepared by radical initiation in a 30 wt% formulation using a 1:4 cross-linker to oligomer content. These formulations developed into distinct soft gels while formulations below 30 wt% typically resulted in amorphous solids. Meanwhile, the non-functionalized gels were mechanically stiffer compared to their functionalized counter parts. $^{1}$H NMR spectroscopy indicated that the functionalized OPF gels quantitively degraded

much faster than the non-functionalized OPF. Finally, the gels were equilibrated in PBS and irradiated followed by incubation at 37 °C or just incubated at 37 °C for 10 days. Mechanical testing indicated that the OPF-NB-50 gels yielded lower compression modulus compared to non-irradiated OPF-NB-50. However, the compression data of the non-functionalized OPF gels remained the same regardless of UV light.

Further work needs to be done to optimize the mechanical properties of the gel such as increasing the cross-linker content to construct a stiffer gel. Overall, the introduction of new cyclization spacer systems presents itself as an attractive quality for potential development within applications of controlled drug release.

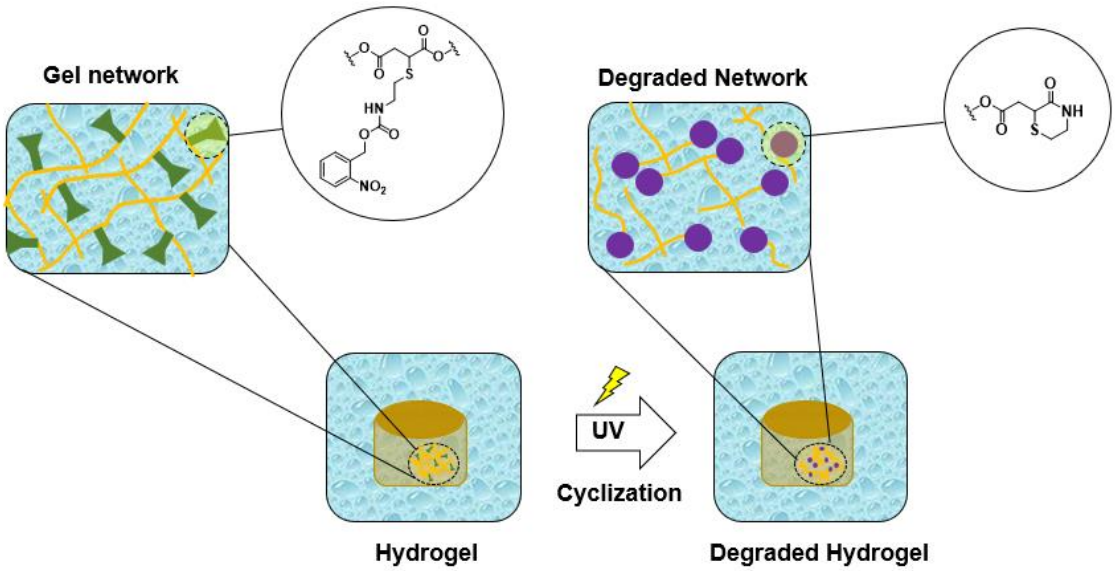


**Figure 4.1.** Schematic presenting a cross-linked OPF hydrogel network functionalized with photo-cleavable groups and irradiated by UV light, triggering a backbone cleavage event through cyclization, thereby leading to the break down of the hydrogel network.

# 4.1 References:


1. Samir, A.; Ashour, F. H.; Hakim, A. A. A.; Bassyouni, M. *npj Mater. Degrad.* **2022,** *6*, 68.
2. Vroman, I.; Tighzert, L. *Materials* **2009,** *2*, 307-344.
3. Bhagabati, P., Biopolymers and biocomposites-mediated sustainable high-performance materials for automobile applications. In *Sustainable Nanocellulose and Nanohydrogels from Natural Sources*, Elsevier: Amsterdam, The Netherlands, 2020; pp 197-216.
4. Panchal, S. S.; Vasava, D. V. *ACS Omega* **2020,** *5*, 4370-4379.
5. Song, R.; Murphy, M.; Li, C.; Ting, K.; Soo, C.; Zheng, Z. *Drug Des. Devel. Ther.* **2018,** *12*, 3117-3145.
6. Luckachan, G. E.; Pillai, C. K. S. *J. Polym. Environ.* **2011,** *19*, 637-676.
7. Gunatillake, P.; Mayadunne, R.; Adhikari, R. *Biotechnol. Annu. Rev.* **2006,** *12*, 301-347.
8. Murthy, N.; Wilson, S.; Sy, J. C. *Polym. Sci: A.* **2012,** 9, 547-560.
9. Liu, Y.; Song, L.; Feng, N.; Jiang, W.; Jin, Y.; Li, X. *RSC Adv.* **2020,** *10*, 36230-36240.
10. Manavitehrani, I.; Fathi, A.; Badr, H.; Daly, S.; Negahi Shirazi, A.; Dehghani, F. *Polymers* **2016,** *8*, 20.
11. Okada, M. *Prog. Polym. Sci.* **2002,** *27*, 87-133.
12. Kasirajan, S.; Ngouajio, M. *Agron. Sustain. Dev.* **2012,** *32*, 501-529.

13. Efthimiadou, E. K.; Theodosiou, M.; Toniolo, G.; Abu-Thabit, N. Y., Stimuli-responsive biopolymer nanocarriers for drug delivery applications. In *Stimuli Responsive Polymeric Nanocarriers for Drug Delivery Applications*, Elsevier: 2018; Vol. 1, pp 405-432.
14. Bu, Y.; Ma, J.; Bei, J.; Wang, S. *Front. Bioeng. Biotechnol.* **2019,** *7*, 98.
15. Seyednejad, H.; Ghassemi, A. H.; van Nostrum, C. F.; Vermonden, T.; Hennink, W. E. *J. Controlled Release* **2011,** *152*, 168-176.
16. Bossion, A.; Zhu, C.; Guerassimoff, L.; Mougin, J.; Nicolas, J. *Nat. Commun.* **2022,** *13*, 2873.
17. Vert, M. *Biomacromolecules* **2005,** *6*, 538-546.
18. Urbanek, T.; Jager, E.; Jager, A.; Hruby, M. *Polymers* **2019,** *11*, 1061-1082.
19. Washington, K. E.; Kularatne, R. N.; Karmegam, V.; Biewer, M. C.; Stefan, M. C. *Wiley Interdiscip. Rev.: Nanomed. Nanobiotechnol.* **2017,** *9*, 1446-1448.
20. Cameron, D. J.; Shaver, M. P. *Chem. Soc. Rev.* **2011,** *40*, 1761-1776.
21. Albertsson, A.-C.; Varma, I. K., Aliphatic Polyesters: Synthesis, Properties and Applications. In *Degradable Aliphatic Polyesters*, Albertsson, A.-C., Ed. Springer Berlin Heidelberg: Berlin, Heidelberg, 2002; pp 1-40.
22. Wei, M.; Gao, Y.; Li, X.; Serpe, M. J. *Polym. Chem.* **2017,** *8*, 127-143.
23. Schattling, P.; Jochum, F. D.; Theato, P. *Polym. Chem.* **2014,** *5*, 25-36.
24. Stuart, M. A.; Huck, W. T.; Genzer, J.; Muller, M.; Ober, C.; Stamm, M.; Sukhorukov, G. B.; Szleifer, I.; Tsukruk, V. V.; Urban, M.; Winnik, F.; Zauscher, S.; Luzinov, I.; Minko, S. *Nat. Mater.* **2010,** *9*, 101-113.
25. Xie, J.; Li, A.; Li, J. *Macromol. Rapid Commun.* **2017,** *38*, 1-14.

26. Gu, Z.; Aimetti, A. A.; Wang, Q.; Dang, T. T.; Zhang, Y.; Veiseh, O.; Cheng, H.; Langer, R. S.; Anderson, D. G. *ACS Nano* **2013,** *7*, 4194-4201.
27. Fernandez, M.; Orozco, J. *Polymers* **2021,** *13*, 2464-2506.
28. Alvarez-Lorenzo, C.; Bromberg, L.; Concheiro, A. *Photochem. Photobiol.* **2009,** *85*, 848-860.
29. Mena-Giraldo, P.; Perez-Buitrago, S.; Londono-Berrio, M.; Ortiz-Trujillo, I. C.; Hoyos-Palacio, L. M.; Orozco, J. *Sci. Rep.* **2020,** *10*, 2110.
30. Carl, L. P.; Chakravarty, K. P.; Katzenellenbogen, A. J. *J. Med. Chem.* **1981,** *24*, 478-480.
31. Alouane, A.; Labruère, R.; Le Saux, T.; Schmidt, F.; Jullien, L. *Angew. Chem., Int. Ed.* **2015,** *54*, 7492-7509.
32. Wang, W.; Alexander, C. *Angew. Chem., Int. Ed.* **2008,** *47*, 7804-7806.
33. Gisbert-Garzarán, M.; Manzano, M.; Vallet-Regí, M. *Chem. Eng. J.* **2018,** *340*, 24-31.
34. Shelef, O.; Gnaim, S.; Shabat, D. *J. Am. Chem. Soc.* **2021,** *143*, 21177-21188.
35. Gavriel, A. G.; Sambrook, M. R.; Russell, A. T.; Hayes, W. *Polym. Chem.* **2022,** *13*, 3188-3269.
36. Dud, M.; Tichotova, M.; Prochazkova, E.; Baszczynski, O. *Molecules* **2021,** *26*, 5160.
37. Noordzij, G. J.; Wilsens, C. *Front. Chem.* **2019,** *7*, 729.
38. Chen, E. K. Y.; McBride, R. A.; Gillies, E. R. *Macromolecules* **2012,** *45*, 7364-7374.
39. Mejia, J. S.; Gillies, E. R. *Polym. Chem.* **2013,** *4*, 1969-1982.

40. Dal Corso, A.; Borlandelli, V.; Corno, C.; Perego, P.; Belvisi, L.; Pignataro, L.; Gennari, C. *Angew. Chem., Int. Ed.* **2020,** *59*, 4176-4181.
41. Kasai, R. D.; Radhika, D.; Archana, S.; Shanavaz, H.; Koutavarapu, R.; Lee, D.-Y.; Shim, J. *Int. J. Polym. Mater. Polym. Biomater.* **2022,** *4*, 1-11.
42. Ahmed, E. M. *J. Adv. Res.* **2015,** *6*, 105-121.
43. El-Husseiny, H. M.; Mady, E. A.; Hamabe, L.; Abugomaa, A.; Shimada, K.; Yoshida, T.; Tanaka, T.; Yokoi, A.; Elbadawy, M.; Tanaka, R. *Mater. Today Bio* **2022,** *13*, 100186.
44. Chyzy, A.; Plonska-Brzezinska, M. E. *Molecules* **2020,** *25*, 5795.
45. Lee, J. H.; Bucknall, D. G. *J. Polym. Sci., Part B: Polym. Phys.* **2008,** *46*, 1450-1462.
46. Majcher, M. J.; Hoare, T., Hydrogel Synthesis and Design. In *Cellulose-Based Superabsorbent Hydrogels*, Springer, Cham: 2018; pp 1-41.
47. Parhi, R. *Adv. Pharm. Bull.* **2017,** *7*, 515-530.
48. Bi, X.; Liang, A., In Situ-Forming Cross-linking Hydrogel Systems: Chemistry and Biomedical Applications. In *Emerging Concepts in Analysis and Applications of Hydrogels*, IntechOpen: 2016; Vol. 86, pp 133-149.
49. Sanchez-Cid, P.; Jimenez-Rosado, M.; Romero, A.; Perez-Puyana, V. *Polymers* **2022,** *14*, 3023.
50. Echalier, C.; Valot, L.; Martinez, J.; Mehdi, A.; Subra, G. *Mater. Today Commun.* **2019,** *20*, 100536.
51. Das, D.; Pal, S. *RSC Adv.* **2015,** *5*, 25014-25050.
52. Tomal, W.; Ortyl, J. *Polymers* **2020,** *12*, 1073.

53. Orakdogen, N.; Okay, O. *J. Appl. Polym. Sci.* **2007,** *103*, 3228-3237.

54. Liu, M.; Zeng, X.; Ma, C.; Yi, H.; Ali, Z.; Mou, X.; Li, S.; Deng, Y.; He, N. *Bone Res.* **2017,** *5*, 17014.

55. Chamkouri, H. *Am. J. Biomed. Res.* **2021,** *11*, 485-493.

56. Kinard, L. A.; Kasper, F. K.; Mikos, A. G. *Nat. Protoc.* **2012,** *7*, 1219-1227.

57. Kinard, L.; Kasper, K.; Mikos, A. *Protoc. Exch.* **2012,** 1-3.

58. Park, H.; Guo, X.; Temenoff, J. S.; Tabata, Y.; Caplan, A. I.; Kasper, F. K.; Mikos, A. G. *Biomacromolecules* **2009,** *10*, 541-546.

59. Kasper, F. K.; Seidlits, S. K.; Tang, A.; Crowther, R. S.; Carney, D. H.; Barry, M. A.; Mikos, A. G. *J. Controlled Release* **2005,** *104*, 521-39.

60. Liang, N.; Flynn, L. E.; Gillies, E. R. *Eur. Polym. J.* **2020,** *136*, 109899.

61. Correa, S.; Grosskopf, A. K.; Lopez Hernandez, H.; Chan, D.; Yu, A. C.; Stapleton, L. M.; Appel, E. A. *Chem. Rev.* **2021,** *121*, 11385-11457.

62. Dyamenahalli, K.; Famili, A.; Shandas, R., Characterization of shape-memory polymers for biomedical applications. In *Shape Memory Polymers for Biomedical Applications*, Yahia, L. H., Ed. Woodhead Publishing: 2015; pp 35-63.

63. Lee, D.; Zhang, H.; Ryu, S., Elastic Modulus Measurement of Hydrogels. In *Cellulose-Based Superabsorbent Hydrogels*, Springer, Cham: 2019; pp 865-884.

64. Bashir, S.; Hina, M.; Iqbal, J.; Rajpar, A. H.; Mujtaba, M. A.; Alghamdi, N. A.; Wageh, S.; Ramesh, K.; Ramesh, S. *Polymers* **2020,** *12*, 2702.

65. Cai, M. H.; Chen, X. Y.; Fu, L. Q.; Du, W. L.; Yang, X.; Mou, X. Z.; Hu, P. Y. *Front. Bioeng. Biotechnol.* **2021,** *9*, 630943.

66. Ma, Y.; Yao, J.; Liu, Q.; Han, T.; Zhao, J.; Ma, X.; Tong, Y.; Jin, G.; Qu, K.; Li, B.; Xu, F. *Adv. Funct. Mater.* **2020,** *30*, 2001820.

67. Zhao, L.; Zhu, L.; Liu, F.; Liu, C.; Shan, D.; Wang, Q.; Zhang, C.; Li, J.; Liu, J.; Qu, X.; Yang, Z. *Int. J. Pharm.* **2011,** *410*, 83-91.

68. Watrelot, A. A.; Tran, D. T.; Buffeteau, T.; Deffieux, D.; Le Bourvellec, C.; Quideau, S.; Renard, C. M. G. C. *Appl. Surf. Sci.* **2016,** *371*, 512-518.

69. Barra, T.; Arrue, L.; Urzúa, E.; Ratjen, L. *J. Phys. Org. Chem.* **2019,** *32*, 3937.

70. Nair, D. P.; Podgórski, M.; Chatani, S.; Gong, T.; Xi, W.; Fenoli, C. R.; Bowman, C. N. *Chem. Mater.* **2013,** *26*, 724-744.

71. Lv, A.; Cui, Y.; Du, F.-S.; Li, Z.-C. *Macromolecules* **2016,** *49*, 8449-8458.

72. Temenoff, J. S.; Athanasiou, K. A.; LeBaron, R. G.; Mikos, A. G. *J. Biomed. Mater. Res.* **2002,** *59*, 429-437.

# Appendix: Supplementary Figures

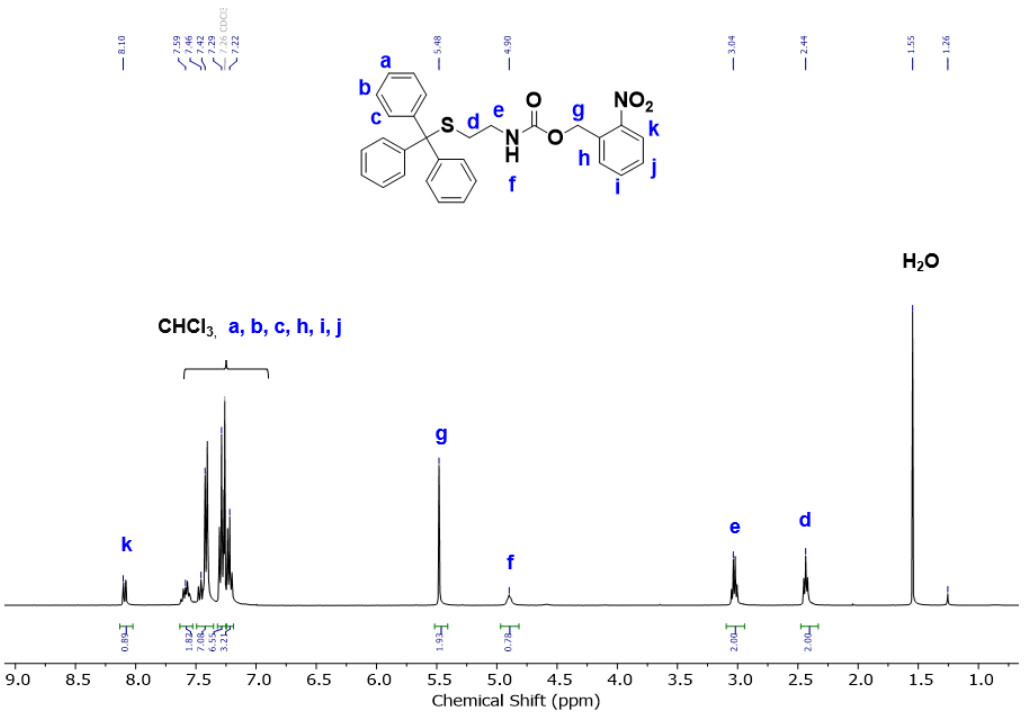


**Figure A1.** $^{1}H$ NMR spectrum of Compound (**3**) ($CDCl_3$, 400 MHz).

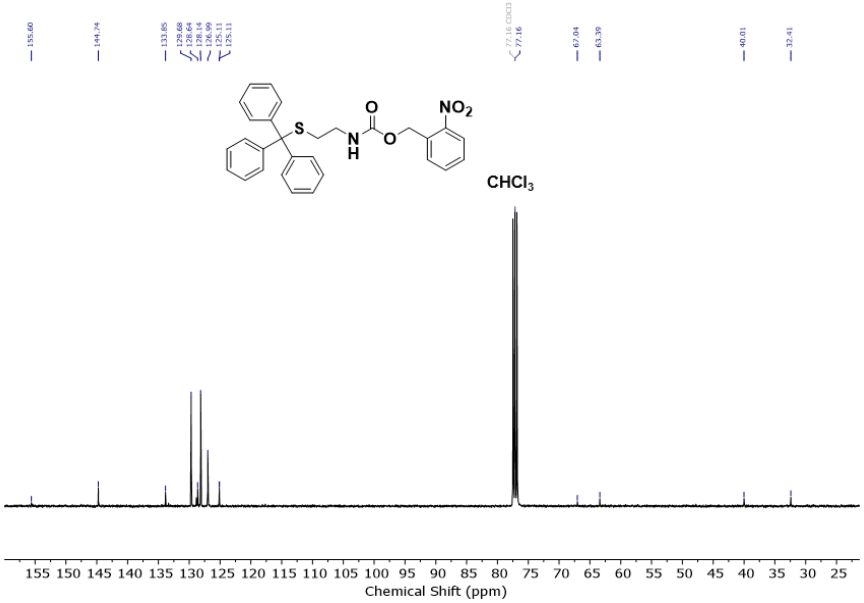


**Figure A2.** $^{13}C$ NMR spectrum of Compound (**3**) ($CDCl_3$, 400 MHz).

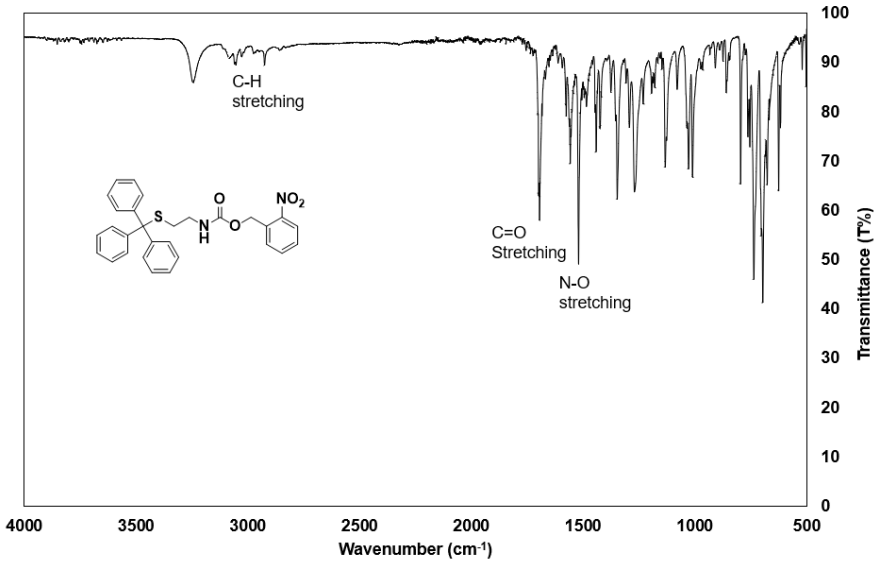


**Figure A3.** FT-IR spectrum of Compound (**3**).

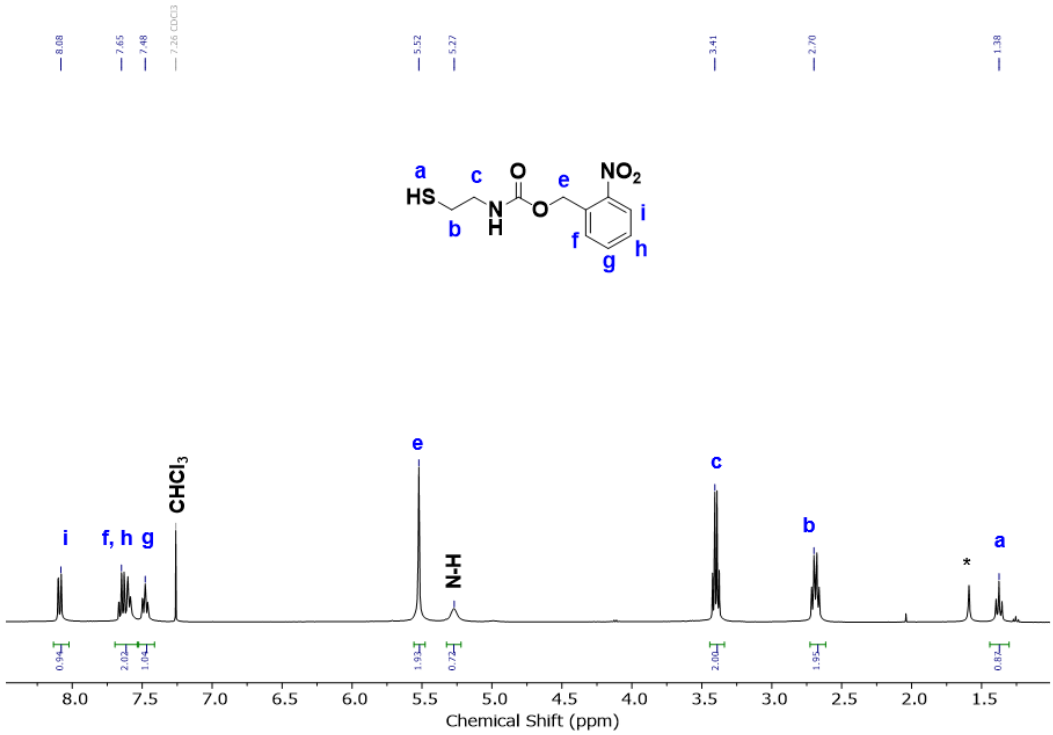


**Figure A4.** $^{1}$H NMR spectrum of Compound (**4**) ($CDCl_3$, 400 MHz) (* corresponds to water).

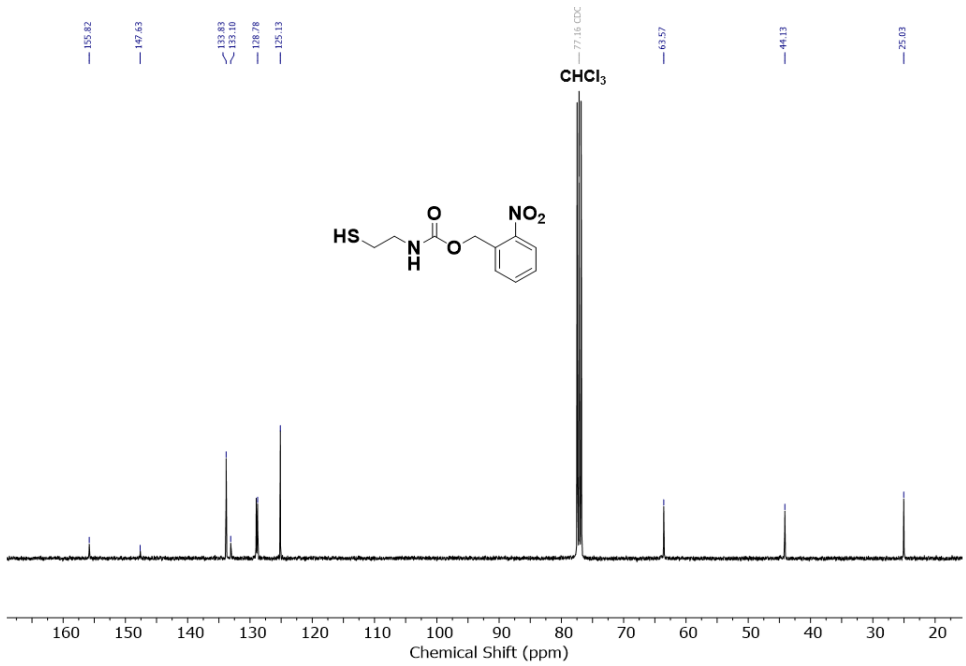


**Figure A5.** $^{13}C$ NMR spectrum of Compound (**4**) ($CDCl_3$, 400 MHz).

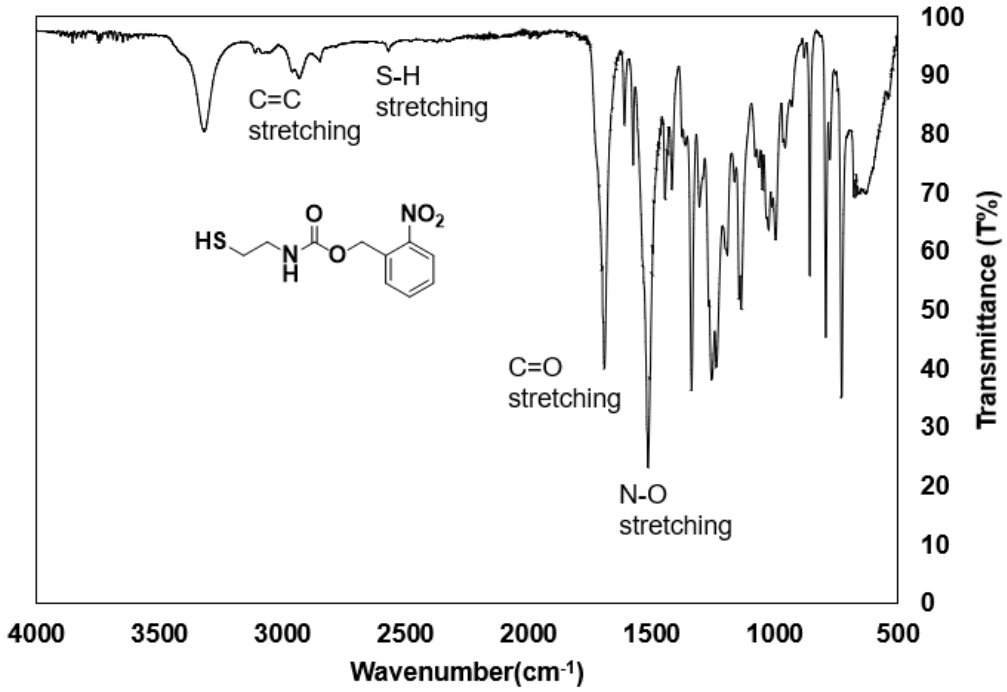


**Figure A6.** FT-IR spectrum of Compound (**4**).

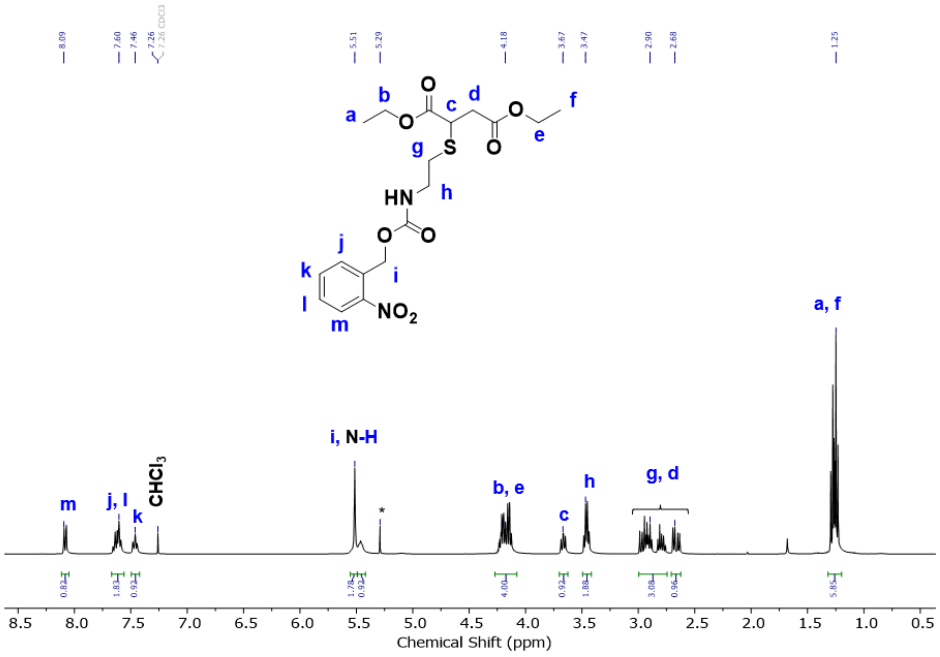


**Figure A7.** $^{1}H$ NMR spectrum of Compound (**5**) ($CDCl_3$, 400 MHz) (* corresponds to $CH_2Cl_2$ peaks).

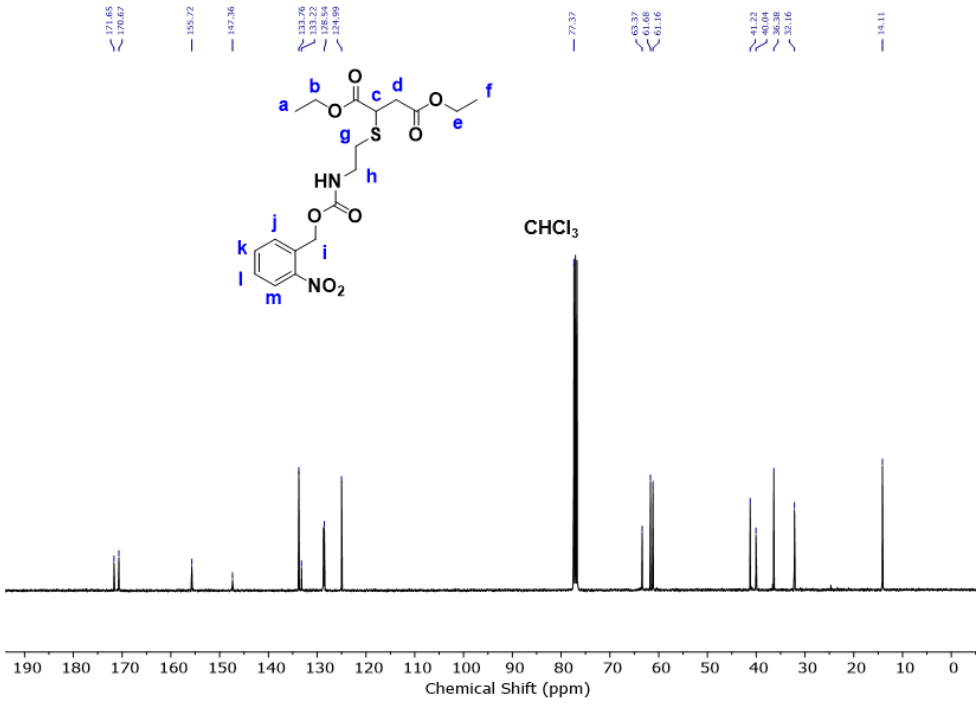


**Figure A8.** $^{13}C$ NMR spectrum of the Compound (**5**) ($CDCl_3$, 101 MHz).

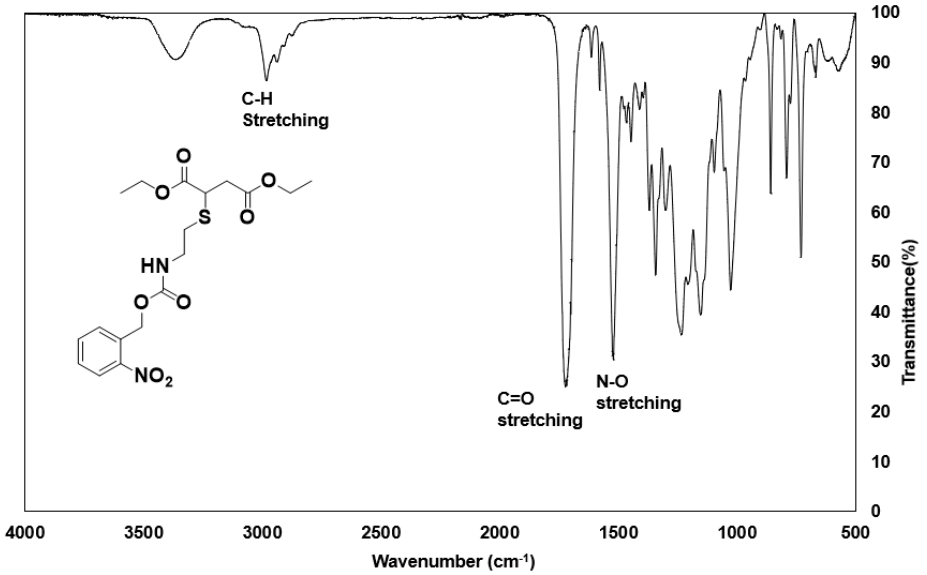


**Figure A9.** FT-IR spectrum of Compound (**5**).

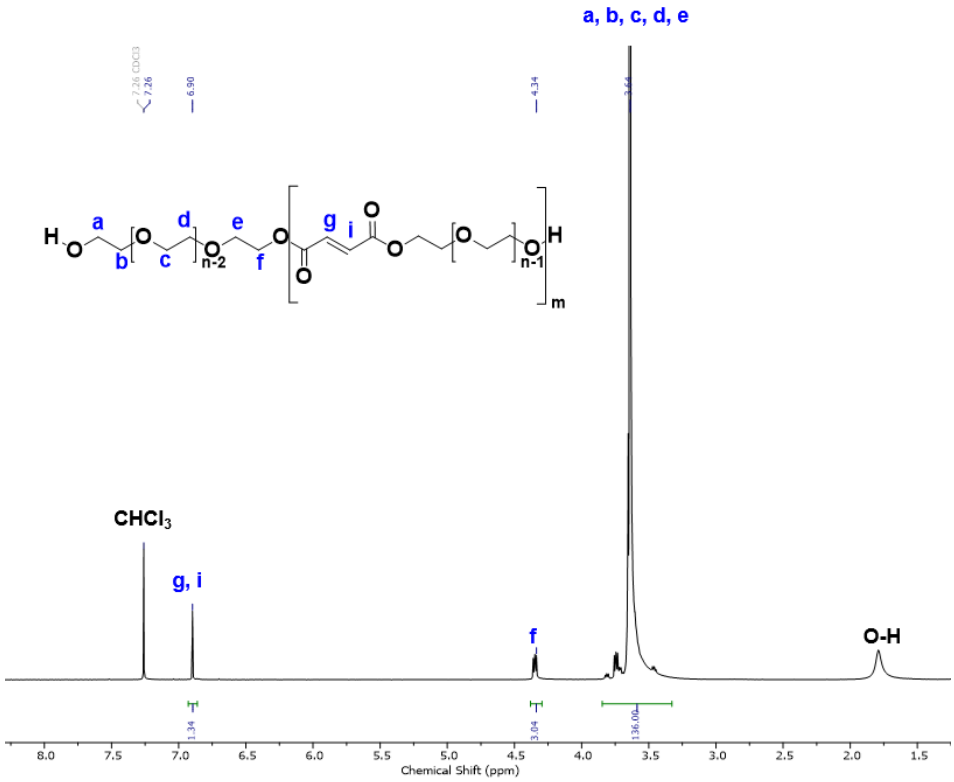


**Figure A10.** $^{1}H$ NMR spectrum of OPF ($CDCl_3$, 400 MHz).

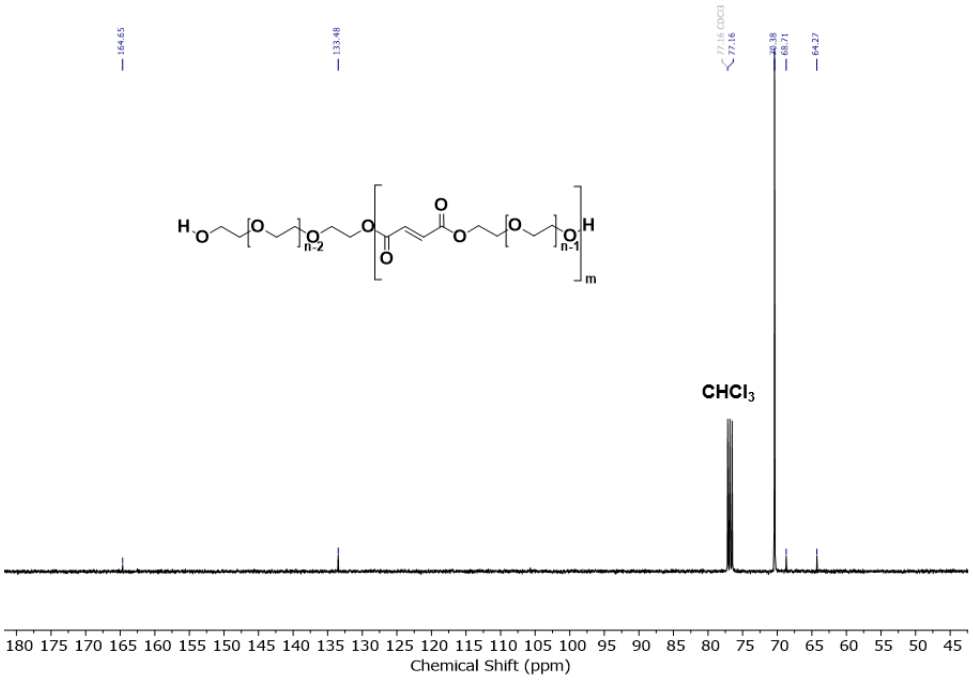


**Figure A11.** $^{13}C$ NMR spectrum of OPF ($CDCl_3$, 400 MHz).

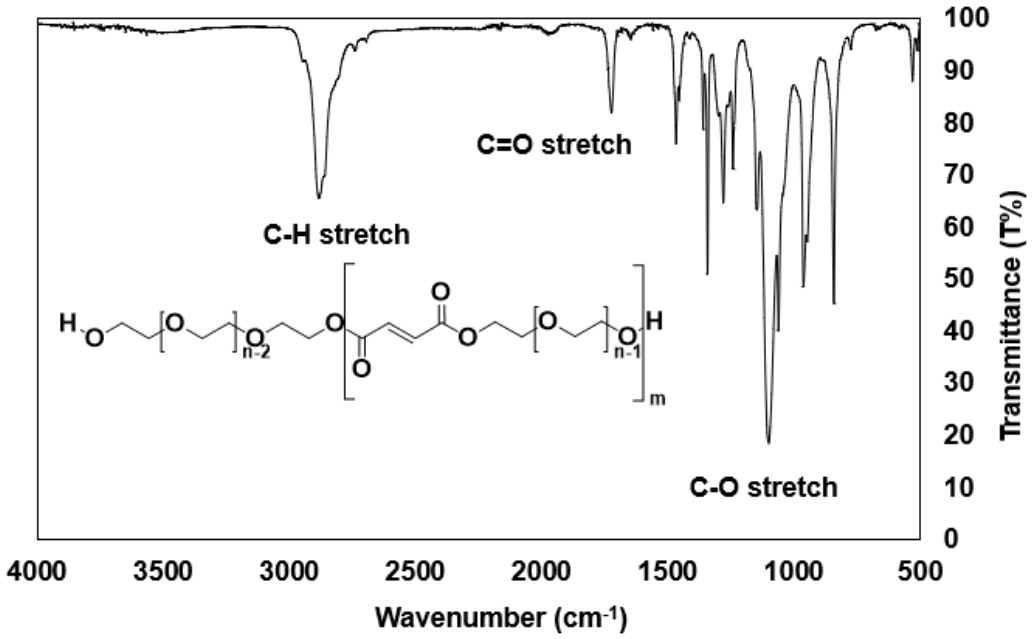


**Figure A12.** FT-IR spectrum of OPF.

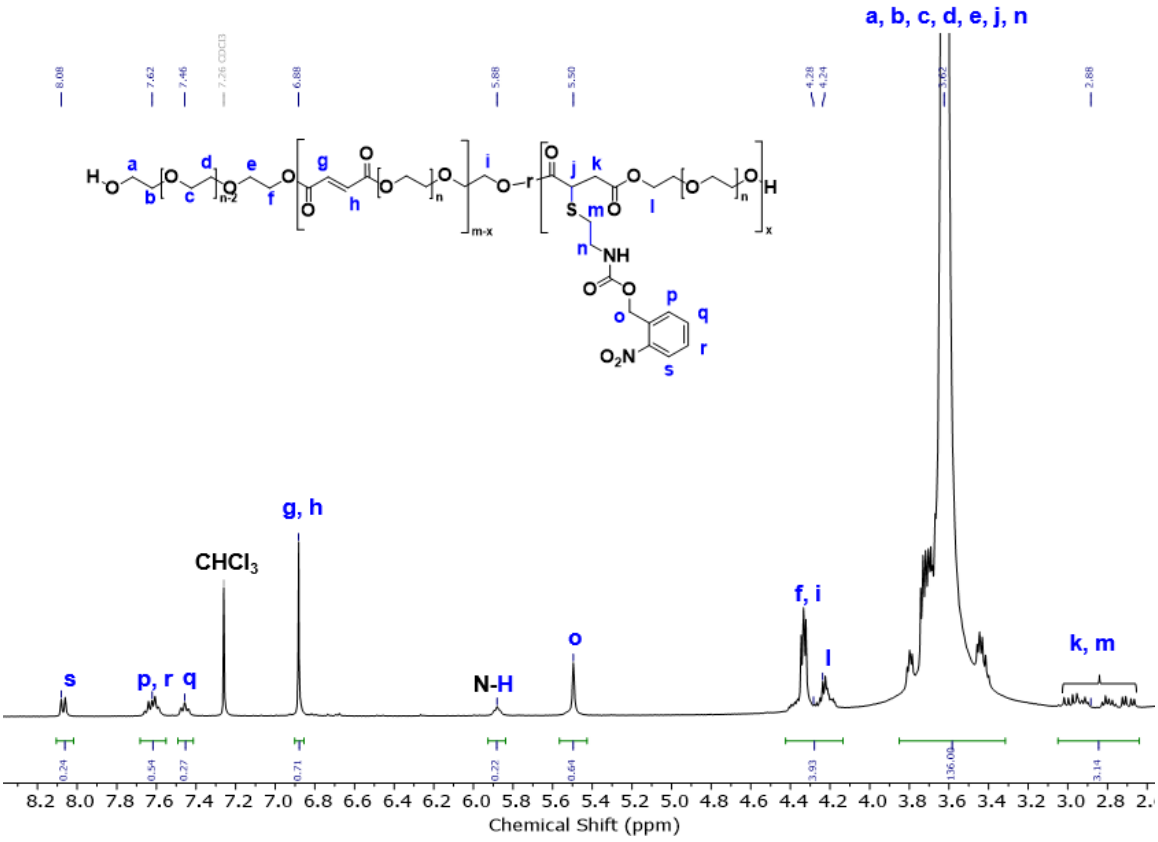


**Figure A13.** $^{1}H$ NMR spectrum of OPF-NB-50 ($CDCl_3$, 400 MHz).

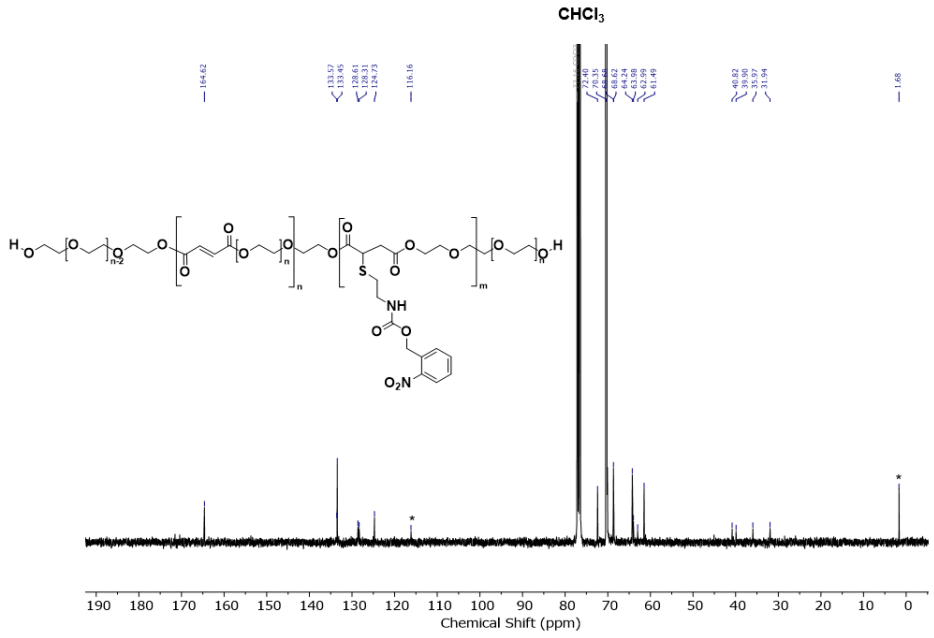


**Figure A14.** $^{13}C$ NMR spectrum of OPF-NB-50 ($CDCl_3$, 101 MHz) ( * corresponds to MeCN peaks).

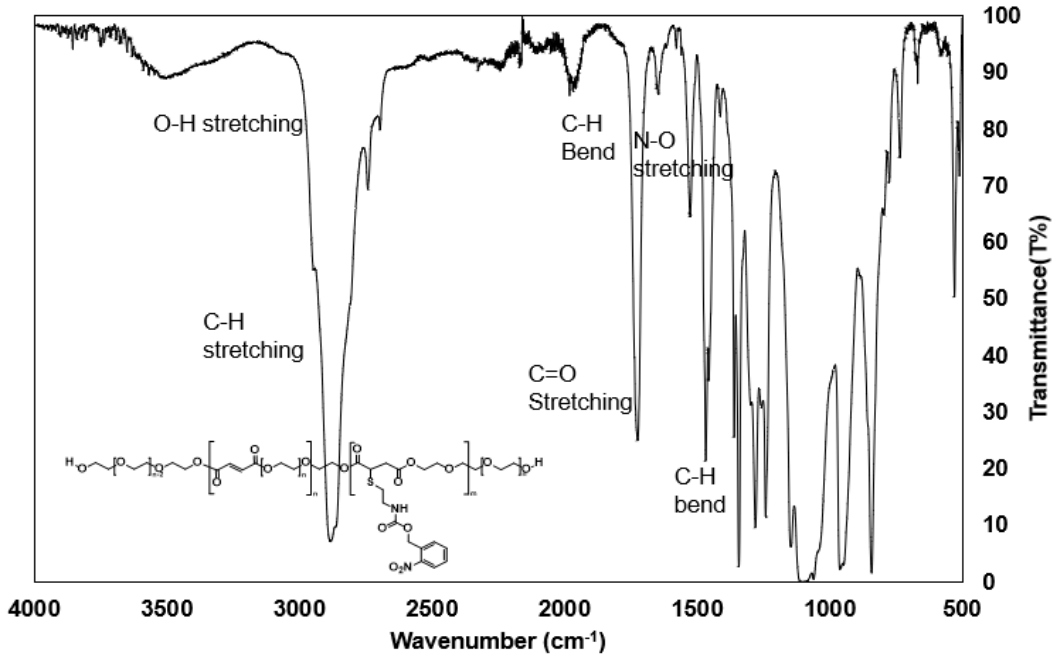


**Figure A15.** FT-IR spectrum of OPF-NB-50.

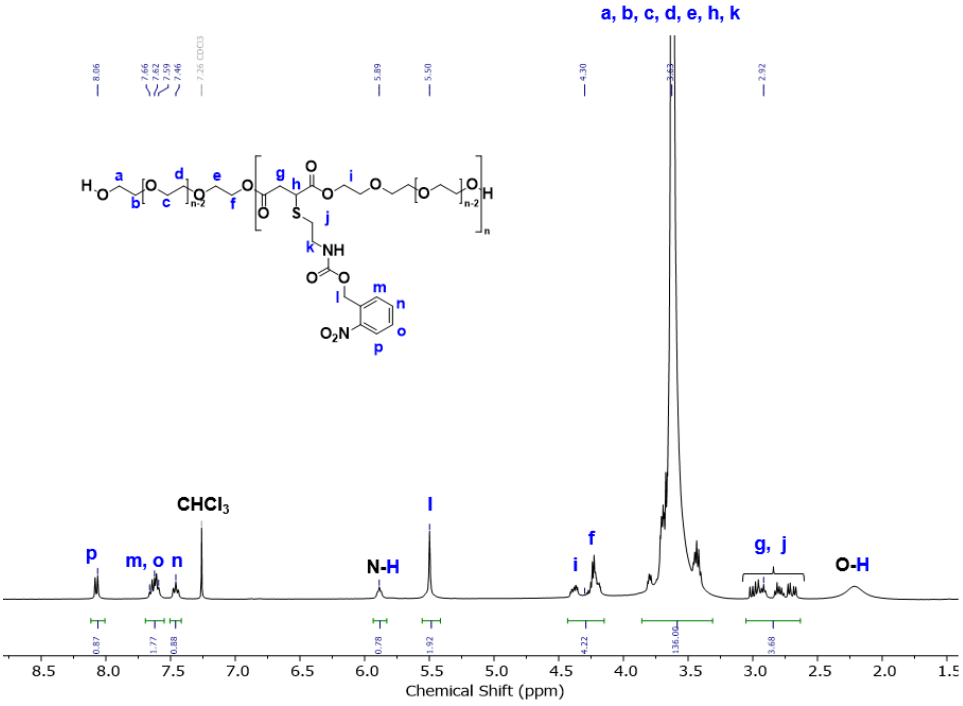


**Figure A16.** $^{1}H$ NMR spectrum of OPF-NB-100 ($CDCl_3$, 400 MHz).

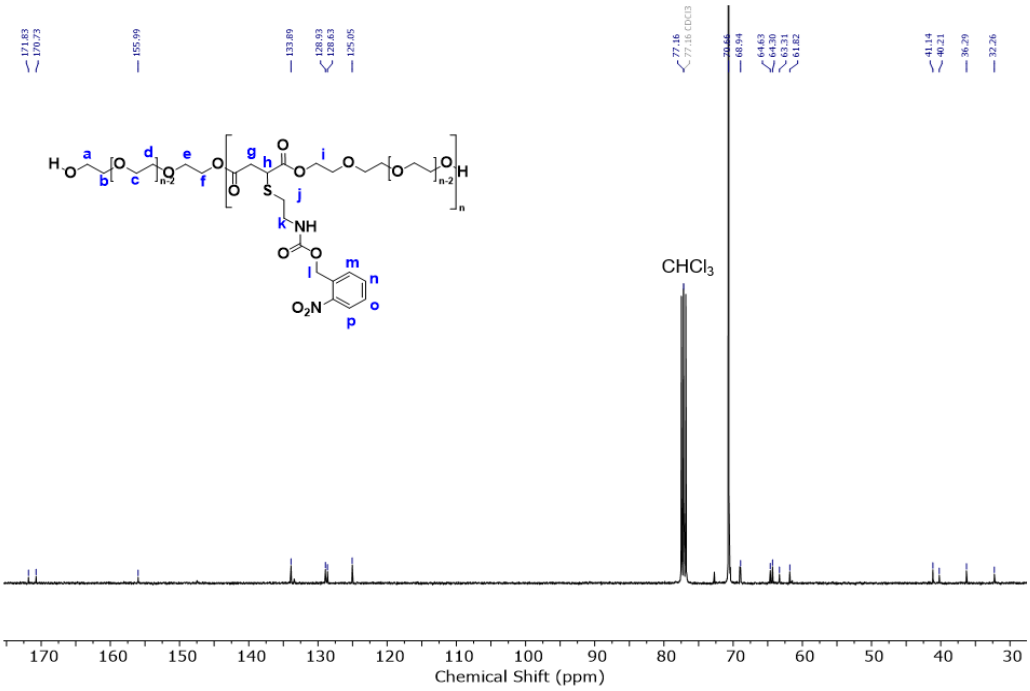


**Figure A17.** $^{13}C$ NMR spectrum of OPF-NB-100 ($CDCl_3$, 400 MHz).

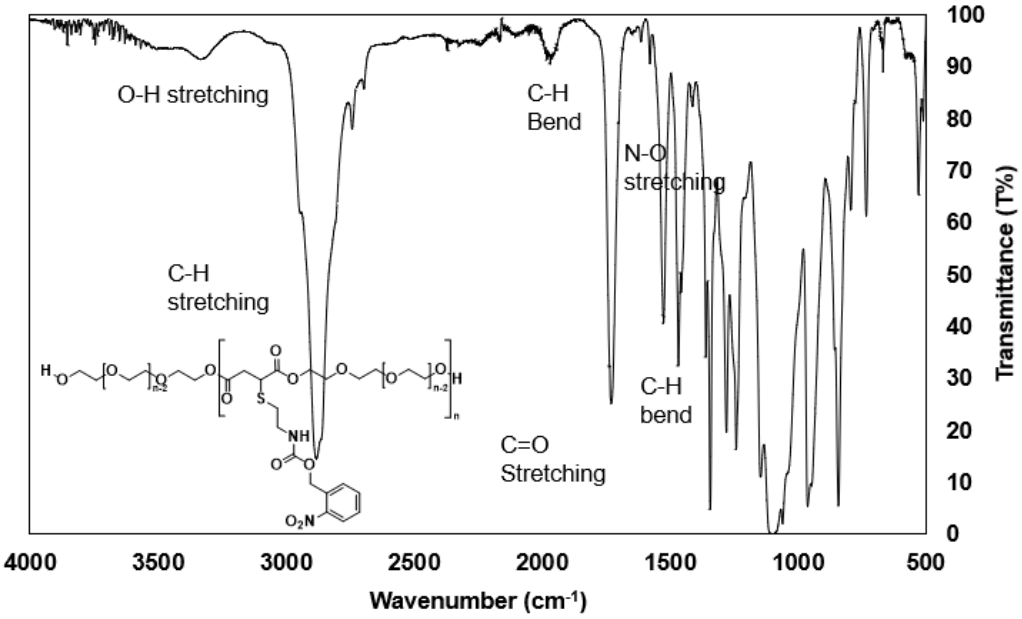


**Figure A18.** FT-IR spectrum of OPF-NB-100.

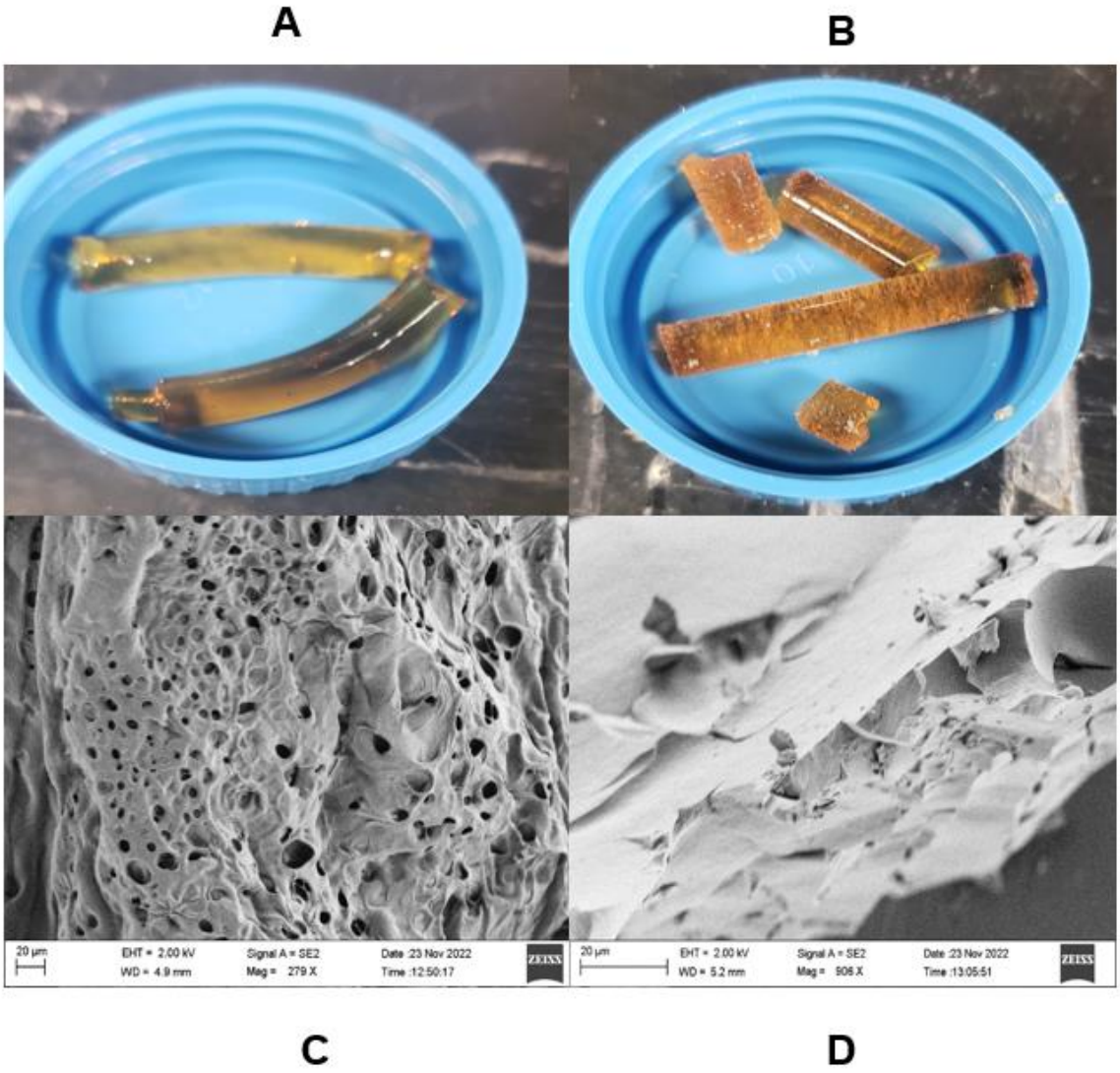


**Figure A19. A)** 30 wt% formulation hydrogel of OPF-NB-50 **B)** 30 wt% formulation hydrogel of OPF **C)** SEM imaging of 30 wt% hydrogel of OPF-NB-50 magnified at 20 µm **D)** SEM imaging of 30 wt% hydrogel of OPF at 20 µm magnified at 20 µm.

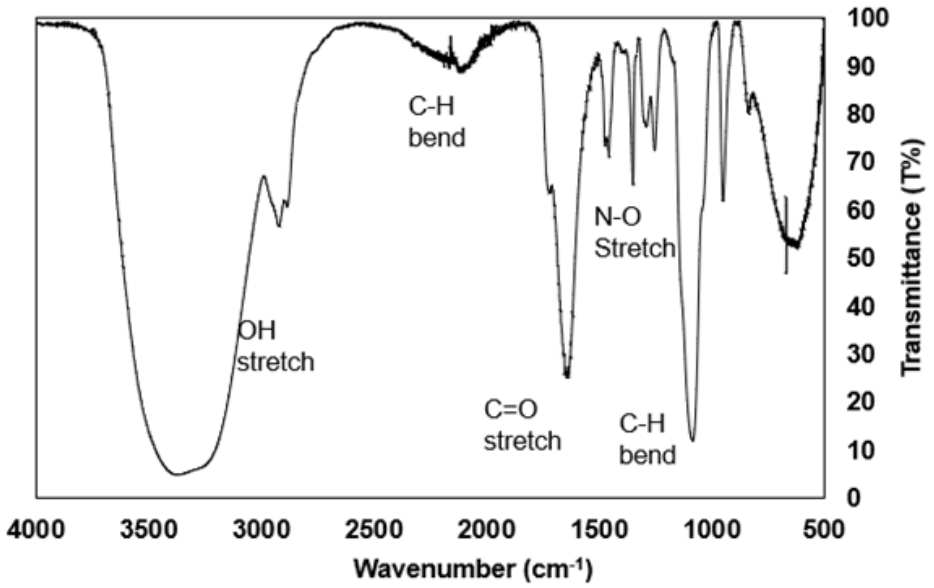


**Figure A20.** FT-IR spectrum of the 30 wt% OPF hydrogel.

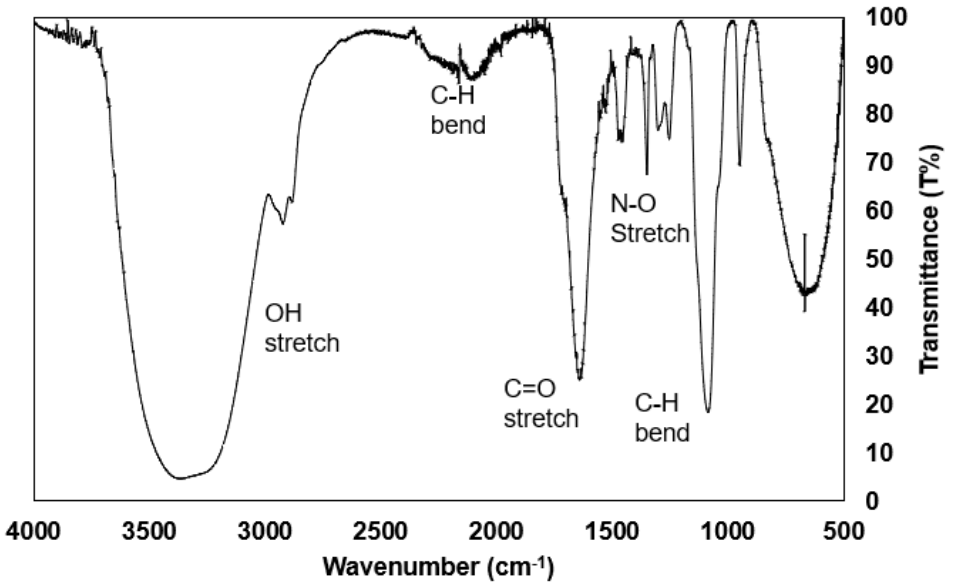


**Figure A21.** FT-IR spectrum of the 30 wt% OPF-NB-50 hydrogel.

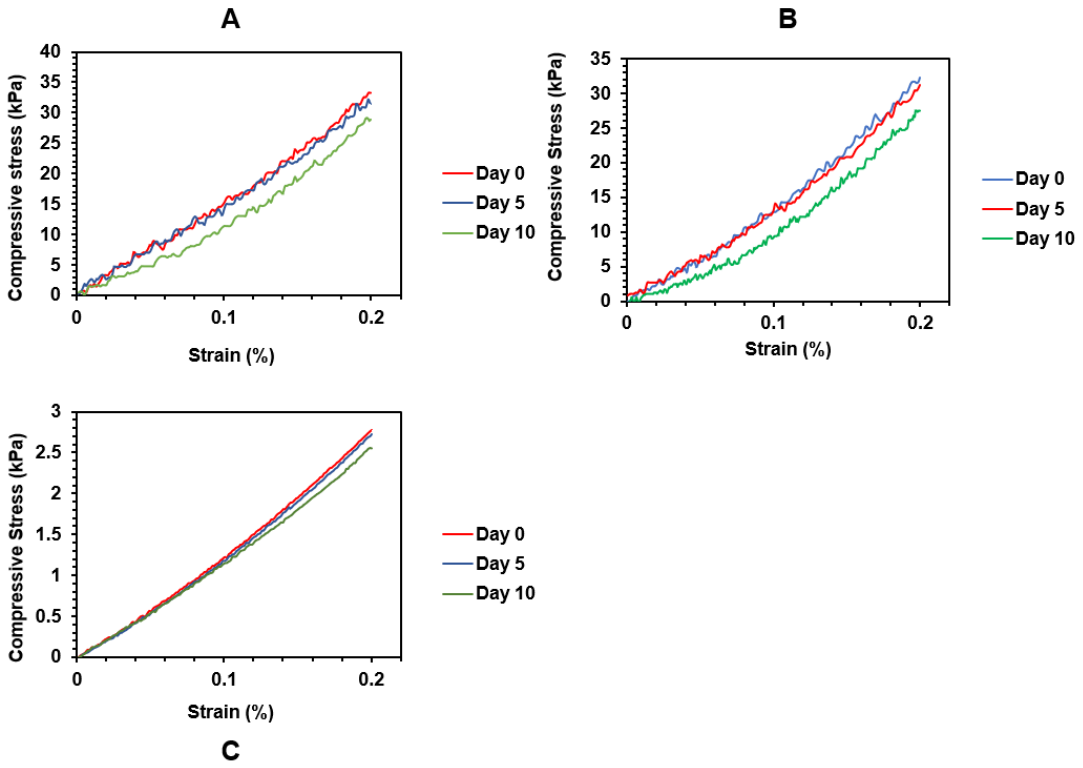


**Figure A22.** Stress-strain curves of **A)** Irradiated OPF **B)** Control group of OPF **C)** Control group of OPF-NB-50.

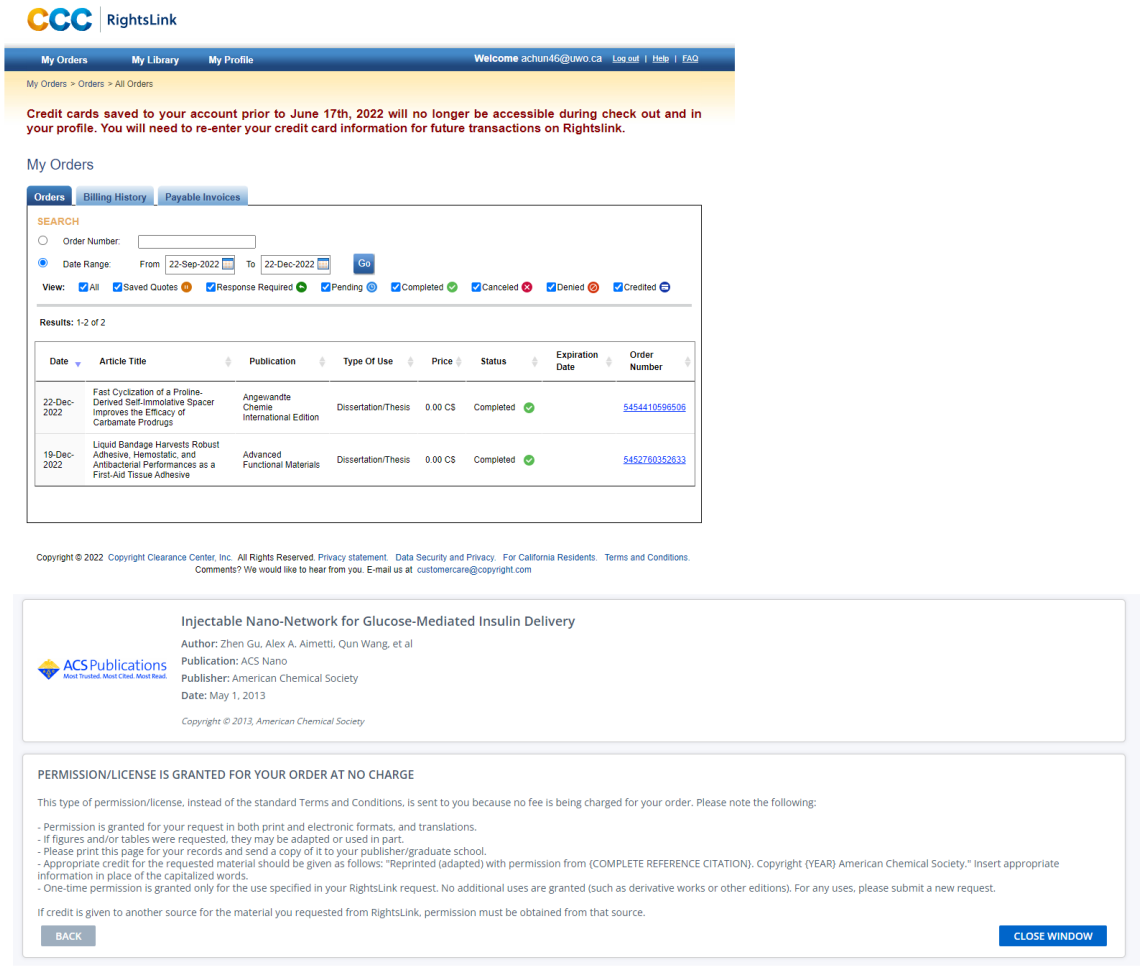


**Figure A23**. Permission to use copyrighted material.

# Curriculum Vitae

**Name:** Andrew Chung

**Education:**

B.Sc Honours in Chemistry
Ryerson University,
Toronto, Ontario, Canada
Sept 2016 – April 2020

M.Sc in Chemistry
The University of Western Ontario,
London, Ontario, Canada
2020 – Present

**Related Work Experience:**

Graduate Research Student
The University of Western Ontario
London, Ontario, Canada
2020 – Present

Graduate Teaching Assistant
The University of Western Ontario
London, Ontario, Canada
2020-2022

Undergraduate Research Assistant
Ryerson University
Toronto, Ontario, Canada
2018-2019

**Conference Presentations:**

*Presenter is underlined*

- Chung. A; Gillies, E.R. Oligo [poly (ethylene glycol) fumarate] hydrogels with photo-sensitive pendent groups Consortium for Industrial Bioproduct Innovation Western University (CIBI-WESTERN). London, Ontario, Canada, 2022. Oral presentation.

- Chung. A; Gillies, E.R. Oligo [poly (ethylene glycol) fumarate] hydrogels with photo-sensitive pendent groups. 39$^{th}$ Canadian High Polymer Forum. Gananoque, Ontario, Canada, **2022**. Poster presentation.